Modelling Physical and Biological drivers of larval retention in reef systems

Thesis submitted by

Paulina Cetina Heredia

MSc. Physical Oceanography (Ensenada, Mexico)

In September 2012

For the degree of Doctor of Philosophy

In the School of Marine & Tropical Biology,

and the School of Engineering and Physics

James Cook University

Statement on the contribution of others

Nature of assistance	Contribution	Names, titles and affilitations of co-contributors
Intellectual support	Discussing research proposal, data analysis, interpretation of results, manuscript and thesis editing	Professor Sean R Connolly (main supervisor)
	Data analysis, discussing interpretation of results, thesis editing	Professor Peter Ridd (supervisor)
	Discussing interpretation of results, facilitating AIMS data provision	Doctor Richard Brinkman (supervisor)
	Taught me to use the Sparse Hydrodynamic Ocean Code and advisor while modifying SHOC's particle tracking algorithm Development of research ideas	Dr. Mike Herzfeld (Department of Marine and Atmospheric Research, CSIRO)
Computer facilities and software	Usage of super-computer	Australian Institute of Marine Science (AIMS)
	IT support with AIMS super- computer	Simon Spagnol (AIMS) Geoff Millar (AIMS)
	IT support with the use of SHOC's visualization software 'plum'	Dr. John Andrewartha (Department of Marine and Atmospheric Research, CSIRO)
Financial support	PhD scholarship and living allowance (3 years)	National COuncil of sCience and Technology CONACyT, (Mexico)
	PhD scholarship and living allowance (1 year) Internal Research Allocation (IRA) $ 2000 AUD Graduate Research Scholarship (GRS), 2008 towards research	James Cook University (JCU) , School of Marine and Tropical Biology, School of Engineering and Physical Sciences , Graduate Research School
	PhD scholarship supplement (3 years)	Secretary of Public Education (SEP), Mexico
	Research money grant: $500 AUD, best poster at the AIMS@JCU student seminar 2007 $1000 AUD, second best oral presentation at AIMS@JCU student seminars 2008 $500 AUD, Conference travelling expenses (11th ICRS)	Australian Institute of Marine Science (AIMS)
	$1000 AUD, Conference travel expenses (11th ICRS)	ARC centre of excellence for coral reef studies

Title of the thesis: Modelling physical and biological drivers of larval retention in reef systems

Name of the candidate: Paulina Cetina Heredia

Chapter #	Details of publication	Nature and extent of the intellectual input of each author	I confirm the candidate's contribution to this paper and consent to the inclusion of the paper in this thesis
2. A simple approximation for larval retention around reefs	Cetina-Heredia P, Connolly SR (2011) A simple approximation for larval retention around reefs, Coral Reefs, Vol 30, Number 3, 593-605	Cetina-Heredia Paulina: Research proporsal, modelling, data analysis and interpretation, writing Connolly Sean R.: suggestions for data analysis and interpretation, editing of the manuscript and thesis	_____ Professor. Sean R Connolly

Acknowledgements

I would like to thank the people from the Ecological modelling team at the School of Marine and Tropical Biology, and the IT people from AIMS and the Department of Marine and Atmospheric research of CSIRO. I would also like to thank CONACyT, SEP, JCU, AIMS and ARC CoE for their financial contribution towards this project.

I am really grateful to my family: Maria del Carmen Heredia Fernandez, Eugenio Augusto Cetina Vadillo, Maria del Carmen Cetina Heredia, Enrique Ortiz Herrasti, Camila Ortiz Cetina, Lucas Ortiz Cetina and Lina Ortiz Cetina; and to my friends for all their support; it motivated me and allowed me to accomplish this work.

I want to thank Dr. Mike Herzfeld for all his help and feedback and to my supervisors Professor Peter Ridd and Dr. Richard Brinkman for their comments and support.

I am immensely grateful to my main supervisor Professor Sean Connolly for his unconditional support, for teaching and motivating me throughout my PhD.

Abstract

Larval dispersal has major effects on ecological and evolutionary processes. Thus, a thorough understanding of mechanisms driving larval transport, and estimates of larval retention, are necessary to inform the conservation and management of marine biodiversity. The overall aim of this thesis was to investigate physical and biological factors driving larval transport in coral reef systems, with particular emphasis on the effect of lee-reef eddies, swimming behaviour, and their interaction.

In the second chapter, I quantified the extent to which lee-reef eddies with different dynamics influence retention of passive larvae close to reefs. Simulations of particle transport at individual reefs with idealized shapes, under the influence of unidirectional and tidal flows, were conducted with the Sparse Hydrodynamic Ocean Code (SHOC), a three dimensional hydrodynamic model, using a reef-scale spatial resolution. I then tested how accurately the Island Wake Parameter (I), a dimensionless number that indicates the degree of turbulence of flow past obstacles under stationary flows in shallow waters, characterized the qualitative nature of the simulated flow past reefs. Theoretical considerations suggest that I~1 implies the formation of stable eddies that remain attached downstream of the reef, and I>10 implies the formation of unstable eddies that detach and dissipate or are advected downstream. I found that the Island Wake Parameter captured adequately the qualitative nature of the flow past idealized reefs. Unidirectional flows induced the formation of stable eddies and were associated with I~1, while tidal flows induced the detachment and downstream advection of eddies and were associated with I>10. These eddies provoked the recirculation of particles, prolonging retention times. Thus, stable eddies (small I values) induced long retention times, and unstable eddies (large I values) induced short retention times. Indeed, a nonlinear regression indicated that the Island Wake Parameter explained 81-92% of the variability in retention time among idealized reefs across the range of flow regimes considered. This

suggests that the Island Wake Parameter is a useful predictor of the formation and duration of eddies past reefs with idealized shapes under unidirectional and tidal flows, and that eddies and their life-spans are key determinants of the retention of passive particles close to reefs.

The findings above suggest that the Island Wake Parameter may be useful for approximating retention of particles close to reefs, when well-calibrated, reef-scale circulation models are not unavailable. To investigate this possibility further, I aimed, first, to examine how well the Island Wake Parameter characterizes the flow past real reefs under non-stationary flows, and second, under these more realistic circulation regimes, to determine effect of eddies on retention of passive larvae, and test the robustness of the relationship between the Island Wake Parameter and mean retention times. To achieve these objectives, in Chapter 3, I implemented SHOC with a reef-scale spatial resolution (~300 m) within the central Great Barrier Reef (GBR), encompassing 14 middle and 6 outer shelf reefs with various shapes (crescentic, lagoonal, planar and patchy), ranging from 1.9 to 27.5 km^2 in size. Comparison of the model outcomes against observed time series of temperature, sea level and currents through correlation, principal components, and spectral analyses, showed that the model reproduces the dynamics in the region adequately. In particular, it characterizes well the formation of eddies downstream of reefs, and the upwelling events associated with these eddies.

Having validated the central GBR model, I turned in Chapter 4 to simulating passive larval transport over two spawning events, and to quantifying retention time at individual reefs. The Island Wake Parameter proved successful at discerning between the presence and absence of eddies. In turn, the presence of eddies, and their duration, strongly influenced larval retention: the longest retention times occurred at reefs where eddies were long-lived, and the shortest retention times when eddies did not form at all. Finally, a common functional relationship characterized how mean retention time depends on the Island Wake Parameter, both for idealized reefs under simplified flows (from Chapter 2), and for reefs along the central

GBR under realistic circulation. These results indicate, first, that lee-reef eddies and their dynamics are accurately depicted by the Island Wake Parameter, and second, that lee-reef eddies are key drivers of passive larval transport close to reefs. Because the Island Wake Parameter is a simple function of upstream flow velocity, reef geometry, and vertical diffusion, these findings suggest that first-order estimates of larval retention may be obtained from relatively coarse-scale characteristics of the flow, and basic features of reef geomorphology. Such approximations may be a valuable tool for modelling meta-population dynamics over large spatial scales, where explicitly characterizing fine-scale flows around reefs would require extensive computational resources and model calibration.

The results of Chapters 2 and 4 indicate that the potential of lee-reef eddies to retain particles is limited by eddy life-span. Stable eddies can facilitate self-recruitment of species whose larvae are passive, or weak swimmers, for a few days after release. However, mean currents along the central GBR are intense and provoke unstable eddies that only retain larvae for periods of less than a day. This suggests that other mechanisms, such as swimming behaviour, might play an important role in larval retention and dispersal patterns of species whose larvae take weeks or months to develop, such as reef fishes.

Consequently, the objective of the fifth chapter was to quantify the extent to which horizontal swimming behaviour of larvae that exploit lee reef eddies can influence retention close to reefs. I incorporated larval behaviour within SHOC's Lagrangian algorithm to simulate the transport of larvae that swim towards regions where lee reef eddies form. The implemented swimming speed of larvae increased with age according to an empirical relationship for Lutjanids. Simulations were conducted at idealized reefs under alternative circulation regimes that produced stable eddies, unstable eddies, and no eddies. Larvae were assumed to be advected into the reef's vicinity at different stages of their development, and the proportion of retained larvae at the end of the pelagic larval duration was quantified for

each larval stage and circulation regime. Depletion of energy reserves by swimming was also considered, based on published data. Results indicate that the potential for swimming behaviour to increase retention close to reefs is highly sensitive to the extent to which larval feeding is sufficient to replenish energy reserves, and on the presence and duration of eddies. If food sources are sufficiently available throughout the planktonic stage to replenish energy expended during swimming, then larval swimming behavior suffices to enhance retention close to reefs and facilitate self-recruitment. However, if food is scarce, the presence of favourable circulation structures, such as eddies with long life-spans, or vertical migration combined with currents flowing in varying directions with depth, are necessary for self-recruitment, and crucial to enhance the retention of late-stage pelagic larvae that arrives close to reefs.

Table of Contents

List of Tables

Chapter 2

Chapter 3

Chapter 4

List of Figures

Chapter 2

Chapter 3

Chapter 4

Chapter 5

Appendix 1

Chapter 1. General Introduction

1.1 Importance of larval transport

Most marine organisms release planktonic eggs or larvae that disperse in the ocean while developing and acquiring competence to settle (Cowen and Sponaugle 2009). In addition, the vast majority of marine life forms have a sessile or sedentary adult life (e.g., Sale 1991). This life cycle connects sub-populations into meta-populations during the larval phase, the dominant or unique dispersal stage (Cowen and Sponaugle 2009). Consequently, larval dispersal has major implications for biogeographical, evolutionary, and ecological processes.

The dispersal of larvae is often necessary for species to colonize new habitats or expand their geographical ranges; consequently, it is a main driver of species distributions (Strathmann et al. 2002). Furthermore, it regulates gene flow amongst sub-populations. As a result, dispersal has repercussions for genetic differentiation within meta-populations (e.g., Hellberg 2002), the possibility for local adaptation (e.g., Brown et al. 2001), and ultimately on speciation (Strathmann et al. 2002).

A variety of ecological processes are also influenced by larval dispersal pathways and distances. For instance, species coexistence at the meta-community level is promoted when competing species have different disproportionate transport of propagules towards or away from particular habitats within a meta-population (Salomon et al. 2010). Moreover, the degree to which populations self-recruit or receive subsidy from external sources has major consequences for population replenishment and dynamics (e.g., Cowen and Sponaugle 2009). In addition, temporal fluctuations in migration rates have been shown to have a stabilizing influence on populations (Strathmann et al. 2002). Finally, the potential for local populations to recover from disturbances is also affected by larval exchange. Those populations that rely mostly on local recruitment will take longer and have difficulties to recover from localized disturbances or overexploitation than populations that import larvae from elsewhere considerably (Steneck 2006). Consequently, understanding which mechanisms drive larval

transport and how they modulate larval supply is crucial for the adequate design of conservation and management strategies (e.g., Botsford et al. 2001).

Marine Protected Areas (MPAs), where fishing and other activities are prohibited, have become an increasingly prevalent approach to ameliorate the loss of biodiversity, alteration of trophic structure of ecosystems, and over-exploitation of particular stocks (Russ et al. 2004). One of the main benefits of MPAs is to provide a spatial refuge where biomass and fecundity of exploited species can increase, and from which larvae are exported, supplementing populations in surrounding areas (e.g., Bellwood et al. 2004; Sale et al. 2005). Effective MPAs must be net exporters of propagules and there must be sufficient self-recruitment within a single reserve or a network of reserves to ensure sustainability when surrounding populations are depauperate (Sale et al. 2005). Hence, estimates of connectivity and its temporal variability are crucial for the effectiveness of reserve design (Botsford et al. 2001, Blowes and Connolly 2012).

The overall aim of this thesis is to improve our understanding of the physical and biological mechanisms driving larval transport in reef systems, with a focus on the role of eddies that form in the lee of reefs – circulation features that have been hypothesized to retain larvae near their natal reefs (e.g., Sponaugle et al. 2002; Swearer et al. 1999).

1.2 Mechanisms driving larval transport

1.2.1 Physical Mechanisms

Due to the variety of mechanisms inducing ocean circulation (e.g., atmospheric pressure gradients, wind, sea level changes), currents mediating larval transport vary over a wide range of spatial and temporal scales (e.g., Legrand et al. 2006). For instance, low frequency currents which are defined over 100-1000 km dictate regional scale larval pathways. Nevertheless, currents with shorter temporal and spatial scales, such as those that are tidally driven, mediate the transport of larvae at local scales. In a similar manner, the interaction of

currents with the ocean floor in shallow or coastal waters induces flow structures that affect considerably the spread and transport of larvae (Parslow and Gabric 1989). For instance, close to reefs, the impact of currents with intricate bathymetry causes the formation of fronts, lee-reef eddies and tidal jets which are coupled with regions of convergence, divergence and vertical water movement (i.e., upwelling and downwelling) (e.g., Black and Gay 1987; Legrand et al. 2006). Larval transport within these types of flow structures is fundamentally different from that associated with homogeneous horizontal velocity fields (e.g., Parslow and Gabric 1987), where topographically-induced flows are absent. In the latter case, larvae are advected in the same direction and over similar distances regardless of their horizontal position. Conversely, when horizontal velocity shear is present, larvae can experience markedly different trajectories depending on their horizontal position. For instance, larvae outside eddies are quickly advected away from a reef, while larvae embedded in eddies remain close to it, and accumulate in regions of flow convergence. As a result, the distribution of larvae is not homogeneous. In fact, observational studies of larval dispersal along the Great Barrier Reef have documented the spread of larvae along streaks associated with fronts and lee-reef eddies (e.g., Oliver and Willis 1987). Hence, flow structure at the scales of hundreds of meters is relevant to retention or flushing times, and consequently to larval transport close to reefs. In addition, vertical stratification can cause the advection of larvae in different directions, depending upon the larval vertical position in the water column. Therefore, a comprehensive understanding of larval transport in reef systems needs to consider three dimensional water movement, not only at the regional scale that meta-populations encompass, but also at the reef scale. This thesis examines the effect of reef-scale flow structure on larval transport.

1.2.2 Biological Mechanisms

The time it takes larvae to develop and become competent to settle has crucial implications for dispersal distances. Marine organisms have a variety of reproductive modes:

some invertebrates release eggs that fertilize in the water column, while others have internal fertilization and release already developed larvae (e.g., Hadfield et al. 2001). Similarly, some fish release their eggs into the water column, while others lay demersal eggs that remain in the benthos until larvae hatch (Leis 2006). These differences in reproductive mode lead to differences in the minimum duration that early life stages of organisms must spend in the plankton before being able to settle. In reef systems, for instance, coral brooders have internal fertilization and are able to settle immediately or within hours after release (e.g., Best and Resing 1987), while spawners, which have external fertilization, typically take at least several days (e.g., Harrison et al. 1984; Connolly and Baird 2010). Similarly, reef-fish larvae that hatch from demersal eggs need a minimum of 30 days to develop, while those developing from planktonic eggs take between 9-30 days (Brothers et. al. 1983; Victor 1986). As a consequence, some organisms are more likely to be retained long enough to settle into their source reef and others are more likely to be dispersed towards downstream reefs before reaching the competent stage.

Another factor mediating the dispersal processes is larval behaviour. The majority of marine invertebrates have weak swimming abilities throughout their pelagic stage (Chia et al. 1984). Thus, physical mechanisms that promote retention are key for settlement to occur in the same habitat where larvae are released, and are also likely to influence settlement in downstream suitable habitats. Nevertheless, marine invertebrate larvae can exhibit diurnal vertical migration (e.g., Valiela 1995). This movement can lead to different dispersal trajectories if currents are not coherent with depth or when vertical stratification is dominant, and has the potential to enhance arrival to settlement grounds. In contrast to most marine invertebrates, fish larvae have a variety of sensorial and locomotion capabilities that allow them to substantially modify their dispersal through oriented horizontal navigation (e.g., Kingsford et al. 2002).

To benefit from their swimming capabilities and enhance settlement probability, larvae of reef-associated organisms need to perceive the presence of a reef. Studies have shown that reef fish larvae have olfactory organs that allow them to distinguish between oceanic and reef waters (Atema et al. 2002). Moreover, Gerlach et al. (2007) found that fish larvae of the families Apogonidae and Pomacentridae show preference for water with a specific chemical signature (i.e., water from their home reef). Similarly, fish larvae are able to hear and respond to the noise associated with reefs (e.g., waves breaking on the reef), performing oriented navigation towards the source of sound. In fact, field studies have found higher concentrations of larvae in light traps that transmitted recorded sounds from reefs, compared to light traps without sound cues (Tolimieri et al. 2004). This indicates that fish larvae have the capability to sense the environment, and more importantly, that they react to these cues (e.g., Kingsford et al. 2002).

In addition, the swimming ability of reef fish has been measured in the laboratory (e.g., Stobutzki and Bellwood 1997; Fisher and Wilson 2004), and found sufficient to overcome currents encountered in many reef systems. For instance, along the GBR, mean current speeds of approximately 0.3 ms^{-1} have been measured close to reefs (e.g., Wolanski and Pickard 1985). Fish larvae from a variety of families are able to sustain swimming speeds between 0.2-0.6 ms^{-1} (e.g. Fisher 2005), implying that larvae can modify their dispersal by oriented navigation (e.g., Stobutzki and Bellwood 1997). In addition, some studies that simulated larval transport at specific locations have found better agreement with observed larval distributions when behaviour is invoked (e.g., Wolanski et al. 1997; Paris et al. 2005). Nevertheless, swimming activity incurs an energetic cost (Stobutzki and Bellwood 1997), limiting the potential of this behaviour on arriving to suitable habitat. Armsworth (2000) used a mathematical framework to explore the extent to which larvae can influence their dispersal through swimming behaviour, and found that those strategies which exploit favourable currents, such as positioning at the bottom where currents are slower, are more beneficial.

Even though there is accumulating evidence that fish larvae can swim to influence their dispersal, the specific swimming strategies that are used and the energetic cost they incur remain unknown. Moreover, how biological factors weigh against oceanographic processes has rarely been investigated. In this thesis I explore the relative effect of swimming strategies that exploit circulation features to achieve arriving to reefs.

1.3 Thesis aims and structure

This thesis examines physical and biological mechanisms driving larval transport in reefs systems, and proposes and evaluates a simple and tractable method to approximate retention times of passive larvae close to reefs as an alternative to the use of fine-scale hydrodynamic models. Throughout the thesis retention time is computed at individual reefs and refers to the time it takes passive or active larvae to be advected outside an area where the reef has an influence on the flow dynamics and from which larvae can be advected back towards the reef due to tidal reversal or recirculation within eddies.

Coral reefs are a good study system because the effects of complex circulation associated with reefs pose a challenge to estimate larval transport. In addition, recent studies have shown that dispersal of reef-fish larvae is rarely explained solely by physical mechanisms. Therefore, examination of how biological factors, such as swimming behaviour and its interaction with physical mechanisms, modify larval dispersal requires further research.

Larval dispersal is commonly investigated using hydrodynamic models to simulate larval transport and estimate connectivity at specific geographical locations (e.g., James et al. 2002; Kool et al. 2010). The development, refinement, and use of such models has immensely enhanced our understanding of dispersal processes (Cowen and Sponaugle 2009). However, the implementation of such models requires the collection of comprehensive oceanographic data sets used not only to force the model but also to test its performance. These sorts of data are not always available. Furthermore, computational capabilities needed to support the

performance of hydrodynamic models are often large. For instance, obtaining one day of circulation along the Great Barrier Reef (GBR) using the sparse hydrodynamic ocean code (SHOC), with a resolution of 3km, takes 20 hours. Not surprisingly, augmenting the spatial resolution and the simulation time over scales relevant to larval transport increases the computational time considerably. For example, simulating one day of larval transport over 100km of the GBR with a reef-scale spatial resolution takes 3 days. Thus, alternative approaches to estimate larval retention or dispersal would be particularly useful at locations where either oceanographic data or computer resources are scarce.

The aim of Chapter 2 was to develop and evaluate a simple and tractable way to approximate passive larval retention close to reefs. With this objective, simulations of passive larval transport at individual reefs with idealized shapes under unidirectional and tidal flows were used to quantify, first, the effect of lee-reef eddies on larval retention; second, the extent to which the Island Wake Parameter, a dimensionless number that indicates the degree of turbulence past obstacles in shallow waters, characterizes the dynamics of eddies formed downstream of reefs; and third, the relationship between the Island Wake Parameter and mean retention time.

In Chapter 3, a three dimensional hydrodynamic model was implemented along the central Great Barrier Reef to explore larval transport in a real reef system under realistic circulation regimes, and to determine whether the relationship between the Island Wake Parameter and mean retention times found for idealized reefs (Chapter 2) holds for real reefs under realistic flows. To solve explicitly the circulation structure at the reef scale, and include the effect of oceanic circulation (i.e., the Coral Sea inflow), nested grids were used, starting with a regional grid that encompassed the whole GBR with a coarse spatial resolution (~3.6km) and finishing with a reef-scale spatial resolution grid extending over the central GBR. This chapter provided a validated model with a reef-scale spatial resolution for the central GBR that

allowed exploring larval transport and testing the potential of the Island Wake Parameter to approximate larval retention at real reefs.

In Chapter 4, the model implemented in Chapter 3 was used to simulate passive larval transport along the central GBR over two spawning events, and to quantify the effect of eddies on larval transport close to real reefs under realistic circulation regimes. Specifically, I tested if the Island Wake Parameter depicts the flow dynamics in the wake of real reefs under non-stationary flows, and I examined how robust is the relationship between the Island Wake Parameter and mean retention time for real reefs. These results provided insight into the potential of lee reef eddies to facilitate self-recruitment or enhance retention of larvae advected close to a reef.

Recent studies on population genetic structure suggest that considerable proportions of reef-fish larvae recruit in their natal reef (e.g., Jones et al. 1999; Harrison et al. 2012). Although physical mechanisms may delay larval flushing, it is unlikely that they consistently induce larval retention for periods of time comparable to the length of the planktonic stage of the majority of reef fish (weeks-months). For example, lee-reef eddies recirculate larvae prolonging retention times; however, their potential to retain larvae is limited by their life-span, which, under intense currents or tidal flows, is rarely longer than hours (Chapters 2 and 4). Thus, other mechanisms, such as larval behaviour, may be relevant for determining patterns of larval dispersal. Bio-physical models that track larvae and incorporate larval life traits and behaviour have been used to test hypothesized mechanisms for observed larval distributions (e.g., Burgess et al. 2007; Paris et al. 2005; Staaterman et al. 2012) or observed population genetic structure (e.g., Foster et al. 2012). The interaction of larval vertical migration and stratified circulation has been identified as a mechanism by which larvae return to the source reef. However, favourable stratified circulation is not prevalent at all locations. In addition, fish larval swimming speeds are comparable to those of oceanic currents (e.g., Fisher 2005). This suggests that larvae might also perform horizontal swimming behaviour to

facilitate reaching suitable habitat for settlement. In fact, modelling studies that invoke larval oriented navigation have found a better match with observed larval distributions (e.g., Wolanski et al. 1997). Nevertheless, the interaction of swimming behaviour with current structure at the reef scale has not been explored.

In Chapter 5, the extent to which horizontal swimming behaviour, and its interaction with lee-reef eddies, modifies larval retention close to reefs is examined. I implemented larval behaviour into the Sparse Hydrodynamic Ocean Code (SHOC) by modifying the particle tracking algorithm to run active larval transport simulations and quantify the effect on larval supply of lee-reef eddies and horizontal swimming behaviour. Studies that used an analytical framework to investigate the effect of behaviour on larval transport have shown that strategies which exploit favourable currents are more likely to increase the extent to which they can influence dispersal since they minimize energetic costs (e.g., Armsworth 2001; Irisson et al. 2004). To consider energy expenditure incurred by performing swimming behaviours, I quantified the extent to which energy depletion due to swimming reduced the proportion of active larvae arriving into suitable habitat. Results from this chapter highlight the importance of considering energy expenditure caused by larval behaviour during dispersal.

The second Chapter of this thesis has been published in *Coral Reefs* with my principal supervisor SR Connolly as a co-author. Hence, it is written in first person plural. The rest of the Chapters are not yet submitted for publication so they are written in first person singular.

Chapter 2. A simple approximation for larval retention around reefs

2.1 Introduction

The dispersal of planktonic larvae influences many ecological and evolutionary phenomena. It affects the persistence of populations (James et al. 2002), the geographical distribution of species (Strathmann et al. 2002); population resilience to local disturbances (Steneck 2006; van Oppen and Gates 2006); population genetic structure (Hellberg et al. 2002), and potential for local adaptation (Done 1982; Willis and Oliver 1990). Therefore, an understanding of connectivity (i.e., the degree to which populations are linked through larval dispersal) is important for management and conservation in marine environments (Sale et al. 2005).

Connectivity is investigated using hydrodynamic models to simulate particle transport, and to quantify larval dispersal at specific geographical locations. Such models frequently predict relatively high levels of connectivity among marine populations (e.g., Roberts 1997; Cowen et al. 2006). However, evidence of substantial self-recruitment exists across species with a broad range of life history traits (Swearer et al. 2002), and, in some cases, there is evidence that larval retention is likely to be higher than that predicted by hydrodynamic models (e.g., Gerlach et al. 2007). For strong swimmers, recent work suggests that larval behavioural strategies, such as oriented navigation, can enhance larval retention and facilitate self-recruitment (e.g., Kingsford et al. 2002). However, many other marine organisms have passive larvae for prolonged time (Nahas et al. 2003), and most marine invertebrates, such as corals, have weak swimming capabilities throughout their larval phase (Chia et al. 1984; Bradbury and Snelgrove 2001). Moreover, species whose larvae have strong swimming ability often take several days to begin swimming (e.g., Irisson et al. 2004). Thus, for the majority of marine organisms, local retention is likely to be substantially influenced by local-scale hydrodynamics, at least over the first few days of larval life. Hence hydrodynamic models used

to estimate dispersal need to characterize adequately the flow structures that induce larval retention around reefs.

In coastal waters, the interaction of currents with the ocean bottom provokes complex flows that in turn dictate particle trajectories. For instance, water flowing past reefs is associated with the formation of fronts, horizontal convergence, divergence, and upwelling. These types of flows, strongly influenced by vertical water movements, can distribute larvae in streaks (Wolanski and Hamner 1988; Wolanski et al. 1989) rather than uniformly across the surface (Parslow and Gabric 1989), and affect particle flushing times. Consequently, the effect of vertical flows is highly relevant for larval dispersal. Moreover, reefs induce friction, and thus turbulence (strong current velocity shear or linear stress); which leads to the formation of downstream reef scale eddies. These eddies have been observed to affect larval distributions (Wolanski et al. 1989; Willis and Oliver 1990; Burgess et al. 2007). Lee eddies can promote larval retention by recirculating larvae or accumulating them in regions where secondary convergent flows occur (Wolanski et al. 1996; Sponaugle et al. 2002). However, such eddies can also accelerate transport across the wake if larvae become entrained in the eddy and travel along its edge where velocities are greater (Sandulescu et al. 2006), or they can enhance larval dispersion by the straining motions of the eddies (Signell and Geyer 1991). Hence, to accurately simulate larval transport in shallow waters, models must not only account for three dimensional hydrodynamics that solve the vertical flow structure, but also utilize a spatial resolution fine enough to depict the effect of complex bathymetry, such as around reefs (Wolanski 1993; Marinone 2006) on the horizontal flow structure.

In order to incorporate a reef scale (hundreds of meters) spatial resolution, and capture the effects of three dimensional flows in hydrodynamic models, substantial computational power is required, even at the scale of individual reefs. However, larval dispersal can occur over great distances (e.g., tens or even hundreds of kilometers; James et al. 2002; Cowen et al. 2006); therefore, dispersal models must cover large geographical areas.

These twin requirements present a substantial logistical challenge for the simulation of dispersal patterns. One approach has been to use high resolution models for regions of shallow waters (e.g., around reefs), nested within coarse resolution models that cover broad geographical areas (e.g., Tang et al. 2006). Most recently, models that allow changes in resolution within the same grid have been developed (Legrand et al. 2006). However, these approaches involve extensive model calibration, which in turn, requires observations at many different locations. Alternatively, advection-diffusion approximations that parameterize smaller-scale flows (Paris and Cowen 2004; Marinone et al. 2008) can be implemented in coarse resolution models that allow a wide geographical coverage. However, diffusion is highly spatially and temporally variable in the ocean (Visser 1997), and thus extensive calibration with observations is required to adequately characterize the flow structure found in the vicinity of reefs when this approach is employed.

In this study, we explore a new approach to overcoming the logistical problems associated with modelling reef scale flow features in a metapopulation context, by investigating how well the larval retention simulated by a reef scale three dimensional model can be estimated with very simple functions that incorporate effects of reef dimension, flow velocity, and bottom friction scales on retention times. In order to determine how reef-scale circulation features affect larval retention, a high-resolution (~100 m), three-dimensional hydrodynamic model was used to estimate larval retention by reefs with different shapes and sizes, under a range of circulation regimes (i.e., under different combinations of unidirectional and tidal flow intensities).

To approximate the effects of reef dimension, flow velocity and bottom friction scales on retention time; we examined a dimensionless number, termed the “Island Wake Parameter” that characterizes the flow behind topographic outcrops in shallow waters (Wolanski et al. 1984). Analogous to the Reynolds number, the Island Wake Parameter indicates whether the flow past an obstacle has turbulent characteristics, such as whether

eddies are expected to form behind the obstacle and how stable these flow structures are (Tomczak 1988; Barton 2001). For Island Wake Parameter values on the order of unity, stable eddies are expected to form behind the obstacle. Smaller values are predicted to produce laminar flow. Larger values are predicted to lead to eddy formation, detachment and dissipation. In previous work, this number has proved successful at predicting these qualitative features of the wake (Neill and Elliot 2004; Pattiaratchi et al. 1986). The present study tests whether differences among reefs in the Island Wake Parameter can explain associated differences in larval retention times induced by a particular circulation regime, and whether the relationship between retention time and Island Wake Parameter varies predictably among circulation regimes. This approach offers the potential to estimate the larval retention induced by three-dimensional, reef-scale flow structure in a simple and tractable way, without the need to explicitly model that flow structure. Moreover, such simple approximations potentially can be applied even at locations where hydrodynamic models can not readily be implemented, due to insufficient oceanographic data.

2.2 Methods

2.2.1 The Island Wake Parameter

The Island Wake Parameter, *I*, is the ratio of advective to frictional terms, relevant to the flow past an obstacle in shallow waters. In this type of environment, bottom drag is the primary source of velocity shear (Dong and McWilliams 2007). Bottom drag causes a stress boundary layer that generates turbulence and vertical momentum transfer. Consequently, the pertinent frictional terms are the vertical turbulent diffusion coefficient K_z, and the water depth H. K_z represents the vertical momentum transfer due to turbulence, it allows the development of eddies and is expected to influence their persistence (Moum et al. 1988). The advection term is determined by the acceleration that the particles experience when they

deviate from their intended path as they approach obstacle. This term is related to the velocity, *V*, of the current that impinges upon the obstacle, and the width, *W*, of the obstacle. Hence, the Island Wake Parameter is given by:

$$I = \frac{VH^2}{K_z W} \qquad \text{eq.2.1}$$

Although the expression for the Island Wake Parameter is simple, many of the constituent terms are not constant. For instance, the velocity upstream of an obstacle may vary over time and space. For consistency, in this study, *V* was determined as the maximum velocity over time found within the region upstream of the obstacle in each simulation. *H* is constant (50 m) for all simulations. This depth is within the range of depths around inner and middle shelf reefs along the Great Barrier Reef (GBR). *W* is the dimension of the reef perpendicular to the incoming flow.

In the field, vertical diffusion (K_z) is highly spatially and temporally variable (even within individual eddies), and is time-consuming to measure (e.g., Bricker and Nakayama 2007). Using such measurements when applying eq. 2.1 would defeat the purpose of a simple approximation based on measuring easily obtainable quantities, such as reef dimensions. Previous uses of the Island Wake Parameter approximate K_z by applying Taylor's theory (1954), accoriding to which vertical diffusion is proportional to the drag coefficient, flow velocity and depth. However, this approximation is problematic because the Island Wake Parameter becomes independent of velocity. Instead, we use a background vertical diffusion specified in the simulations (0.01 ms^{-1}). This quantity represents the extent of vertical momentum transfer in the ocean's interior, and it is a lower bound on the total vertical diffusion, which is:

$$K_z = K_b + \alpha\mu H(1+3.33R_i)^{-3/2} \qquad \text{eq. 2.2}$$

where μ is the maximum of the surface and bottom friction velocities, α is a constant, and R_i is the Richardson number, dependent on the vertical stratification and vertical velocity shear (Herzfeld and Waring 2012).

2.2.2 Hydrodynamic & Particle tracking model

The Sparse Hydrodynamic Ocean Code (SHOC) was used to compute velocity fields and track individual passive particles. SHOC was developed by the Environmental Modelling group at the Commonwealth Scientific and Industrial Research Organization (CSIRO) and was previously termed the Model for Estuaries and Coastal Oceans (MECO) (Parslow et al. 2001; Wolanski et al. 2003). It has proved useful for investigating circulation in coastal areas (Walker 1999), larval transport in estuaries (Condie et al. 1999) and more recently across and along shelf connectivity in Western Australia (Condie and Andrewartha 2008). Briefly, SHOC is a finite difference model based on the three dimensional equations of momentum that uses the hydrostatic and Boussinesq approximations. The equations are solved in an Arakawa C grid, and are written for a curvilinear orthogonal horizontal mesh and a set of chosen 'z' coordinates in the vertical (Herzfeld and Waring 2012). The turbulence closure scheme implemented was the k-ε (Buchard et al. 1998), and a Lagrangian particle tracking algorithm contained within SHOC, was used to obtain simultaneously the velocity field and the particle location for the entire simulation time.

A common grid with nine depth layers was used for the simulations. Given that particles were initially located above the reef, and the reef surface was 5 m underwater, a higher vertical resolution (0.5 m) near the surface, and a coarser vertical resolution (5 m) in the rest of the water column was adopted for all simulations.

Research on the nature of lee reef eddies, including modelling (Black and Gay 1987), remote sensing and *in situ* observations (Wolanski et al. 1984), have reported that the size of these circulation features is 1-2 times the size of the reef's side perpendicular to the incoming

current. In order to capture the dynamics of a vortex, a minimum of three grid points across the gyre are necessary. Because the simulations were run for reefs with widths ranging from 600-3600 m, a spatial resolution of ~200 m was used to ensure a minimum of three grid points across the smallest of the expected eddies. Every time step, the particles were advected with the velocity explicitly solved by the hydrodynamic model plus a random diffusion velocity. This diffusion velocity was determined by drawing a random number from a Gaussian distribution with mean zero and standard deviation equal to the diffusion coefficient relevant to spatial scales smaller than the grid size, that is ~0.09 $m^2 s^{-1}$ (Okubo 1971).

Our use of a constant resolution, allowed implementing the same horizontal diffusion coefficient to induce particle diffusion caused by sub-grid flows in all simulations. However, this approach does imply more grid cells behind larger reefs than behind small reefs, and thus potentially poorer resolution of eddy structure behind smaller reefs. However, preliminary simulations with finer horizontal resolution resulted in retention times within 3% of one another, even for smaller reefs, which suggests that scaling grid cell size to reef size would have had a negligible effect on results.

For each simulation, 10^4 passive particles were released randomly distributed in the water column above the reef. The time, relative to the tidal cycle, at which particles were released had a negligible effect on particle retention; therefore particles were released at time zero.

2.2.3 Scenarios

This study examines how well *I* captures the characteristics of the flow past obstacles and can be used as a statistical predictor of retention times. As noted above (eq. 2.1), I is a function of: the reef dimension perpendicular to the incoming flow, the flow magnitude and the vertical diffusion coefficient. Therefore, to determine the relationship between I and retention time, this study analyses simulations for a range of reef shapes, reef dimensions, and

flow speeds generated by different combinations of unidirectional and tidal flows of different intensities.

Rectangular and triangular reef morphologies were used, because they resemble common reef shapes along the GBR; kidney-shaped reefs also were examined to incorporate the effects of a semi-enclosed central reef lagoon on larval retention (Figure 2.1). For each of these shapes, length and width dimensions were varied in order to encompass a wide spectrum of geometries. In total, we ran simulations for twelve rectangular, six triangular and eight kidney reefs (see Table 2.1). Bathymetry was uniform, with reefs submerged 5 m from the surface, rising straight from a 50 m flat bottom.

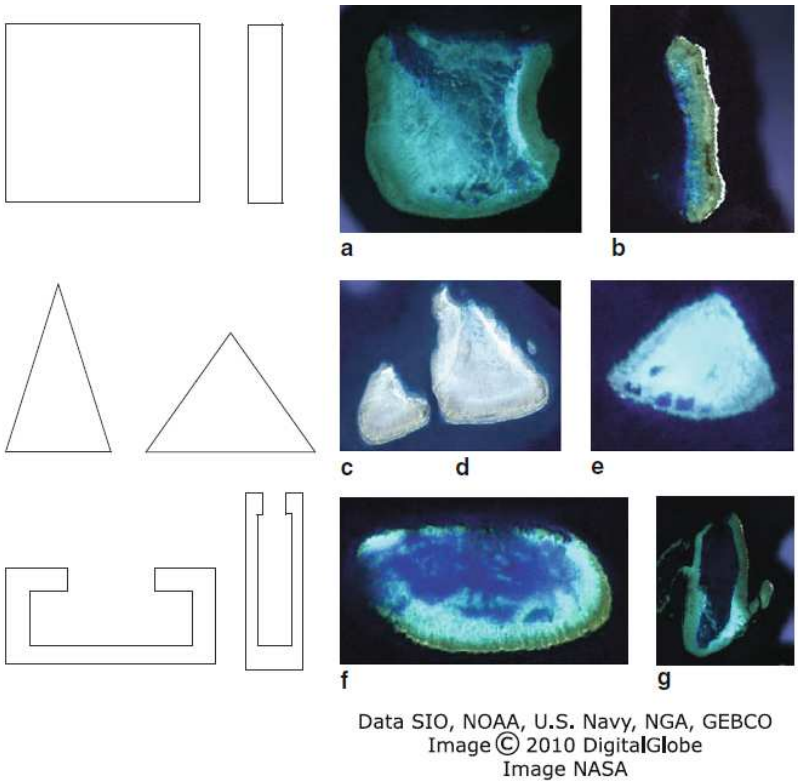

Figure 2.1 Modelled reef geometries and reef images along the GBR from Google Earth, examples for: a and b) rectangle, c d and e) triangle, and f and g) kidney shaped reefs. The reef images are oriented parallel to the coastline (main direction of the EAC). Their longitude and latitude are: a) 149° 49'E, 20°04'S, b) 145° 45'E, 15° 16'S, c) 145° 20'E, 14° 47'S, d) 145° 20'E, 14° 45'S, e) 150° 50'E, 21° 09'S, f) 147° 03'E, 18° 37'S, and g) 150° 19'E 20° 06'S.

Because I incorporates only the upstream obstacle flow intensity, we first implemented a unidirectional flow. Simulations were run for all rectangular reefs, for a range of intensities (~0.06-0.77 ms^{-1}). For each flow intensity, the relationship between I and mean retention time was quantified as described under *Methods: Statistical Analysis*, below. Estimated parameters characterizing this relationship were compared across flow intensities, to determine whether and how the functional relationship between I and retention time varied. To determine whether these relationships were robust to reef shape, simulations for the triangular and kidney shapes were run for two of these flow intensities, which we term "weak" and "strong", *wU* and *sU*, respectively, where *w* denotes weak, *s* denotes strong and *U* denotes unidirectional flow.

A unidirectional flow resembles a dominant alongshore low frequency current (e.g., Eastern Australian Current, EAC). However, circulation in reefs systems can also be influenced by high frequency tidal currents. It is therefore important to test the effect of such flows on I and its functional relationship with residence times. Therefore, circulation regimes that consisted of both, a unidirectional flow, plus a perpendicular tidal flow were implemented. Although tidal currents are not always perpendicular to low frequency currents, this is particularly common along the Eastern Australian coast where the GBR is located (Wolanski and Pickard 1985). Moreover, because I implicitly accounts only for flow in one direction, implementing tidal currents flowing perpendicularly to such flow provides a particularly stringent test of the robustness of I as a statistic describing circulation around reefs. Three different scenarios combining unidirectional and tidal flows were implemented: weak unidirectional and weak tidal (*wUwT*), weak unidirectional and strong tidal (*wUsT*), and strong unidirectional and strong tidal (*sUsT*).

2.2.4 Boundary forcing

The grid is oriented in a north-south east-west direction, has dimensions of 80 by 45 grid cells (16 by 9 km), and has four open boundaries through which we forced the model. The reefs were located seven grid cells south of the northern boundary, and at least twenty grid cells away from the east and west boundaries. Simulations using alternative distances indicated that this was far enough from the domain limits to avoid any effect of the boundaries on particle transport. To simulate the unidirectional flow scenarios, we constrained the current magnitudes at the south and north boundaries to remain constant in both magnitude and southward direction. To model effects of flow intensity, these current magnitudes were constrained to specific values ranging between 0.05-0.65ms^{-1}. This generated maximum flow magnitudes between 0.065 and 0.77 ms^{-1} within the model domain, consistent with the range of reported magnitudes for low frequency currents along the GBR (Wolanski and Pickard 1985). For simulations investigating effects of reef shape, and presence of tidal flows, the "weak" and "strong" unidirectional flow scenarios corresponded to southward magnitudes of 0.05 and 0.12 m s^{-1} at the boundaries (generating maximum flows of 0.11-0.51 ms^{-1} within the model domain). To implement the tidal flows we forced the east and west boundaries with synthetic sea level elevation time series (e.g., Wolanski et al. 1989). Specifically, the sea level time series were generated as the sum of diurnal and semidiurnal harmonics with amplitudes that would generate maximum tidal current magnitudes of 0.16 ms^{-1} and 0.44 ms^{-1} for the weak and strong tidal flow scenarios, respectively. This encompasses a range of tidal current magnitudes which are consistent with observational studies along the GBR (Griffin et al. 1987). The necessary forcing to generate a strong unidirectional flow provoked simultaneous strong tidal flows. Hence, it was not feasible to recreate the effect of a strong unidirectional flow coupled with a weak tidal flow.

2.2.5 Particle abundance and retention time

For all simulations, each 3D particle position was recorded every 30 minutes for the duration of the simulation (10-15 d). Particles were designated as "retained" if they remained within a region where they could be either entrained in a wake eddy, and ultimately brought back to the reef, or to be advected back over the reef after a tidal reversal. We delimited the retention area by counting 18 grid cells (the dimensions of the largest observed lee eddy) to the south of each simulated reef. Simulations indicated that eastward and westward displacement of eddies by tidal flows were of similar magnitude, so we extended the retention area east and west of the reef edges by 18 cells also. We adopted this approach, rather than scaling retention area to expected eddy size separately for each reef, to make our test of I more conservative. Specifically, smaller reefs tend to have larger I (equation 2.1). Using a smaller retention area would also tend to reduce retention times, and thus potentially amplify the expected negative relationship between I and mean retention time. In all simulations, all larvae that left the retention area did so past the southern boundary. This indicates that the designated retention area was sufficiently large to account for any east-west tidal recirculation or northward diffusion of larvae and that extending the area to the north, east, or west of the reef any further would have had no effect on the results.

The number of particles inside the retention area was calculated to obtain particle abundance over time, and the time at which each particle was advected out of this area was recorded. Mean retention time is the average time at which particles were flushed from the retention area. To evaluate how the potential for local self-recruitment varied among reef shapes, reef dimensions, and circulation regimes, we also estimated the percentage of larvae remaining inside the reef vicinity after 12 hours, 2 days, and 4 days. We chose 4 days as our maximum for this calculation because it is approximately the time required for broadcast-spawning corals to become competent to settle (Nozawa and Harrison 2008; Gilmour et al. 2009). It is also approximately the time required for some fish to develop swimming ability

(Irisson et al. 2004). Similarly, broadcast-spawned sponge larvae take between 12-54 hours, to metamorphose and settle (Leys and Degnan 2001; Whalan et al. 2008a).

2.2.6 Statistical analysis

I<1 represents laminar flow I~1 the formation of eddies that remain attached downstream the obstacle, and I>1 the formation and detachment of eddies. This could provoke shorter retention times as I increases above 1. Therefore, to quantify how well I predicts retention times, we used a power-law relationship, modified to include an offset term:

$$R = a\ I^b + c \qquad \text{eq. 2.3}$$

where *R* denotes retention time, I the Island Wake Parameter, and *a, b,* and *c* are fitted regression parameters. *b* represents the steepness of the relationship between the retention time and the Island Wake Parameter, as I increases from low values and the flow changes from friction-dominant to advection-dominant. We expected this parameter to be negative (i.e., shorter retention times for larger values of I). Consequently, the first term in equation (2.2) should approach zero as I increases, and thus *c* represents an asymptotic minimum possible retention time (i.e., retention time as I approaches infinity). The existence of such a minimum is plausible on physical grounds because, as friction becomes overwhelmed by advection, at very large I values some minimum time may still be required for larvae to be flushed from the retention area. To test for such a minimum, we also fit regression models where *c* was fixed at zero, and only *a* and *b* were estimated; where likelihood ratio tests did not indicate significant support for the full three-parameter model, we used the simpler model. The parameter *a* represents the additional retention due to the presence of an ideal stable eddy; that is, *a+c* is the predicted retention time when I=1. I was log-transformed for analysis, to homogenize residual variances.

First, regressions were conducted separately for all rectangular reefs and each unidirectional flow speed, to determine whether the relationship between retention time and I varied systematically among unidirectional flow intensities (i.e., different *a*, *b*, and *c* parameters for each unidirectional flow regime). A regression was also conducted by pooling the data across unidirectional flow intensities (i.e., a single *a*, *b*, and *c* parameter applies to all unidirectional flows). We used a likelihood ratio test to determine whether the model with separate parameters was significantly better than the pooled model.

Secondly, we conducted regression and likelihood ratio test to determine how well equation (2.3) predicted retention time for rectangular reefs under the flows with and without tides, and whether there were significant differences in parameters *a*, *b*, and *c* depending in the tidal regime.

Thirdly, to test the effect of reef shape on the relationship between the retention time and I, regressions were conducted for each reef shape separately (i.e. different parameters *a*, *b*, and *c* for the rectangular, triangular and kidney shaped reefs), and compared with a regression in which all reef shapes were pooled in a single analysis. A likelihood ratio test was used for model selection between the pooled model and the models with different regression parameters for each reef shape.

Finally, we pooled the results for all simulations (all reef shapes, unidirectional flow intensities and tidal regimes) in a single regression to determine how well a single fit of equation (2.3) could approximate retention time across the entire set of simulations.

Table 2.1 Percent of particles remaining inside the retention area 12 hours, 2 days and 4 days after release for each reef and circulation regime.

	Reef dimensions		**Time**													
	Length (km)	**Width (km)**	**12 h**					**2 d**					**4 d**				
			Circulation regime													
			wU	***wUwT***	***wUsT***	***sU***	***sUsT***	***wU***	***wUwT***	***wUsT***	***sU***	***sUsT***	***wU***	***wUwT***	***wUsT***	***sU***	***sUsT***
Rectangle	4.0	0.6	100	99.98	99.95	50.26	30.80	0.03	0.03	0.32	0.03	0.03	0.03	0.03	0.03	0.03	0.03
	4.2	0.6	99.81	99.74	99.82	63.44	55.18	0.13	0.59	1.36	0.01	0.01	0.01	0.01	0.02	0.01	0.01
	3.0	0.6	99.99	99.98	99.99	71.08	66.68	0.28	0.28	1.72	0.01	0.01	0.01	0.01	0.01	0.01	0.01
	1.6	0.8	99.99	99.96	99.92	71.24	49.73	1.55	0.86	0.77	0	0	0	0	0	0	0
	0.8	0.8	99.99	100	99.96	82.21	53.12	11.46	5.17	1.25	0.37	0.07	0.05	0.02	0.01	0	0.02
	2.0	1.0	100	100	100	90.51	84.24	19.38	12.65	8.34	2.36	0.04	0.43	0.02	0.08	0.10	0
	1.4	1.0	100	99.97	99.93	89.87	75.82	19.14	14.42	4.81	2.47	0.18	0.39	0.08	0.01	0.04	0.01
	1.2	1.2	100	99.99	99.97	93.54	74.32	25.85	23.30	5.26	10.03	0.38	1.97	1.00	0.04	0.54	0.01
	1.0	1.4	100	100	99.96	95.46	80.98	45.09	40.26	5.25	25.24	0.84	9.07	5.92	0.05	4.14	0
	1.6	1.6	100	100	99.99	95.02	84.06	41.87	35.74	20.11	22.24	1.22	9.61	4.44	3.03	4.04	0.02
	1.0	2.0	100	100	99.96	98.44	89.31	68.77	57.89	9.77	51.56	1.03	31.21	24.67	0.26	20.82	0.02
	1.0	2.8	100	99.99	99.97	99.62	94.61	79.59	61.17	17.92	55.82	0.83	46.29	30.56	2.89	34.29	0

Continuation Table 2.1

	Reef dimensions		Time													
	Length (km)	Width (km)	12 h					2 d					4 d				
			Circulation regime														
			wU	*wUwT*	*wUsT*	*sU*	*sUsT*	*wU*	*wUwT*	*wUsT*	*sU*	*sUsT*	*wU*	*wUwT*	*wUsT*	*sU*	*sUsT*
Kidney	2.8	1.0	100	99.99	99.97	85.08	80.02	19.22	16.45	17.31	3.86	3.68	5.24	5.80	6.90	1.02	0.65
	2.0	1.0	99.94	99.89	99.98	80.47	66.27	18.12	14.17	14.89	3.97	1.82	4.83	4.42	4.50	0.72	0.28
	1.4	1.0	100	100	99.98	90.25	86.00	22.91	19.40	11.52	4.42	19.95	4.81	3.81	3.08	0.67	18.00
	1.0	1.4	100	100	99.98	96.51	86.00	61.13	56.84	29.00	40.30	19.95	32.11	29.00	19.37	22.16	18.00
	1.0	2.0	100	100	99.98	98.74	90.89	74.09	66.33	20.66	51.07	3.35	40.33	33.58	2.85	20.34	0.13
	1.0	2.8	100	100	100	99.75	96.45	86.88	75.88	44.35	66.23	27.72	64.03	53.51	29.63	49.57	26.15
	1.4	2.8	100	100	99.99	99.41	96.35	76.16	65.94	47.18	47.00	11.81	48.73	39.30	20.31	27.27	0.76
	1.8	3.6	100	100	99.99	99.18	94.68	78.16	68.81	35.20	52.86	4.73	48.12	40.20	8.87	28.47	0.18
Triangle	1.0	1.0	100	99.99	99.95	88.34	71.16	22.30	7.28	3.08	5.82	0.03	0.86	0.01	0.01	0.24	0.01
	1.4	1.6	100	99.98	99.91	92.82	76.40	44.77	24.23	5.42	25.22	0.09	10.58	0.98	0.02	4.54	0.01
	1.4	1.2	100	100	99.94	97.29	75.13	53.39	28.08	1.30	31.77	0.19	14.97	1.62	0.01	6.85	0.01
	2.0	1.4	100	100	99.99	98.53	74.88	62.65	38.92	2.76	47.07	0.24	28.93	9.70	0.02	18.78	0.02
	2.2	1.2	100	99.99	99.77	98.79	72.50	73.42	39.02	1.94	53.13	0.24	38.18	9.86	0.01	24.57	0.03
	3.4	1.0	100	100	100	100	98.95	86.59	64.88	22.45	66.58	1.38	54.18	24.78	2.68	44.22	0.04

2.3 Results

2.3.1 Island Wake Parameter and retention time values

I ranged between 0.6 to 31, implying a range of flow structures without lee eddies, to those with unstable eddies. Comparisons between I and the corresponding velocity and vorticity fields showed that I ~1 values were associated with persistent eddies behind the obstacle (Figure. 2.2a), and large I >1 values were consistently associated with strong vorticity gradients (Figure. 2.2b, 2.2c).

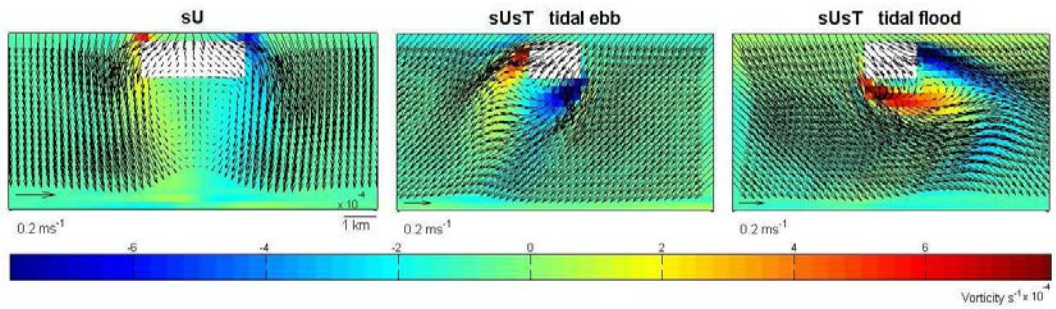

Figure 2.2 Top view snapshots of the velocity field (arrows) and vorticity or horizontal velocity shear (color-scale) for different flow regimes: a) strong unidirectional (*sU*), b) strong unidirectional strong tidal (*sUsT*) at ebbing time, and c) strong unidirectional strong tidal (*sUsT*) at flooding time. Each panel shows the retention area and reefs are shown in white.

Overall, mean retention times obtained from the simulations varied by approximately an order of magnitude: from 0.48-5.74 days. After 12hours, the majority of the particles (50-100%) are retained at all but one reef, regardless of the circulation regime. By 4 days, most particles had been flushed away from most of the reefs but with considerable variation (Table 2.1); for narrow rectangular reefs, <1% of particles remained in the retention area regardless of circulation regime; for kidney-shaped reefs, retention time was substantially greater, ranging up to 64% of particles remaining, and for triangular reefs, retention times varied widely, from <0.1% retained particles for narrow reefs under strong flows, to >50% for wide reefs in weak flows.

The scaling of the mean and variance of retention time, calculated over the whole simulation time period (10 – 15 days), was fairly similar across reef shapes and sizes, and among circulation regimes (Appendix 1, Figure A1), suggesting that differences in mean retention time provide a good description of overall differences in retention patterns among reefs and circulation regimes. Therefore, the analyses below focus on mean retention time as the response variable for identifying the effects of reef size, shape, and of circulation regime, on larval retention.

2.3.2 Relationship between retention time and Island Wake Parameter

The wake structure, characterized by I, on particle distribution was evident (Figure. 2.3). Strong statistical relationships were found between retention time and I in all the analysis reported below. All regressions were statistically significant, and explained >80% of the variation in the simulated mean retention times. For the analysis of different unidirectional flow speeds, regressions account for a large proportion of the variability shown in the data (84-92%). The likelihood ratio tests showed no significant support for the inclusion of parameter *c*. Although parameters *a* and *b* appear to increase slightly towards an asymptote across the examined flow speeds (Appendix 1, Table A1), the changes are small, so the likelihood ratio test supports the pooled model, in which a single set of regression parameters describes the relationship across all flow speeds ($G=27.9$, critical $\chi^2_{(18,0.05)}=28.86$, P=0.06 Figure 2.4, Table 2.2). The relationship between I and retention time remains excellent for circulation regimes with tidal flows (Appendix 1, Table A2). Parameter *c* is significantly different from zero when weak tidal flows are present (Appendix 1, Table A2). Again, however, a likelihood ratio test favors the pooled model, where a single set of model parameters applies across all tidal regimes ($G=5.11$, critical $\chi^2_{(7,0.05)}=14.07$, P=0.65) (Figure 2.5, Table 2.2). Differences between reef shapes modify the intensity of changes in retention times due to changes in I. Specifically, the steepness, or parameter *b*, is smallest for kidney reefs, and largest for triangular shaped

reefs (Appendix 1, Table A3). Again, however, a likelihood ratio test favours a single set of regression parameters across all shapes (*G=14.38*, critical $\chi^2_{(8,0.05)}=15.50$, *P*=0.07) (Figure. 2.6, Table 2.2).

Finally, a single regression between I and retention times, pooling all the circulation regimes and reef shapes, also provides an excellent fit, explaining 82% of the variation in retention time (Figure. 2.7 Table 2.2).

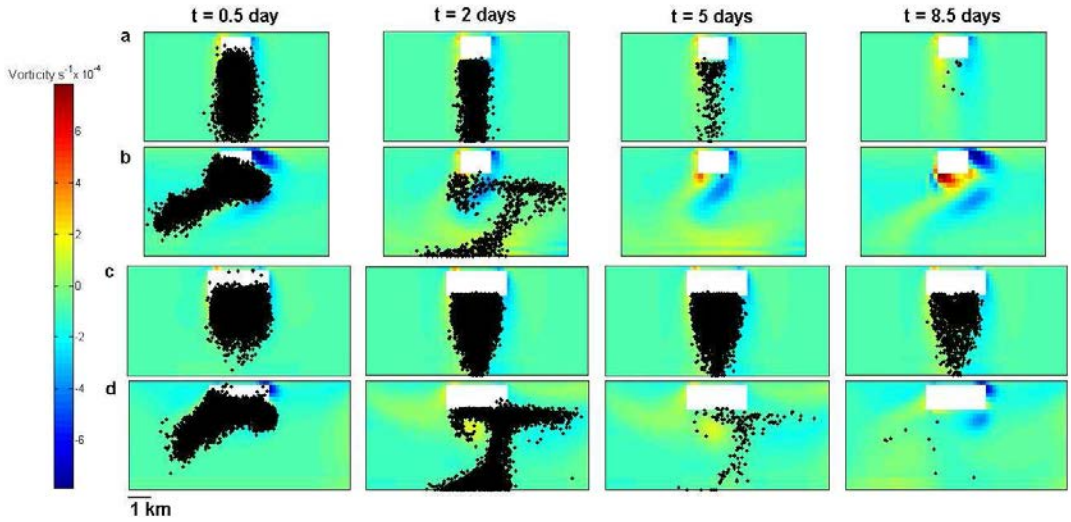

Figure 2.3 Top view snapshots of particle distribution (black dots) and vorticity field over times (*t* = 0.5, 2, 5, and 8.5 days) for: (a) reef A under strong unidirectional flow (*sU*), (b) reef A under strong unidirectional and weak tidal flow (*sUwT*), (c) reef B under strong unidirectional flow (*sU*), and (d) reef B under strong unidirectional weak tidal flow (*sUwT*). Each panel shows the retention area and reefs are shown in white.

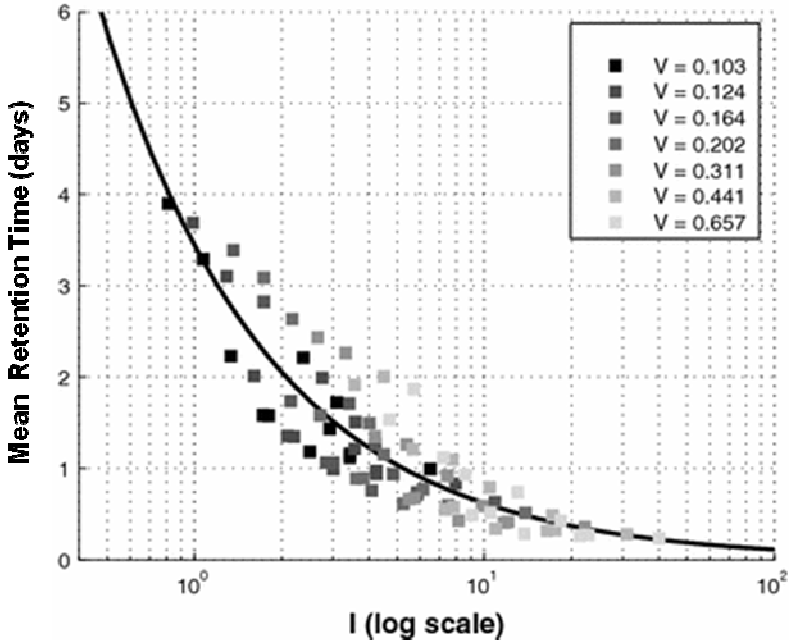

Figure 2.4 Relationship between the Island Wake Parameter (*I*) and mean retention time from the unidirectional flow simulations. Each square represents a particular reef size, and each shade of grey corresponds to a particular flow intensity. The line is the regression for the rectangular reefs with all unidirectional flows intensities pooled.

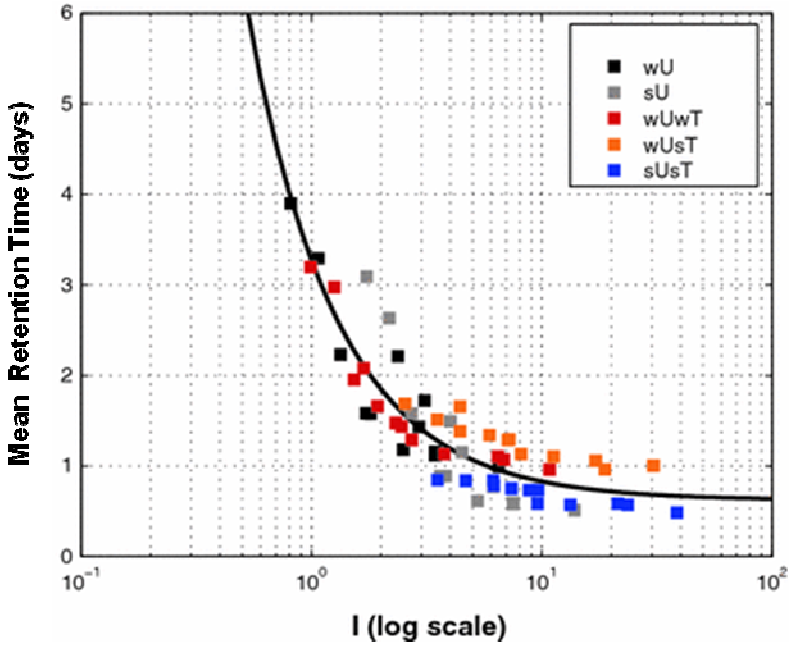

Figure 2.5 Relationship between the Island Wake Parameter (*I*) and mean retention time showing the effects of tidal regime. Each square represents a particular reef size, and each color corresponds to a particular flow regime. The line is the regression for the rectangular reefs pooled across circulation regimes: weak unidirectional (*wU*), strong unidirectional (*sU*), weak unidirectional and weak tidal (*wUwT*), weak unidirectional and strong tidal (*sUwT*), and strong unidirectional and strong tidal (*sUsT*).

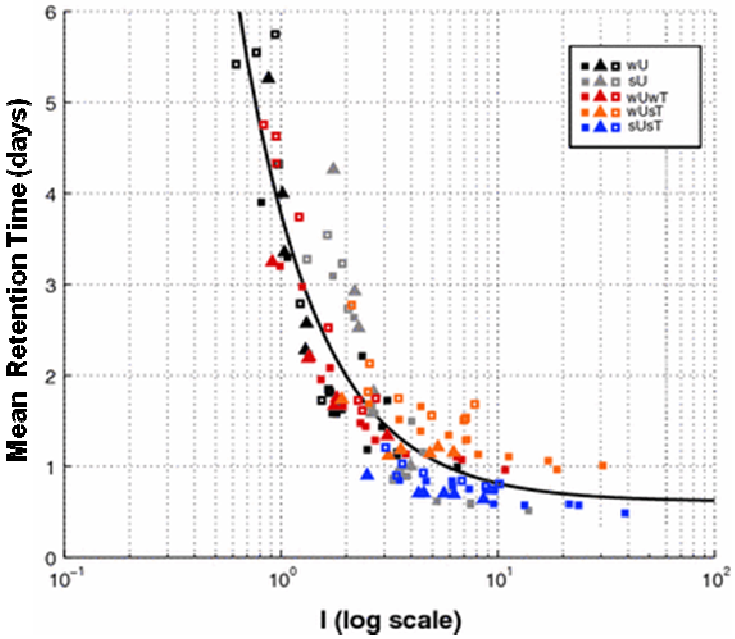

Figure 2.6 Relationship between the Island Wake Parameter (I) and mean retention time showing the effects of reef shape: Squares indicate kidney-shaped reefs, Filled squares indicate rectangular reefs, and Filled triangles indicate triangular reefs. Each color corresponds to a particular flow regime. The line is the regression pooled across reef shapes (rectangles triangles and kidneys) and across circulation regimes: weak unidirectional (*wU*), strong unidirectional (*sU*), weak unidirectional and weak tidal (*wUwT*), weak unidirectional and strong tidal (*sUwT*), and strong unidirectional and strong tidal (*sUsT*).

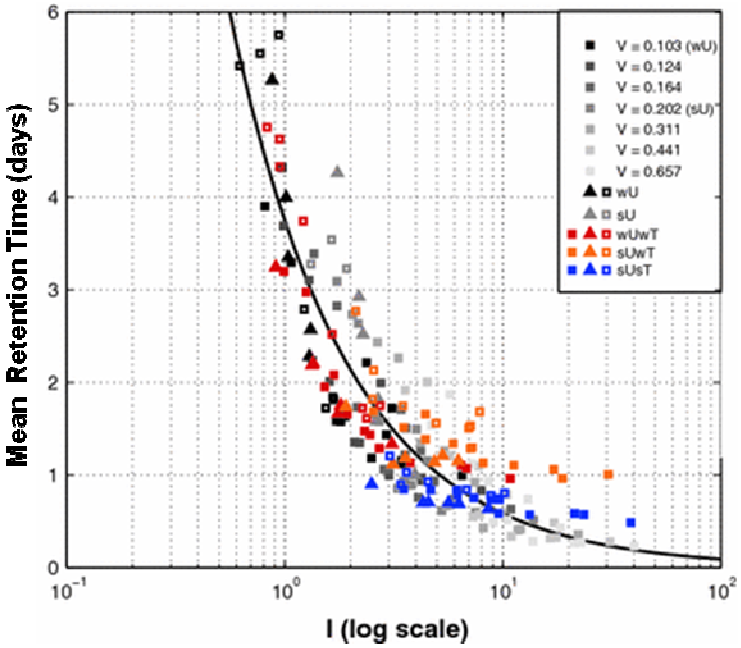

Figure 2.7 Relationship between the Island Wake Parameter (I) and mean retention time for all simulations combined. Each symbol represents and individual reef size and shape. Grey shading, colors and symbols are as indicated in figures 2.4-2.6. The line is the regression pooled across all reef shapes (rectangles triangles and kidneys) and all circulation regimes (i.e. all unidirectional flow intensities (V m s^{-1}) and weak unidirectional and weak tidal (*wUwT*), weak unidirectional and strong tidal (*sUwT*), and strong unidirectional and strong tidal (*sUsT*)).

Table 2.2. Regression parameters with 95% confidence bounds, coefficient of determination (R^2), F statistic, *p* values, and likelihood ratio (*G*) for the favored regression models between the Island Wake Parameter (I) and Retention time. *G*>3.841 indicates statistically significant support for a non-zero value of *c*. *F* statistics indicated that all reported regressions were highly statistically significant (*p*<<0.01 in all cases).

Circulation regime	**Reef shape**	**G**	**c (95% cb)**	**a (95% cb)**	**-b (95% cb)**	R^2	***F***	***P* value**
all unidirectional flow speeds pooled	**Rectangular**	0.0024	NA	3.44 (3.15 3.73)	0.74 (0.66 0.74)	0.81	1680	<0.001
wU/sU/wUwT/wUsT/sUsT pooled	**Rectangular**	11.57	0.62 (0.38 0.87)	2.64 (2.31 2.98)	1.11 (0.79 1.42)	0.82	128	<0.001
wU/sU/wUwT/wUsT/sUsT pooled	**All**	5.11	0.61 (0.35 0.86)	3.12 (2.83 3.50)	3.49 (1.20 0.96)	0.82	290	<0.001
all unidirectional flow speeds /wUwT/wUsT/sUsT pooled	**All**	1.61	NA	3.75 (3.57 3.92)	0.81 (0.75 0.88)	0.82	891	<0.001

2.4 Discussion

2.4.1 Island Wake Parameter, qualitative flow characteristics and retention time

This study confirms that the ratio of advection to bottom friction, as expressed by I, characterizes qualitatively the flow structure behind topographic mounts in shallow waters. The Island Wake Parameter values and associated flow fields obtained in this study are consistent with theoretical predictions. I values close to unity were found for wide reefs under weak and strong unidirectional flows and indeed, a pair of persistent eddies rotating clockwise and anticlockwise were formed behind the obstacle (Figure. 2.2a). These circulation regimes also exhibited long retention times. Thus, this study supports the hypothesis that lee eddies act as a mechanism for retaining larvae close to their natal reef (Sponaugle et al. 2002). However, larval retention is enhanced only when eddies remain attached to the obstacle. Larger I values were found in simulations with tidal flows. The simulated tidal currents promote the displacement of lee eddies to the east and west sides of the reef during tidal reversal (Figures 2.2b, 2.2c). These eddies were subsequently detached by jet currents, advected downstream and eventually dissipated. Retention times were shorter when tides were included (Figure 2.7). Hence, the presence of transient eddies might also accelerate larval flushing by increasing diffusion, or by entraining particles in the rim of the eddy, provoking faster advection than that caused by the mean flow (Sandulescu et al. 2006). Snapshots of particle distribution over time show how, under unidirectional flows, particles circulate around prevailing lee eddies and have longer retention times (Figures 2.3a, 2.3c) than particles trapped on eddies that, with the effect of tidal flows, detach from the reef and are advected downstream (Figures 2.3b, 2.3d).

The Island Wake Parameter is designed to capture the characteristics of unidirectional flow past obstacles in shallow waters. Variations in the flow that approaches the obstacle, such as the effect of perpendicular tidal flows, or variations in reef shapes (i.e., the presence of a

lagoon for the kidney shaped reefs), might well be expected to hinder the performance of the Island Wake Parameter. Therefore, we expected the relationship between retention times and I to vary amongst circulation regimes and reef shapes. A surprising finding of our study was that any such differences were sufficiently small that a single set of regression parameters explained most of the variation in retention times.

For a given unidirectional flow speed entering the model domain from the north, the presence of tides indirectly increases the speed of the southward flow within the model domain, in addition to directly producing oscillating east-west flows. Consequently, I is larger, compared to simulations with the same unidirectional flow magnitude (apparent in Figures 2.5 and 2.7 by the rightward shift of points with tidal flows). However, the presence of tides did not markedly affect the relationship between I and retention time, apparent in the strong evidence against separate regression parameters for the different tidal regimes provided by the likelihood ratio test (P>0.6), and the lack of a tendency for simulations with stronger tidal flows to lie consistently above or below simulations with weaker tides, for a given I (Figure 2.5).

Nevertheless, the differences between parameter estimates for different unidirectional flow intensities and reef shapes were only marginally non-significant (P=0.06 and 0.07, respectively), and there was some apparent structure to the residuals from the fits of the pooled models, both of which suggest that there may be small differences in how retention time responds to I that are consistent with our understanding of the physics of lee eddies.

Specifically, in the simulations with unidirectional flow, there is some evidence that stable eddies promote longer retention times when they occur in the presence of more intense flows. For instance, inspection of Figure 2.4 suggests that, when I is in the range of 1-6, high unidirectional flow speeds tend to cause longer retention times than low flow speeds (light gray squares tend to lie below dark gray squares in this region). This might be because, in

the presence of stable eddies, stronger flows produces stronger convergence at eddy rims, for a given I. Consistent with this interpretation, parameter *a* increases with flow speed, indicating higher predicted retention at I=1 when regressions are conducted separately for different flow speeds (Appendix 1 Table A1). However, because retention times are very similar across unidirectional flow speeds for large I, parameter *b* must also be higher for stronger flows, so that predicted retention for stronger flows converges with predicted retention for weaker flows at large I (Appendix 1 Table A1).

The principal apparent difference between reef shapes is that regression parameter *b* is larger for the triangular and smaller for the kidney shaped reefs (Appendix 1 Table A3). Signell and Geyer (1991) studied the effect of flow past different geometric obstacles. They note that sharper obstacles, such as triangular shaped reefs, are more likely to induce eddy formation. We might expect this to provoke lower retention for such reefs if eddies are detached and advected downstream. Conversely, the lagoons formed by kidney shaped reefs might be expected to promote retention. Careful inspection of Figure 2.6 provides some support for this, but only for intermediate I values. When I~1, all reef shapes form stable eddies, and there is little difference in retention time suggesting that these eddies, rather than particle entrapment at the lagoon, is the main mechanism for retention. When I>>1, eddy shedding occurs regardless of reef shape, and as again retention times are similar amongst shapes. In between, when tides are present, retention appears to be slightly lower for triangles (red, orange and blue triangles generally appear below other shapes of the same color in Figure 2.6), and higher for kidneys (red, orange and blue open squares generally appear above other shapes of the same color in Figure 2.6). The lower retention times for triangular reefs may occur because eddy shedding occurs more frequently at these reefs. Conversely, the higher retention times for kidney-shaped reefs may indicate that the retention in the reef lagoon becomes relatively more important as eddies become unstable, but before flows become strong enough to quickly transport larvae out of the lagoon.

2.4.2 Implications for self-recruitment

The present study shows that reef-scale circulation features lead to a wide range of retention times for an array of circulation regimes and reef morphologies reminiscent of the variety of shapes observed in nature. For self recruitment to occur, larvae must be retained at the natal reef until they acquire competence to settle. Many marine invertebrates are able to settle within a few days or even hours after spawning. Our study shows that substantial larval retention can occur over such time scales, for wide reefs of various shapes and circulation regimes. Indeed, the levels of larval retention modeled in this study may well substantially underestimate relative levels of self-recruitment relative to locally produced larvae which recruits elsewhere. For instance, coral larvae acquire settlement competence quickly and can retain it for extended periods of time (Connolly and Baird 2010). However, a larger proportion of retained larvae than flushed larvae would be likely to successfully recruit, because flushed larvae would have to be transported to another reef, and survive the journey. Even with strong unidirectional and tidal flows, retention can be high, particularly for reefs with semi-enclosed lagoons (Table 2.1). These findings indicate that reef-scale circulation features can facilitate self-recruitment for weak swimming larvae, or larvae that develop swimming capabilities at late developmental stages.

In addition, this study shows that the Island Wake Parameter is likely to be a useful tool for approximating larval retention, without the need to explicitly model local-scale three-dimensional circulation in the vicinity of reefs for a variety of reef shapes and prevailing circulation regimes. Specifically, a single regression between I and retention time (equation 2.3), explained 82% of the variation in retention time across all of our reef shapes and circulation regimes (Table 2.2). Moreover, separate regressions for different flow regimes suggested that the parameters characterizing the relationship between retention time and I change systematically across flow speed, indicating that it may be possible to comprehensively

calibrate small differences in this relationship under different flow magnitudes, and thus explain an even higher proportion of the variation in retention time.

Estimating the effects of reef-scale, three dimensional flows on larval retention in the vicinity of reefs is a significant problem for understanding, and predicting, larval dispersal patterns and the meta-population and evolutionary dynamics that they influence. This study identifies one approach to making such estimates in a simple, tractable way that does not require detailed, computationally intensive, and expensively calibrated reef-scale hydrodynamic models to be run for every location and time that is of interest.

Chapter 3. Modelling reef-scale circulation on the central Great Barrier Reef (GBR)

3.1 Introduction

The ocean's circulation determines several aspects of marine ecosystems. For instance, circulation patterns are main drivers of larval transport and allow for connectivity or the exchange of larvae between sub-populations of species that have a bipartite life cycle (i.e., planktonic larvae and a sedentary adult phase), (e.g., Cowen et al. 2009). Hydrodynamic models have the capability to provide predictions of oceanographic variables enabling ecological forecasts; for instance, they can be used to understand the role of circulation on larval transport through predictions of the state of the ocean (Rothstein et al. 2006). In this chapter I implemented and validated the 3D Sparse Hydrodynamic Ocean Code (SHOC) along the central Great Barrier Reef (GBR) using a reef-scale spatial resolution. I then use the validation model to examine larval transport in a realistic reef ecosystem (Chapter 4).

The Great Barrier Reef supports a wide diversity of life, and was selected as a world heritage site in 1981; it extends more than 2300 km along the eastern Australian Coast over a 60-200 km wide continental platform, and it is composed of roughly 3000 reefs (GBRMPA). The GBR was selected as a study area because of its ecological importance, its geophysical variation (that is, the presence of inshore, middle, and offshore reefs with a variety of shapes), and the data availability to implement a hydrodynamic model. Because the scope of this thesis centers on the effect of lee-reef eddies in larval retention, and as shown in Chapter 2, the formation and dynamics of eddies varies with reef width and depth, choosing a study region with the presence of reefs with different morphologies, and located across the continental platform, is crucial.

Coastal and ocean models use a wide range of data to define their forcing. BLUElink, an Australian government initiative developed an operational ocean predicting system that

couples outputs from the Ocean Forecast Australian Model (OFAM) with observational data to provide current vectors, temperature, salinity, and sea level of the ocean around Australia (Brassington et al. 2007). In addition, the Australian Bureau of Meteorology runs a numerical weather prediction system that generates atmospheric data. Therefore, high quality data, necessary to force a hydrodynamic model with the potential to produce reliable outputs, is available for the GBR.

In addition, due to the topographic complexity of the GBR, circulation features have a wide range of spatial scales, from 100km to 100m; however, connectivity in the region has only been studied at a spatial resolution on the order of kilometers, utilizing simplified 2 dimensional hydrodynamic models (e.g., Brinkman et al. 2001; James et al. 2002; Luick et al. 2007). Recently, Lambrechts et al. (2009) developed an unstructured grid model to explore circulation along the GBR, considering flow structure from small to regional scales. Yet, larval retention caused by eddies formed downstream of reefs of the central GBR remains unexplored. Hence, this Chapter provides the first 3D validated hydrodynamic model that considers flow features at the reef scale for the Central GBR, and allows investigating patterns of particle retention in the region with particular emphasis on the effect of lee-reef eddies on passive larval retention.

3.3.1 Background on the circulation and winds along the central Great Barrier Reef

On a regional scale (100-1000 km), the circulation over the Great Barrier Reef (GBR) is controlled by exchanges with the Coral Sea (e.g., Brinkman et al. 2001). The wind, atmosphere-ocean heat exchange, and tides, modify the mean regional flow locally over spatial scales of 10-100 km (Legrand et al. 2006). Finally, the interaction of currents with the complex bathymetry induces circulation features such as current jets or wake eddies at the reef scale ~100 m (Wolanski and Hamner 1988). All these components determine the circulation patterns of the region.

The regional mean flow along the GBR is driven by the Southern Equatorial Current SEC which is the northern branch of the South Pacific gyre, and which flows westward from the Coral Sea towards the Australian continental platform. The SEC divides into the North Vanuatu Jet NVJ and the North Caledonia Jet NCJ close to Fiji and Vanuatu (Gourdeau et al. 2008). When the NCJ reaches the Australian shelf it gives origin to the western boundary southward flowing Eastern Australian Current EAC (Choukroun et al. 2010) (Figure 3.1). The bifurcation point or location where the EAC originates varies seasonally. During the monsoon season (December to February) the inflow and bifurcation point moves north, to approximately 14 °S (Scully and Power 1973), but it can occur as south as 18 °S (Church et al. 1987).

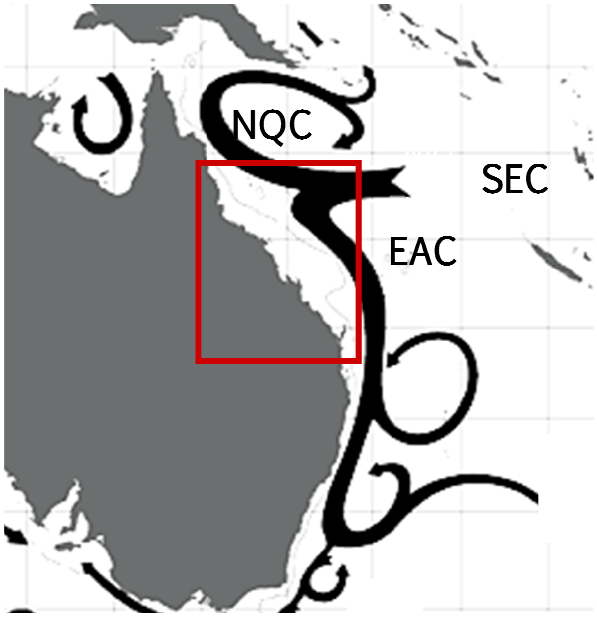

Figure 3.1 Schematic of major currents in the Southwest Pacific showing the South Equatorial Current (SEC) flowing eastwards, dividing into the North Vanuatu Jet (NVJ) and the North Caledonia Jet (NCJ), which in turn give rise to the north-westward flowing North Queensland Current (NQC), and the south-eastward flowing Eastern Australian Current (EAC) respectively when reaching the continental platform. (Modified from http://www.bom.gov.au/oceanography/forecasts/forecast-help.shtml, CSIRO). The red square illustrates the area over which the GBR extends.

The EAC is well defined in the outer shelf and influences the circulation on the continental platform. At roughly 17°S this long-shore current extends over the whole platform and has a subsurface maximum of 0.15 ms^{-1}. Between 18 and 22°S, the current attaches to the

coast, intensifies (Ridgway and Dunn 2003), and has typical magnitudes of 0.3ms^{-1} (e.g., Wolanski and Pickard 1985; Luick et al. 2007). Thus, currents over the shelf within the study area are oriented along-shore in a predominant south-eastward direction. However, near the bifurcation point, the surface currents vary in strength and direction (Choukroun et al. 2010) occasionally reversing in the most superficial layers, especially when south-easterly winds are strong (Andrews and Furnas 1986). Wyrtki (1962) described the existence of a northward flow from 11-19 °S from March to November and mostly southward from December to February. Similarly, during November, Church and Boland (1983) observed a northward current just off the GBR shelf at 18-19 °S reaching magnitudes of 0.8ms^{-1}, while in February the currents had a main southward direction. Hence, within the central GBR, current reversals can be induced due to either, variations of the latitude at which the NCJ approaches the continent, or the effect of strong south-easterly winds. Within the GBR lagoon, tides are semi-diurnal and the co-tidal lines are roughly parallel to the shelf break (Wolanksi and Pickard, 1985), thus, tidal currents are normally oriented across-shelf.

The movement of high pressure systems at mid-latitudes and low pressure systems over the tropics are main drivers of the intensity and direction of winds. Along the GBR, the distribution of pressure systems induces east to south-east trades (e.g., Creswell and Greig 1978) with typical magnitudes of 5-7 ms^{-1} (Pickard et al. 1977). During the Austral summer (December-February), however, winds from the northerly quadrant are also common, due to a low pressure system formed in the north-east of Australia which causes the monsoon or wind reversals (Pickard 1977). The initial monsoon onset occurs in late December but later onsets are often associated with El Nino conditions while earlier onsets can be triggered by La Nina (Suppiah 1992).

3.2 Methods

3.2.1 Model Description and Implementation

3.2.1.1 Hydrodynamic Model

The Sparse Ocean Hydrodynamic Code (SHOC) was implemented in the Central region of the Great Barrier Reef (CGBR) with a spatial resolution of 300 m, and validated against observations over the summer periods of 2005-2008. The model is described in the Methods section of Chapter 2. Briefly, SHOC was developed by the Environmental Modelling group at CSIRO and is fully described by Herzfeld and Waring. (2012). SHOC resolves the three dimensional primitive equations discretized on a finite difference stencil, applying the hydrostatic and Boussinesq approximations. The equations are written for a curvilinear orthogonal horizontal mesh and a set of chosen 'z' coordinates in the vertical. SHOC has been extensively used for case studies on the Australian shelf and coastal margins regarding, for instance, oceanographic processes and induced connectivity at estuaries (Herzfeld et al. 2010a), and fluxes of nutrients in oligotrophic marine channels (Wild-Allen et al. 2009). More recently it has been implemented along the GBR with a 4 km resolution to produce velocity fields used by CONNIE, an online tool developed by CSIRO, which allows rapidly estimating connectivity statistics between reefs (Condie et al. 2012).

3.2.1.2 Domain

The complex bathymetry of the Great Barrier Reef (GBR) requires high spatial resolution for accurate modelling (Luick *et al*. 2007). Similarly, it is desirable that all the dominant physical processes, including the Coral Sea inflow and its interaction with the continental shelf, are captured. Hence, two rectangular grids, hereafter referred to as intermediate and fine, were nested inside a larger curvilinear regional grid that covers the entire GBR. In this manner, a spatial resolution that solves the reef-scale circulation features was obtained for the central section of the GBR, and the meso-scale circulation of the region

was incorporated. The regional grid follows the continental platform, thus it is wider in the middle of the GBR and narrower in the northern and southern areas. This configuration allows incorporating the effect of oceanic currents, such as the intrusion of the North Caledonian Jet (NCJ), and gives a variable spatial resolution throughout the domain (3 – 6 km), with finer resolution inside the platform where the bathymetry is more complex. The Intermediate grid is located in the Northern – Central region of the GBR (17.4°S – 19.9°S latitude and 145.8°E – 148.4°E longitude) and extends from the shore to the continental shelf break; it is oriented parallel to the coastline and has a resolution of approximately 1.6 km. The fine grid encompasses middle and outer shelf reefs located within 18°S - 19°S latitude and 146.9°E 147.8°E longitude. It also has an orientation parallel to the coastline and a spatial resolution of approximately 300 m. (Figure 3.2). The regional grid has 39 vertical layers with a resolution that decreases with depth from 3 m at the surface to 150 m at 2500 m deep. The intermediate grid has 36 vertical layers with resolution of 1 m at the surface and 100 m at 1200 m deep. Finally, the fine grid has 36 vertical layers whose resolution decreases from 0.6 m at the surface to 100 m at 760 m deep. The bathymetry was provided by GeoScience Australia (Whiteway 2009), and it is spatially interpolated within SHOC to the respective grid resolution. The minimum water depth was set to 5m to minimize the wetting and drying of coastal cells with tidal changes and to depict the effect of the reef platform.

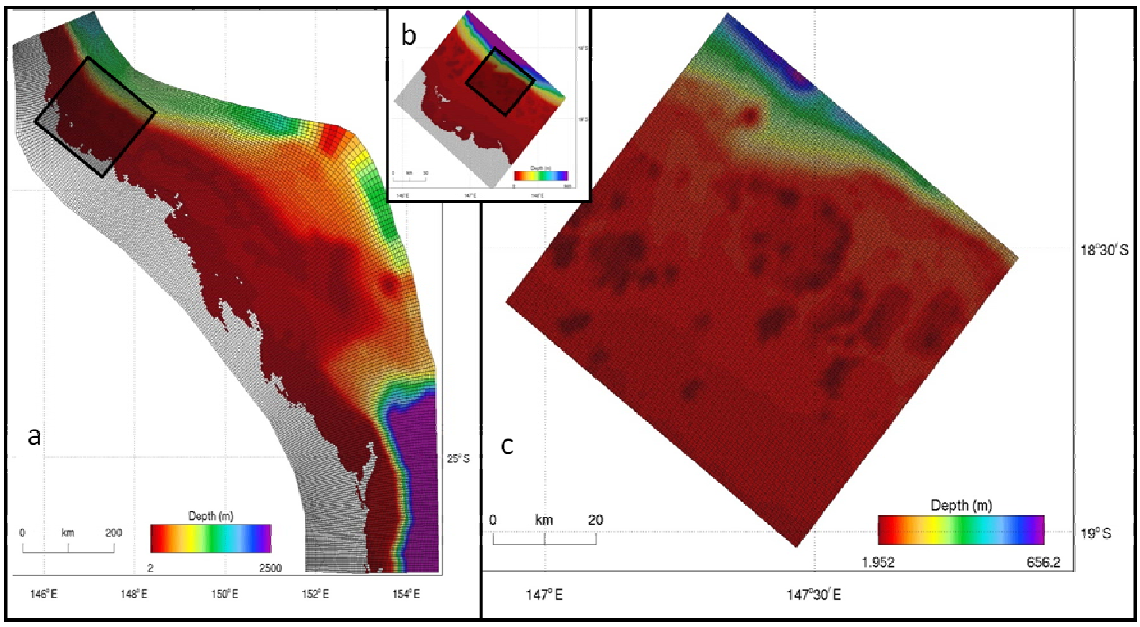

Figure 3.2 Nested grids: a) Regional, b) Intermediate, and c) Fine, and the region's bathymetry (colour scale). The black rectangles delimit the extent of the corresponding nested grid.

3.2.1.3 Forcing variables, atmospheric and oceanographic models

The model requires as inputs atmospheric variables (i.e., wind, atmospheric pressure, cloud cover) over the whole domain, and oceanographic variables, in particular: sea level, temperature and salinity, at the boundaries. These variables were obtained from meteorological and oceanographic models, respectively, and are described more extensively below.

SHOC was forced with atmospheric variables obtained with a meteorological meso-scale model (MesoLAPS). MesoLAPS is a higher resolution version of the Limited Area Prediction System (LAPS), a numerical weather prediction model with data assimilation described by Puri et al. (1997) and developed by the Bureau of Meteorology Research Centre (BMRC). The meso-scale model has a horizontal resolution of 12 km and 29 levels in the vertical with finer vertical resolution in the boundary layer, and an hourly time-step. The outcomes for the first layer, that is, 10 m above the ocean's surface (σ = 0.9988), were interpolated onto SHOC's time-step and spatial grid for forcing.

The model incorporates realistic oceanographic forcing, including tides and a large scale (10 km resolution) circulation taken from global model outputs with data assimilation (Bluelink Reanalysis, BRAN). BRAN was developed between CSIRO, the Bureau of Meteorology (BoM) and the Royal Australian Navy; it is a multi-year integration of the Ocean Forecasting Australian Model (OFAM) with data assimilation once every seven days (Brassinton et al. 2007). Observations assimilated include Sea Level Anomalies (SLA) from satellite altimetry, satellite derived sea surface temperature (SST) and *in situ* temperature and salinity profiles. Conceptually, BRAN is a three-dimensional time-varying synthesis of oceanic observations that uses OFAM as a dynamic interpolator (Oke et al. 2008). OFAM is a global general circulation model based on the Modular Ocean Model MOM (Griffies et al. 2004) that has a 1/10 horizontal resolution around Australia (90°E-180°E longitude, south of 17°N latitude) (Oke et al. 2008).

3.2.1.4 Schemes and Parameterization

3.2.1.4a Time step

The time step has to comply with the Curant-Friedrichs-Levy stability condition which prohibits a perturbation moving at a speed equal to the wave speed (*C*) plus the maximum advective speed expected (U_{max}) from crossing one grid cell in one time step (Herzfeld et al. 2010b). The wave speed was calculated from:

$$C = 2\sqrt{gH} + U_{max} \qquad \text{eq. 3.1}$$

where *g* is the acceleration (ms^{-2}) due to gravity, and *H* is the water depth (m) (Herzfeld et al. 2010b). The order of an appropriate time step (Δt) is then computed as:

$$\Delta t \leq \frac{1}{C}\left[\frac{1}{h_1^2} + \frac{1}{h_2^2}\right]^{-\frac{1}{2}} \qquad \text{eq. 3.2}$$

where h_1 and h_2 are the grid cell size (m) in each horizontal dimension (Herzfeld et al. 2010b). Following this constraint, the utilized time steps are 100, 72 and 35 seconds for the regional, intermediate and fine grids respectively.

3.2.1.4b Bottom friction

In SHOC, the bottom stress ($\overrightarrow{\tau_{bott}}$) is calculated as a quadratic drag law:

$$\overrightarrow{\tau_{bott}} = \rho C_d U \max(|U|, U_f) \quad \text{eq. 3.3}$$

where ρ is the water density, C_d is the drag coefficient, U is the bottom velocity, and U_f is a small background friction velocity (Herzfeld and Waring 2012). In here U_f = 0.0001 ms^{-1}, below this threshold value the friction law changes to:

$$\overrightarrow{\tau_{bott}} = \rho C_d U_f \quad \text{eq. 3.4}$$

(Herzfeld and Waring. 2012), C_d has lower limit, here C_d = 0.0025, and depends upon a bottom roughness length z_o, set to z_o = 0.016 m for the regional grid, and z_o = 0.0004 m for the intermediate and fine grids.

3.2.1.4c Horizontal mixing

The advection of momentum and tracers were solved using a second order and a Van Leer (1979) discretization scheme. Horizontal diffusion in hydrodynamic models is used to capture sub-grid turbulent processes. Hence, the diffusion coefficient varies with the grid cell size. Moreover, a specific range of horizontal diffusion is required to stabilize the numerical tracer and momentum advection. The advection scheme needs a minimum diffusion ($A_H\,min$), given by:

$$A_H \min = 0.5 U^2 \Delta t \quad \text{eq. 3.5}$$

where Δt is the time step and U is the current speed. (Herzfeld et al. 2010b). Simultaneously, a maximum value of diffusion ($A_H\,max$) is constrained by:

$$A_H \max \leq \frac{1}{4\Delta t}\left[\frac{1}{h^2{}_1}+\frac{1}{h^2{}_2}\right]^{-1} \qquad \text{eq. 3.6}$$

where Δt is the time step, h_1 and h_2 are the grid cell size (m) in each horizontal dimension (Herzfeld et al. 2010b). The *a priori* prescribed horizontal diffusion values required by SHOC, were chosen to be well under the maximum threshold to avoid smoothing of tracer's advection, above the minimum to allow numerical stability, and in agreement with the grid's cell size. The horizontal diffusion values were set to 120 ms^{-2} and 10 ms^{-2} for the intermediate and fine grids respectively. Even though the intermediate and fine grids are rectangular, there are slight differences in size between cells. Therefore, the horizontal diffusion was also scaled linearly to the individual cell size by:

$$\frac{\Delta x}{\Delta x_m} \qquad \text{eq. 3.7}$$

where Δx is the gird cell size and Δx_m is the mean grid cell size (Herzfeld and Waring 2012). Because the regional grid had a larger variation in cell sizes, the Smagorinsky (1963) formulation was implemented. This formulation parameterizes horizontal sub-grid scale processes by computing the horizontal diffusion coefficient at each grid cell based on the velocity shear encountered at that cell and does not require an *a priori* horizontal diffusion value (Herzfeld and Waring 2012).

3.2.1.4d Vertical mixing

Hydrodynamic models require a parameterization of the vertical diffusivities of momentum and mass. The Mellor Yamada scheme has been recognized to depict the dynamics of lee reef eddies appropriately (Blaise et al. 2007). In addition, Burchard et al. (1998) argued that both, the Mellor Yamada and the k-ε are good at representing the relationship between the vertical mean flow and turbulence explained by the Monin Obukhov similarity theory. Both schemes (Mellor Yamada and k-ε) include prognostic equations for turbulent kinetic energy,

and a length scale related parameter, which are used to calculate eddy viscosity and vertical diffusivities (Herzfeld et al. 2010b). Comparison between these two schemes has proved not to affect modelling outcomes (Burchard et al. 1998). Therefore, in order to parameterize vertical diffusion I used the Mellor Yamada scheme for the regional grid, and the k-ε for the intermediate and fine grids. The background viscosity and diffusivity coefficients were set to $5*10^{-5}$ ms^{-2} and $1*10^{-5}$ ms^{-2} for the regional and intermediate grids, and to $5*10^{-5}$ ms^{-2} and $1*10^{-2}$ ms^{-2} for the fine grid respectively. For the k-ε a minimum turbulent kinetic energy of $7.6*10^{-6}m^2s^{-2}$ was prescribed, and for the Mellor Yamada a surface length scale of 1m was implemented.

3.2.1.5 Forcing conditions at the boundaries

The regional (coarser) grid is forced at the boundaries with sea level elevation, temperature and salinity time series obtained from the BLUEllink Ocean Data Assimilation System (BODAS). These data corresponds to a low-frequency signal. The sea level elevation is also forced by imposing the effect of the tides from the global tidal model of Cartwright and Ray (1990). In addition the Raymond and Kuo (1984) radiation condition was imposed at all boundaries so that the transient response of the domain is transmitted through the boundary while allowing the boundary to respond to the prescribed forcing (Herzfeld and Waring 2012).

When nesting, the boundaries are forced with the tangential and normal current velocity components obtained from the simulation of the immediate larger resolution grid. However, due to resolution differences in bathymetry between grids, and consequently in the cross sectional area of the boundary, there is no guarantee that the flux through the open boundary is identical for the coarser and finer grids. This may cause an overfilling or emptying of the domain. To avoid this, the velocities are adjusted in order to generate a specific sea level at the boundary every certain time. We used this technique with a time-scale adjustment of 14

seconds for the intermediate grid, and of 6 seconds for the fine grid, and a relaxation input time step of 10 minutes.

3.2.1.6 Forcing conditions at the surface

The sea level elevation obtained from either BODAS or results of coarser resolution simulations are applied throughout the surface of the domain to force the model. Similarly, the wind, atmospheric pressure, air temperature (wet and dry bulb), and cloud cover obtained from MesoLAPS are also supplied. The wind stress is calculated using the Large and Pond (1981) parameterization (Herzfeld and Waring 2012). The heat flux scheme is a bulk formulation and long wave parameterization that also calculates the short wave radiation. It requires the air temperature, wind, and cloud cover (Herzfeld and Waring 2012). The sensible heat flux is considered proportional to the product of the wind speed and the difference between the model surface layer temperature and the air temperature (Herzfeled and Waring 2012). The latent heat flux requires a wet-bulb temperature to calculate specific humidity. The scheme used to calculate latent and sensible heat fluxes is from Kondo (1975). The short wave radiation is calculated from cloud cover data and it is distributed throughout the water column by specifying an attenuation coefficient and transmission. The net heat flux involves the long and short wave radiation and the sensible and latent heat.

3.2.2 Model validation

3.2.2.1 Sea level

Sea level time series from tidal gauges at nine stations along the Great Barrier Reef, collected and provided by the Australian Bureau of Meteorology (BoM), (Table 3.1, Figure 3.3), were compared with those obtained with the model. Both modelled and observed sea level time series were filtered to separate the high frequency, or tidal signal, from the low frequency signal using a Lanczos filter (Duchon 1917) with a cut of frequency of 2 days. The

modelled and observed time series were compared calculating determination coefficients from linear regressions with slope one and intercept zero.

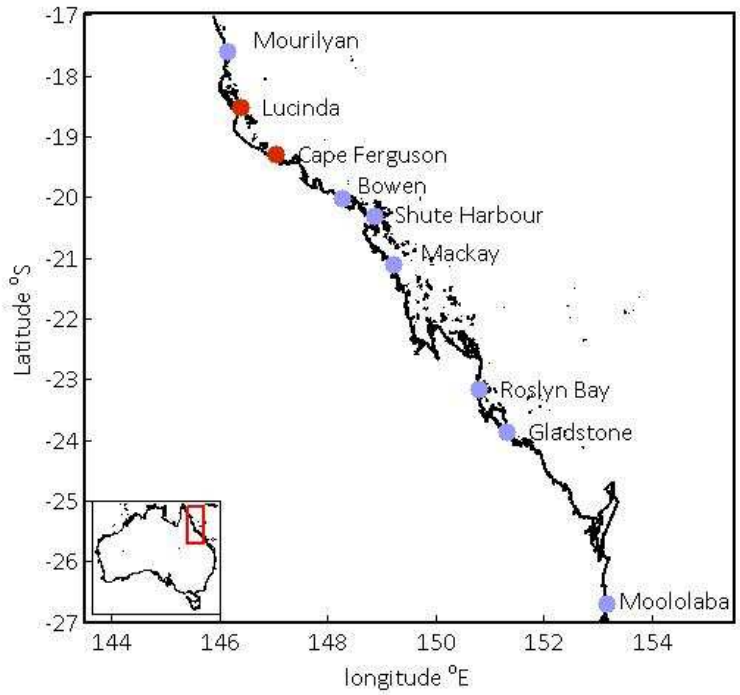

Figure 3.3 Location of the sea level stations along the eastern Australian coast as indicated by the red rectangle in the lower left. Red dots indicate stations that lay within the fine grid, and blue dots indicate stations that lay outside the fine grid.

Table 3.1 Location of tidal gauge stations, time period of the observations, coefficient of determination (R^2), *p* values and degrees of freedom (*df*) for regressions with slope one and intercept zero between the modelled and observed high and low frequency sea level time series. Significant R^2 values are bold.

Station	Location		Time period (month.year)	High frequency		Low frequency	
	Latitude °S	Longitude °E		R^2	*P* value/*df*	R^2	*P* value/*df*
Gladstone	23.8538	151.3136	Dec.05-Feb.06	**0.980**	<0.01/2.5	0.135	0.07/15.5
Lucinda	18.5216	146.3853	Dec.05-Feb.06	**0.987**	<0.01/4.4	**0.677**	0.03/3.5
Mackay	21.1066	149.2258	Dec.05-Feb.06	**0.971**	<0.01/2.7	**0.590**	0.01/5.9
Bowen	20.0245	148.2506	Dec.05-Feb.06	**0.931**	<0.01/4.0	**0.594**	0.03/4.1
Rosslyn Bay	23.1666	150.7916	Dec.05-Feb.06	**0.861**	<0.01/2.9	**0.431**	0.01/9.5
Cape Ferguson	19.2800	147.0500	Dec.05-Feb.06	**0.734**	<0.01/5.8	**0.670**	0.03/3.8
Moololaba	26.6979	153.1505	Dec.05-Feb.06	**0.956**	<0.01/2.9	0.133	0.07/16.1
Mourilyan	17.5971	146.1478	Dec.05-Feb.06	**0.989**	<0.01/4.7	**0.607**	0.03/4.1
Shute Harbour	20.3020	148.8546	Dec.05-Feb.06	**0.938**	<0.01/3.3	**0.533**	0.02/5.4

3.2.2.2 Temperature

Sea Surface Temperature satellite images provide a synthesis of the ocean temperature variation over regional scales (i.e., across the whole GBR). Therefore, as a first diagnosis of model performance, the spatial variation of sea surface temperature (SST) obtained from simulations with the regional grid for 5 days over the summer period of 2006 was visually compared with that observed with a 5 day composite SST satellite image (31/January/2006 – 4/February/2006). The comparison between the SST produced by the model and the satellite image allowed testing qualitatively if the horizontal diffusion is well parameterized in the model.

In addition, observations from temperature loggers were obtained from the Australian Institute of Marine Science (AIMS). Their temperature monitoring program provides time series obtained with temperature loggers deployed at the reef flat (RF), reef upper slope (SL) and/or reef deep slope (DS). I retrieved data for the simulated time period at locations inside the model domain. A total of 27 time series from 17 different locations were used to verify the model outcomes. The observations were compared with time series obtained with the model by interpolating the gird outcomes of the closest depth to the corresponding latitude and longitude. Table 3.2 summarizes details of the *in situ* measurements and model outcomes, and Figure 3.4 shows their location. The modeled and observed temperature temporal mean and standard deviation were computed for each location. Correlation coefficients for the original time series, and the low frequency time series, obtained with a Lanczos filter using a 2 day cut-off frequency, were computed and tested for significance taking into account the number of independent data for each pair of time series following Emery and Thomson (2001). Spectral analysis was also performed for both the modelled and observed original temperature time series to compare the most energetic periodicities.

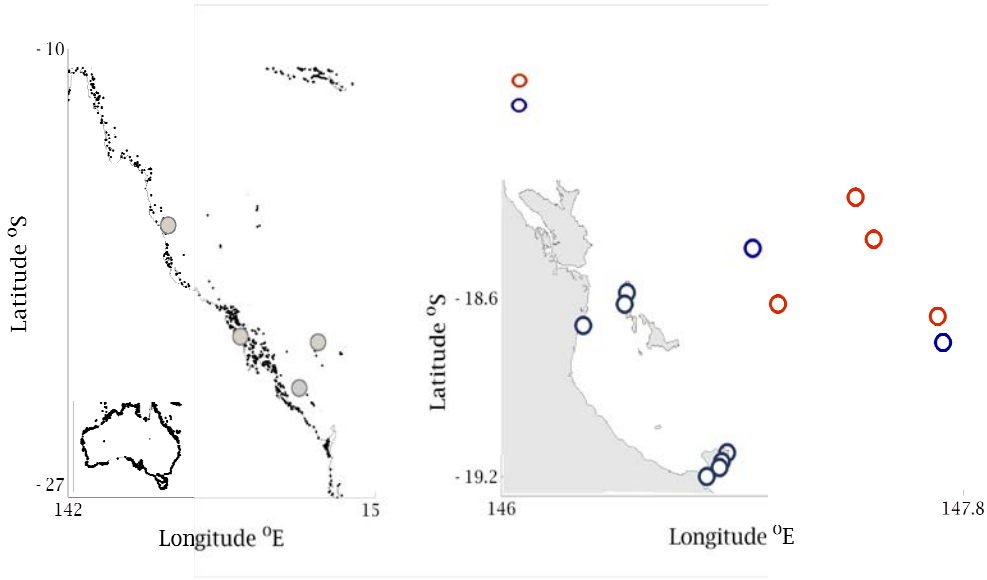

Figure 3.4 Location of the temperature loggers. a) zoom of the rectangle indicated in the map of Australia showing the location of stations that lay within the regional grid (grey dots); b) zoom of the rectangle along the eastern Australian coast showing the stations that lay within the intermediate grid (blue dots) and within the fine grid (red dots).

Table 3.2 Information of the water temperature stations/loggers. Class refers to the reef location/depth at which the temperature loggers were deployed: FL is reef flat below lowest astronomical tide level, SL is reef upper slope (~ 5-9m), and DS is reef deep slope (~20 m). REG, INT and FIN refer to the regional, intermediate and fine girds respectively.

Name	Location (observation)				Location (model)		Time period (both series)
	Latitude °S	Longitude °E	class	Depth (m)	Depth (m)	Grid	
Moore Reef	16.89	146.19	FL	2	1	REG	01/Dec/05-11/Jan/06
Hay Point	21.25	149.31	SL	5	7.7	REG	19/Dec/05-05/Feb/06
East Cay	21.47	152.57	SL	9.97	7.7	REG	22/Dec/05-28/Feb/06
Tryon Island	23.25	151.78	SL	11	7.7	REG	01/Dec/05-28/Feb/06
Kelso Reef	18.43	146.98	FL	0.1	1	INT	01/Dec/05-01/Mar/06
Kelso Reef	18.42	146.98	SL	5.2	7.7	INT	01/Dec/05-01/Mar/06
Kelso Reef	18.46	146.97	DS	19	20	INT	01/Dec/05-01/Mar/06
Lucinda	18.69	146.32	FL	0	1	INT	12/Dec/05-01/Mar/06
Lucinda	18.51	146.37	SL	5	7.7	INT	01/Dec/05-01/Mar/06
Cattle Bay	18.58	146.49	FL	3.52	1	INT	01/Dec/05-01/Mar/06
Cattle Bay	18.57	146.47	SL	6.53	7.7	INT	01/Dec/05-01/Mar/06
Pioneer Bay	18.62	146.48	SL	7.65	7.7	INT	01/Dec/05-01/Mar/06
Davis Reef	18.75	147.72	FL	4	1	INT	01/Dec/05-01/Mar/06
Davis Reef	18.75	147.72	SL	9	7.7	INT	01/Dec/05-01/Mar/06
Florence Bay	19.12	146.88	SL	9	7.7	INT	16/Jan/05-01/Mar/06
Geoffrey Bay	19.15	146.86	FL	2.13	1	INT	01/Dec/05-22/Dec/06
Geoffrey Bay	19.15	146.86	SL	4	7.7	INT	01/Dec/05-22/Dec/06
Nelly Bay	19.17	146.85	FL	2.37	1	INT	01/Dec/05-22/Dec/06
Nelly Bay	19.17	146.85	SL	5.09	7.7	INT	01/Dec/05-22/Dec/06
Middle Reef	19.20	146.80	SL	6.89	7.7	INT	01/Dec/05-16/Jan/06

Continuation Table 3.2

Name	Location (observation)				Location (model)		Time period (both series)
	Latitude °S	Longitude °E	class	Depth (m)	Depth (m)	Grid	
Myrmidon Reef	18.26	147.38	FL	2.5	1	FINE	02/Oct/05-15/Dec/06
Myrmidon Reef	18.26	147.38	SL	9	7.7	FINE	02/Oct/05-15/Dec/06
Myrmidon Reef	18.26	147.38	DS	20	20	FINE	02/Oct/05-15/Dec/06
Diploria Reef	18.40	147.45	SL	9	7.7	FINE	02/Oct/05-28/Nov/05
John Brewer Reef	18.62	147.08	SL	8	7.7	FINE	02/Oct/05-28/Nov/05
Chicken Reef	18.66	147.71	FL	1	1	FINE	02/Oct/05-15/Dec/06
Chicken Reef	18.65	147.71	SL	9	7.7	FINE	02/Oct/05-15/Dec/06

3.2.2.3 Currents and wind

Current data used for model verification were obtained by AIMS monitoring programs using bottom-mounted Acoustic Doppler Current Profilers (ADCP's), near Chicken, Pith and Myrmidon reefs (Table 3.3, Figure 3.5). The north-south *v*, east-west *u*, and vertical *w* velocity components were measured by the ADCP at different depths over time. The velocity time series were filtered to separate the high from the low frequency signals using a Lanczos filter with a cut off frequency of 2 days. To test the model performance, correlation coefficients between the model and observed time series were first computed at each depth and tested for significance considering the effective degrees of freedom for each pair of time series following the method described by Emery and Thomson (2001). Secondly, a principal component analysis of the low and high frequency time series was performed to obtain the main flow orientation and the range of magnitudes of the flow along the principal axis for both the modelled and observed velocity time series.

Monthly wind variability ellipses (that is, the axis that accounts for most of the temporal variance, and the orthogonal axis), were calculated over the fine grid domain following Emery and Thomson's method (2001) to elucidate the intensity and variability of the wind field used to force the model.

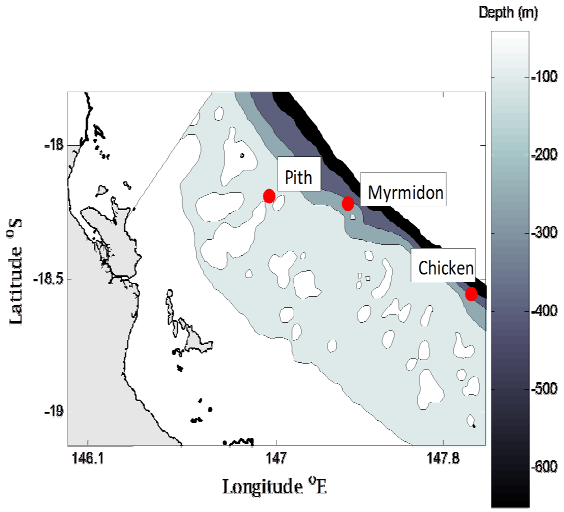

Figure 3.5 Location of the ADCPs, the colour-scale shows the depth.

Table 3.3 ADCP location and time period that overlaps with modelled currents.

Reef	Latitude	Longitude	Depth (m)	Time period
Chicken	18.2196	147.3437	190	Oct-Mar 2005-2006
Pith	18.1902	146.9665	5 meters from bottom	Dec-Mar 2005-2006
Chicken	18.5565	147.9333	190	Dec-Mar 2006-2007
Myrmidon	18.2196	147.3437	190	Dec-Mar 2007-2008

3.2.2.4 Lee-reef eddies, upwelling and downwelling

The interaction of currents with reefs can cause the formation of eddies downstream. In addition, upwelling and downwelling occurs as a consequence of the flow approaching and going around reefs (White and Wolanski 2008), or due to the formation of eddies (Bakun 2006). Upstream of reefs, water converges and provokes downwelling; in addition, at the tip of reefs the flow veers and accelerates inducing water from the bottom to replace the rapidly moving surface waters (White and Wolanski 2008). Similarly, water converges/diverges in the centre of cyclonic/anticyclonic eddies (southern hemisphere) inducing downwelling/upwelling in the centre and upwelling/downwelling at the edges of the eddy (Bakun 2006). In order to verify the formation of eddies and the occurrence of upwelling and downwelling events, inspection of the depth-averaged horizontal velocity field and vertical flow magnitude downstream of reefs was conducted. Similarly, profiles of vertical flow across the centre of reef eddies, and across sections downstream of the tip of the reef were plotted to examine if upwelling was indeed caused by either the presence of eddies or the acceleration of flow around the reef tip.

3.3 Results

3.3.1 Sea Level

The determination coefficients are significant at 9 out of 9, and 7 out of 9 stations for the high and low frequency sea level signals, respectively (Table 3.1). The southernmost stations (Gladstone and Moololaba) are the only ones associated with non-significant determination coefficients of the low frequency signal.

3.3.2 Temperature

The SST satellite image shows a spatial temperature variation between ~24°C in the south and ~31°C in the north; this same distribution is observed in the model outputs (Figure 3.6). In both, the satellite image and model outputs, ramifications of colder or hotter surface waters are visible, for instance, a ramification of colder water extends towards the north close to shore while hot water extends towards the south closer to the outer shelf.

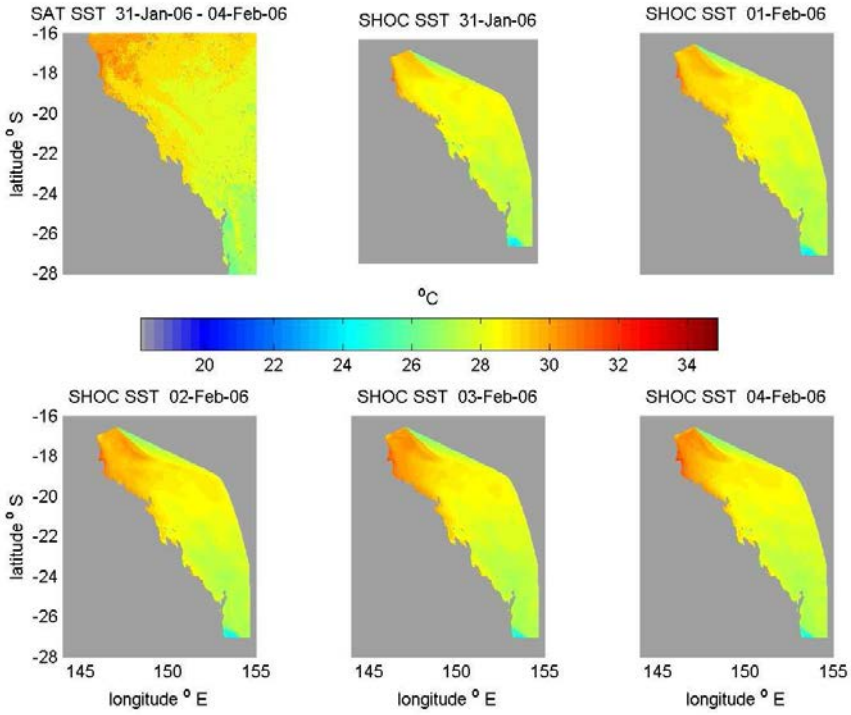

Figure 3.6 Composite satellite SST image over 5 days (31/Jan/06-04/Feb/06) (top left panel), and modelled SST for each of the 5 days. The colour scale represents the temperature (°C) and the grey represents land or part of the ocean that is not covered by the grid.

In addition, water temperature in both observed and modeled time series, varies across stations, with a tendency to increase towards the north and inshore. Mean temperatures calculated over the summer (Dec/05-Mar/06) show lower values at stations which correspond to offshore reefs (i.e., Davis Chicken and Myrmidon), or southern stations (i.e., East Cay and Tryon Island) (Table 3.4). Larger temperature variability is associated with stations close to shore such as Lucinda or those located around Magnetic Island in the reef flat (Geoffrey and Nelly Bay) (Table 3.4).

Table 3.4 Temporal mean and standard deviation (std) in degrees Celsius for all stations (observed and modelled). Correlation coefficients and corrected degrees of freedom between the observations and model outcomes for the original and low frequency temperature time series. Significant correlation coefficients are bold and stations referred in the text are in blue (lowest mean temperatures), green (larger variability).

Name	Class	Observation		Modelled		Pearson's correlation		Degrees of Freedom	
		Mean	Std	Mean	Std	original	low frequency	Original	low frequency
Moore Reef	FL	28.37	0.37	28.34	0.43	**0.63**	**0.84**	14	8
Hay Point	SL	30.15	0.63	30.15	0.51	**0.73**	**0.70**	8	7
East Cay	SL		0.26	29.14	0.30	**0.57**	**0.69**	16	9
Tryon Island	SL		0.59	28.59	0.51	**0.79**	**0.85**	9	7
Kelso Reef	FL	30.34	0.59	28.53	0.31	0.27	0.18	49	39
Kelso Reef	SL	30.22	0.54	28.18	0.38	0.27	0.32	19	14
Kelso Reef	DS	29.86	0.80	30.33	0.66	0.50	0.58	7	5
Lucinda	FL	29.86	0.93	29.85	0.73	**0.44**	0.45	23	14
Lucinda	SL	30.63	1.2	29.53	0.48	0.62	0.64	5	5
Cattle Bay	FL	29.63	0.76	29.55	0.45	**0.65**	0.66	12	6
Cattle Bay	SL	29.60	0.68	29.63	0.49	0.68	**0.77**	5	5
Pioneer Bay	SL	29.38	0.67	28.65	0.51	**0.91**	**0.95**	5	4
Davis Reef	FL		0.41	28.52	0.31	**0.67**	**0.69**	23	15
Davis Reef	SL		0.40	29.67	0.36	**0.65**	**0.69**	10	8
	SL	30.29	0.69	31.65	0.76	0.49	0.48	12	11
Geoffrey Bay	FL	31.29	0.85	31.52	0.70	**0.81**	**0.91**	4	3
	SL	30.93	0.68	31.84	0.72	**0.86**	**0.91**	4	3
Nelly Bay	FL	31.22	0.99	31.79	0.72	**0.77**	0.86	5	3
	SL	31.23	0.80	30.15	0.72	**0.91**	**0.92**	3	3
Middle Reef	SL	30.05	0.65	28.53	0.79	0.39	0.28	18	16

Continuation Table 3.4

Name	Class	Observation		Modelled		Pearson's correlation		Degrees of Freedom	
		Mean	Std	Mean	Std	original	low frequency	Original	low frequency
Myrmidon Reef	FL		0.42	28.94	0.36	**0.95**	**0.97**	3	3
Myrmidon Reef	SL		0.38	28.78	0.29	**0.95**	**0.98**	3	3
Myrmidon Reef	DS		0.45	28.00	0.37	**0.92**	**0.93**	3	3
Diploria Reef	SL		0.28	28.28	0.29	**0.95**	**0.98**	3	3
John Brewer Reef	SL		0.43	28.35	0.31	**0.95**	**0.98**	3	3
Chicken Reef	FL		0.50	27.95	0.49	**0.91**	**0.96**	3	3
Chicken Reef	SL		0.44	27.87	0.55	**0.92**	**0.95**	3	3

The temporal variation in temperature found with the model also agrees with those shown by the observations; significant correlation coefficients were found for 74% and 67% of the stations for the original and low frequency signals respectively. More importantly, all the outcomes for stations that lay inside the fine resolution grid are significantly correlated with the observations (Table 3.4). The temperature at any station varies a maximum of ~1.5°C over the summer period (December-March). However, a constant increment from ~25 to ~28 °C can be observed at stations in the Central GBR from October to December; this rise in temperature is hind-casted properly by the model (Figure 3.7).

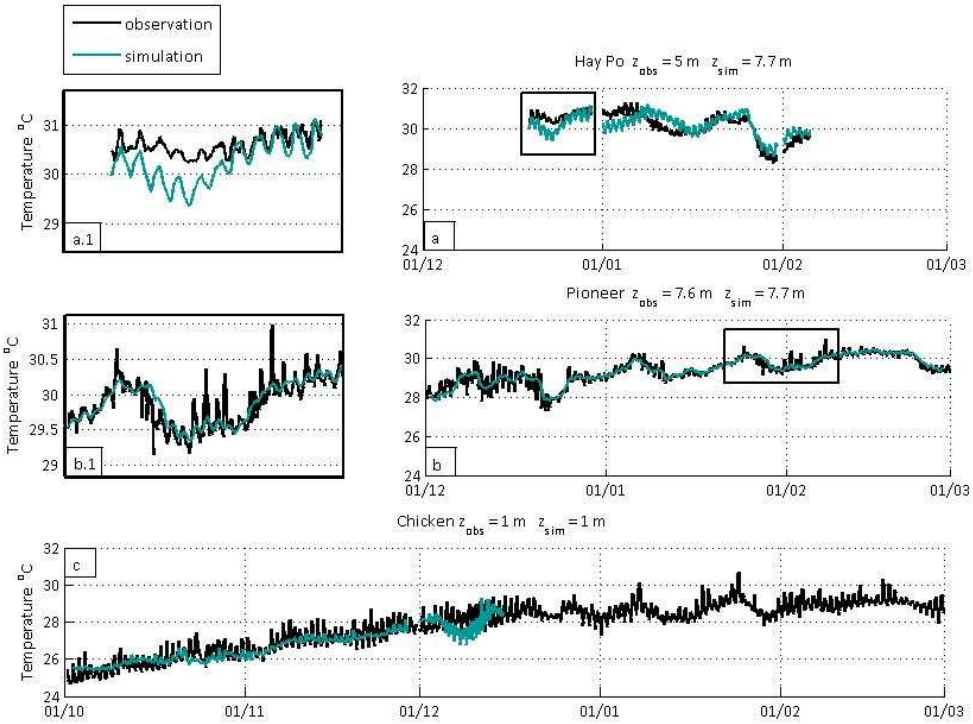

Figure 3.7 Observed (black line) and modelled (blue line) temperature time series for a) station in the regional grid, b) station in the intermediate grid, and c) station in the fine grid. Upper left hand side panels (a.1 and b.1) show a zoom from the rectangles indicated on panels a, and b respectively. The time series correspond to years 2005-2006. The name of the station and the depth of the observation and modelled time series are indicated.

An apparent difference between the modelled and observed time series is the magnitude of the fluctuations. The observed series have larger fluctuations (see standard deviation values on Table 3.4), and are more energetic (Figure 3.8). Poor correlations for both the original and low frequency signals were found for stations that were located at the grid

boundary (Kelso), close to shore (Lucinda and Florence Bay) or between Magnetic Island and the continental shoreline (Middle Reef).

The simulated time period corresponds to the end of autumn and all austral summer; hence, the seasonal variability is not present in the data. However, a spectral analysis revealed that the most energetic signals have similar frequencies for both the observed and the modelled temperature time series; most of the variability is semidiurnal, and a second less evident peak lies between the 10-20 day periodicity (Figure 3.8).

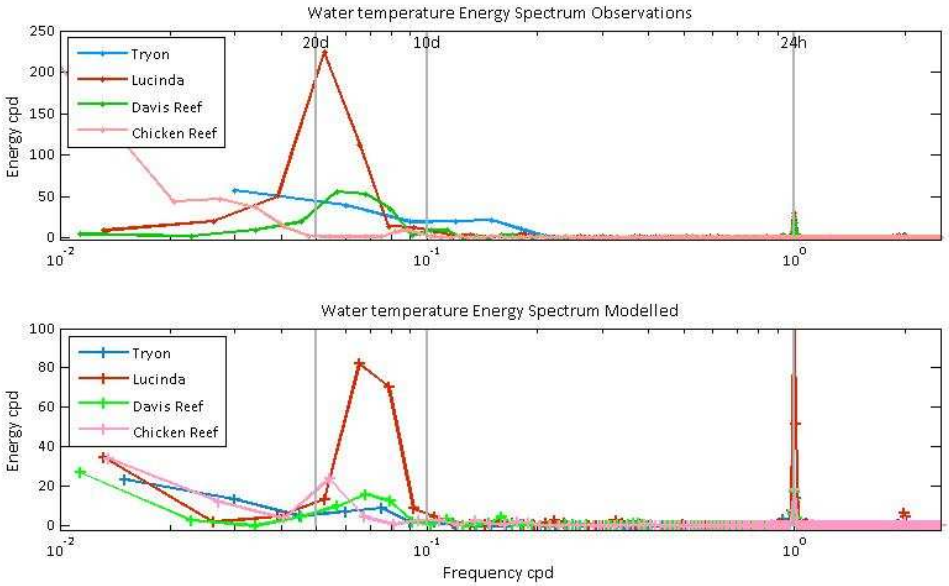

Figure 3.8 Water temperature energy spectrums for 4 stations, the upper panel corresponds to observed time series and lower panel corresponds to modelled time series.

3.3.3 Currents and wind

Larger correlation coefficients were generally obtained for the high frequency signals. However, the vast majority (i.e. 94%) of the correlation coefficients is significant ($p<0.05$, Table 3.5). The principal component analysis indicates that the low frequency currents for both observations and model are oriented roughly along-shore between 288-322° from the East. In addition, the high frequency currents from both observations and model are oriented roughly across shore, between 50.2-64.7° degrees from the East (Table 3.6, Figure 3.5). The range of magnitudes of the low and high frequency currents oriented along the principal axis for both

the observed and modelled currents show that the currents reverse (i.e. the current magnitudes vary from negative to positive, Table 3.6). The range of current magnitudes of the observation and the model differ but they have the same order of magnitude. Moreover, the model and observed currents are in phase, showing flow reversals at the same time (Figures 3.9-3.10). For example, figure 3.9 shows that three out of the four times that the observed south-east flow intensifies (indicated by open head arrows), the flow obtained with the model also strengthens. Similarly, events of flow reversal (indicated by close head arrows) are also simultaneous in the observations and the model outcome. The only discrepancy in the temporal fluctuation of the current orientation between the model and the observations occurs at Pith reef from February-March 2006. During this period, the observed current flows mainly towards the south-east, while the model reproduced north-west flows.

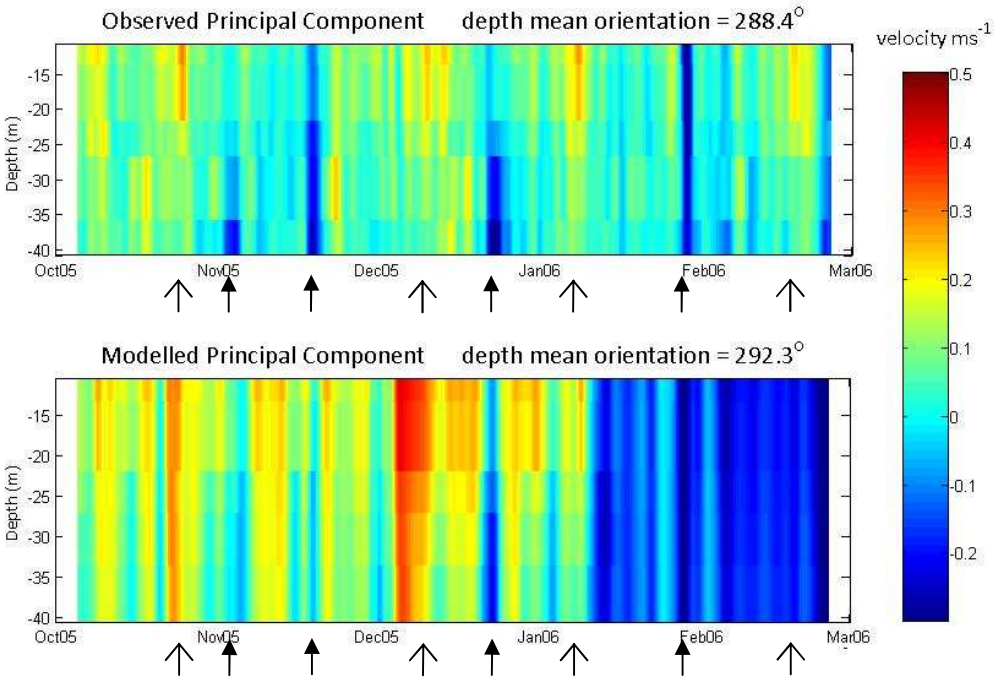

Figure 3.9 Observed (upper panel) and modelled (lower panel) low frequency currents rotated along the principal axis from Pith reef (Dec2005-Mar2006). The depth-averaged orientation is given in degrees relative to the East, the colour-scale shows the magnitude of the flow, where blue indicates south-east and red indicates north-west. The arrows indicate events when the observed flow intensifies: towards the north-west, and towards the south-east. The same arrows are shown for the modelled flow to facilitate their comparison.

Table 3.5 Correlation coefficients and effective degrees of freedom between the observations and model outcomes for the low and high frequency signal of *u* and *v* time series at 3 different reefs over summer periods of 2005-2008. Significant correlation coefficients are in bold.

Depth (m)		Low frequency				High frequency			
		U		*V*		*U*		*V*	
Observation	Model	Correlation coefficient	Degrees of freedom	Correlation coefficient	Degrees of freedom	Correlation coefficient	Degrees of freedom	Correlation coefficient	Degrees of freedom
Chicken Oct/2005-Mar/2006									
30.5	27	**0.38**	27			**0.43**	83	**0.32**	46
35.5	33	**0.35**	33			**0.37**	145	**0.30**	61
40.5	40	**0.34**	34			**0.37**	130	**0.29**	53
60.5	58	**0.37**	35			**0.37**	90	**0.30**	63
80.5	81	**0.31**	43	**0.32**	42	**0.34**	60	**0.29**	126
Pith Dec/2005-Mar/2006									
10.77	10.6	**0.40**	43	**0.32**	36	**0.72**	12	**0.68**	12
13.77	13.5	**0.35**	49	**0.34**	35	**0.74**	12	**0.70**	11
21.77	22	**0.32**	53	**0.36**	42	**0.78**	11	**0.70**	11
26.77	27	**0.38**	50	**0.40**	53	**0.79**	11	**0.71**	10
35.77	33.5	**0.36**	32	**0.41**	68	**0.74**	13	**0.71**	11
40.77	40.5			**0.42**	70	**0.61**	20	**0.63**	12
Chicken Dec/2006-Mar/2007									
33.5	32	**0.56**	12	**0.67**	14	**0.55**	19	**0.69**	32
40.5	40	**0.66**	9	**0.72**	13	**0.64**	14	**0.64**	25
58	56	**0.70**	10	**0.72**	14	**0.64**	14	**0.66**	29
81	80	**0.57**	17	**0.55**	21	**0.61**	17	**0.64**	57
110	108	**0.34**	35	**0.32**	28	**0.53**	28	**0.49**	81
Myrmidon Dec/2007-Mar/2008									
32	32	**0.41**	15	**0.26**	40	**0.20**	189	**0.26**	107
44	44	**0.38**	22	**0.29**	45	**0.27**	113	**0.29**	85
56	56	**0.34**	33	**0.39**	51	**0.25**	90	**0.29**	82
68	68	**0.34**	35	**0.45**	54	**0.26**	136	**0.27**	95
76	76	**0.30**	36	**0.46**	60	**0.23**	161	**0.27**	107
88	88	**0.33**	36	**0.42**	83	**0.17**	297	**0.26**	183
100	100	**0.36**	28	**0.34**	109	**0.18**	284	**0.27**	510

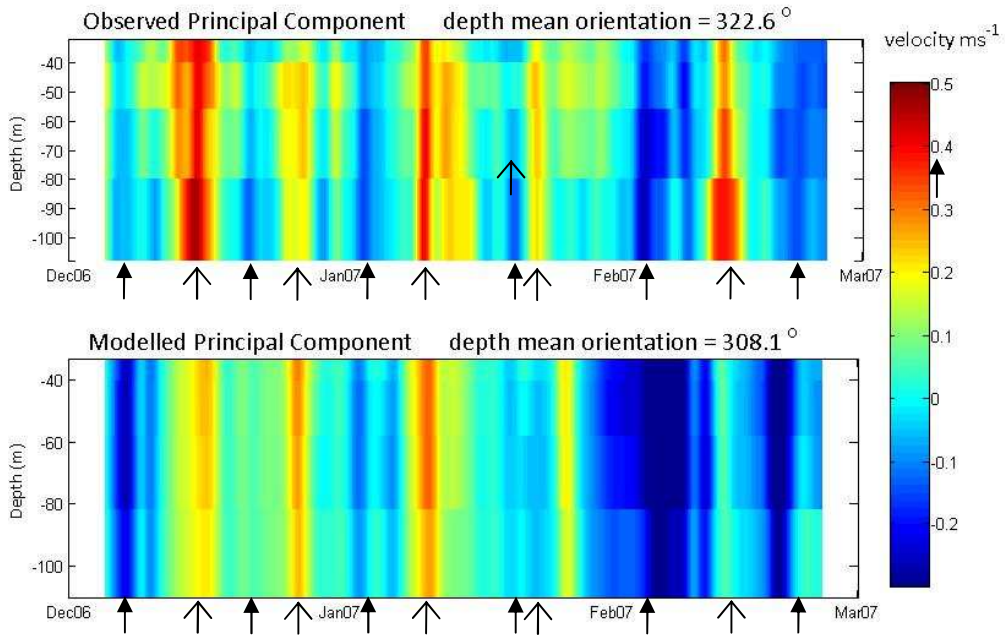

Figure 3.10 Observed (upper panel) and modelled (lower panel) low frequency currents rotated along the principal axis from Chicken reef (Dec2006-Mar2007). The depth-averaged orientation is given in degrees relative to the East, the colour-scale shows the magnitude of the flow, where blue indicates south-east and red indicates north-west. The arrows indicate events when the observed flow intensifies: towards the north-west, and towards the south-east. The same arrows are shown for the modelled flow to facilitate their comparison.

The monthly wind variability ellipses show changes in the wind direction and intensities; in turn, these are related to the modelled low frequency current main direction. The wind variability ellipses obtained for October-December 2005 show wind blowing from the northwest or west (Figure 3.11), and the simultaneous modelled low frequency current has a main south-east direction (Figure 3.9). Conversely, the wind variability ellipses obtained for February 2006 show strong south-easterly winds (Figure 3.11); accordingly, the modelled low frequency current has a north-west direction (Figure 3.9).

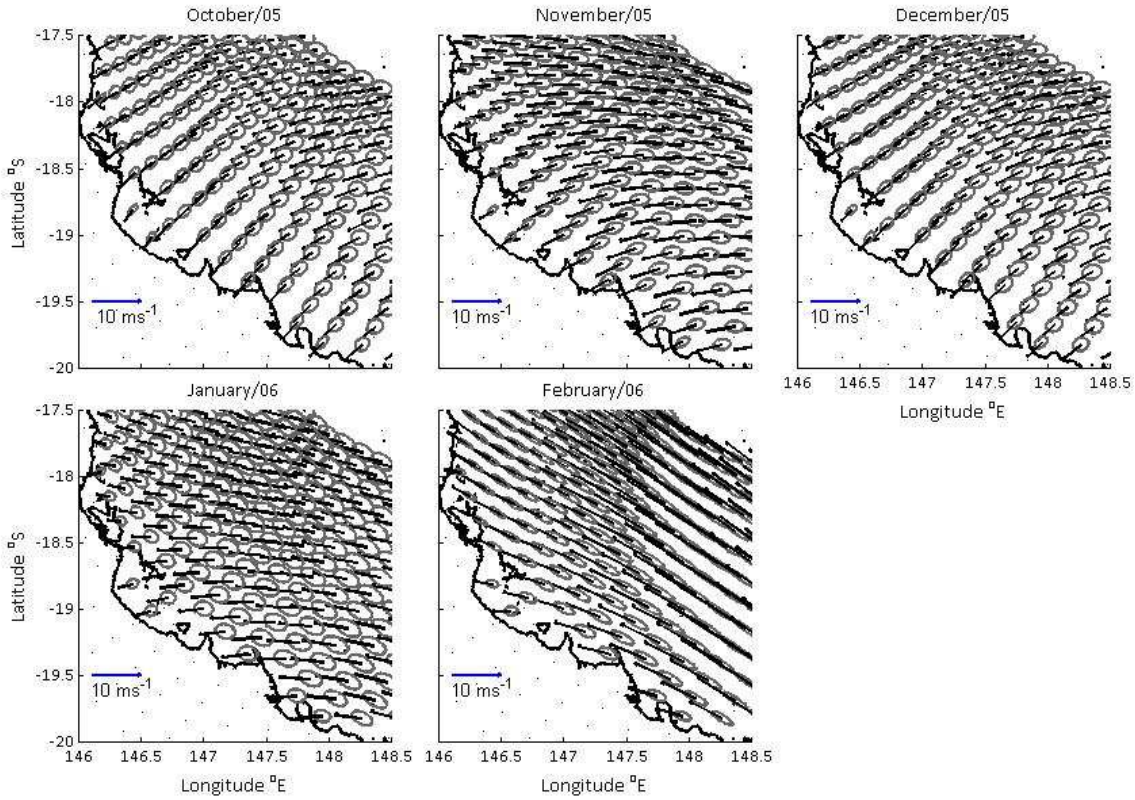

Figure 3.11 Monthly wind variability ellipses and mean wind velocity (ms^{-1})

3.3.4 Lee-reef eddies, upwelling and downwelling

The modelled depth-average vertical flow magnitude downstream of reefs showed that downwelling and upwelling occurred upstream and at the tip of the reefs, respectively (see Figure 3.12 as an example). In addition, upwelling events caused by both the acceleration of the flow over the reef's tip (right hand panels in Figure 3.13), and the presence of low pressure eddies (left hand panels in Figure 3.13), were also observed in the model outcomes. The inspection of the modelled depth-averaged horizontal flow field downstream reefs show the formation of eddies at most of the reefs of the central GBR (see results Chapter 4).

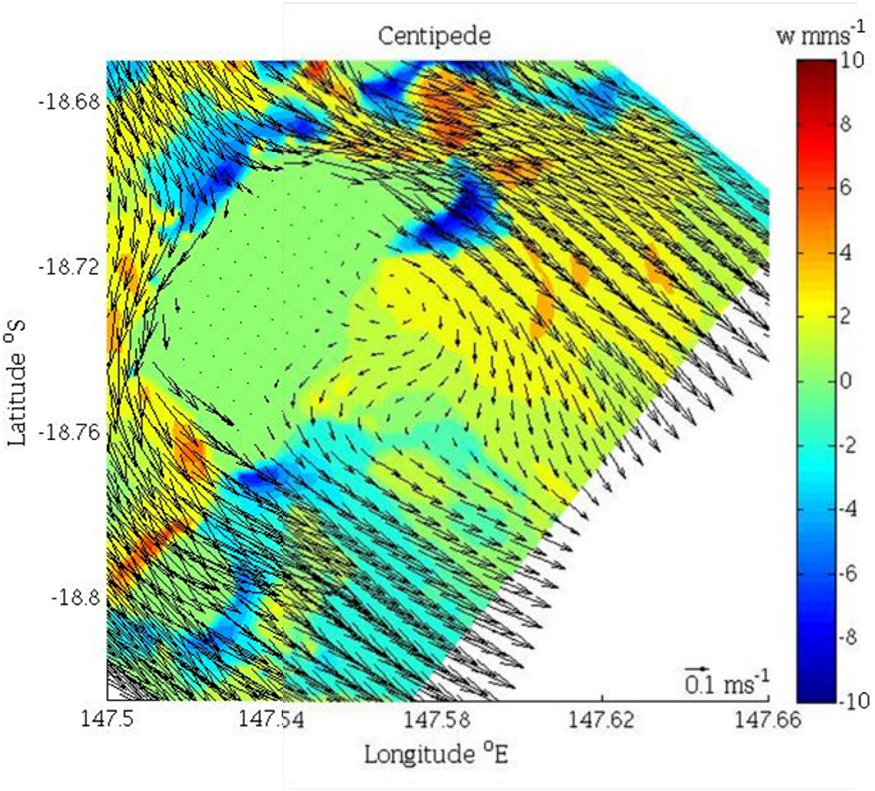

Figure 3.12 Top view snapshot of the depth-averaged horizontal velocity field (arrows) and vertical flow magnitude (colour scale) around Centipede reef (central GBR), obtained with the fine resolution grid of the model.

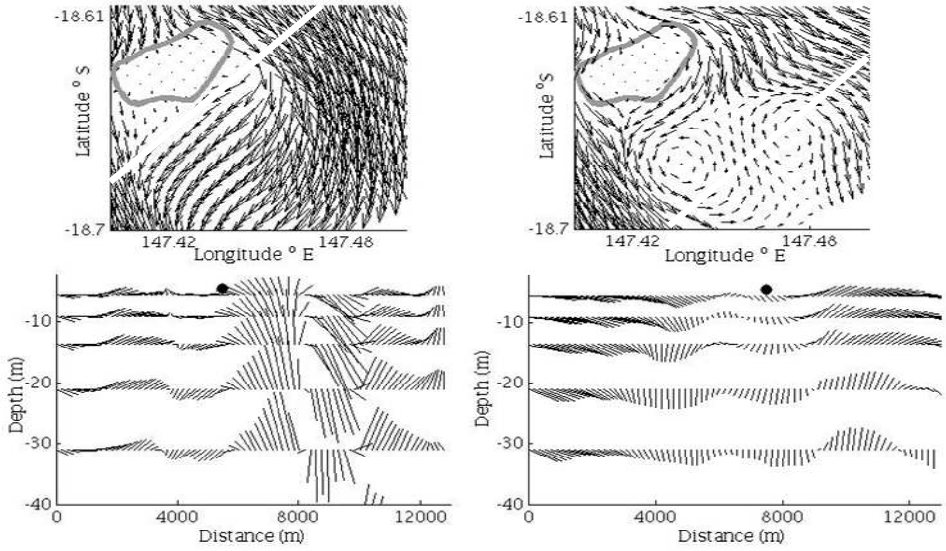

Figure 3.13 Upper panels show a snapshot top view of the depth-averaged horizontal flow field (arrows) around Centipede reef (grey contour) in the central GBR. Lower panels show vertical flow sticks over depth across the sections indicated in the upper panels; the balck dot indicates the position of the centre of the eddy across the section.

3.5 Discussion

The comparisons of the simulation outcomes with observations show that the model performs adequately. It reproduces current magnitudes and orientations that are in agreement with observations previously conducted along the GBR (e.g., Wolanski and Pickard 1985, Luick et al. 2007). In addition, the reef-scale flow structure, such as the formation of lee-reef eddies and associated upwelling events, are also reproduced by the model. Thus, the implementation of SHOC along the central GBR achieved in this Chapter is adequate for further examination of larval transport in a realistic reef system (Chapter 4).

The similarly of the extent of SST spatial structure and complexity degree between the model outputs and the satellite images indicates that the horizontal mixing is well parameterized. The sea level changes due to tides are extremely well reproduced and the low frequency sea level changes are reasonably captured, particularly at stations within the intermediate and fine resolution grids. Similarly, the temporal variability of temperature obtained with the model correlates significantly with observations at most of the stations. The fact that non-significant values occurred at stations close to shore and at Middle Reef (between Magnetic Island and the coastline) suggest that the discrepancies are most likely due to the limited precision in the implemented bathymetry (i.e., Middle reef is not well represented) and not to limitations of the model skills. Nevertheless, the most energetic periodicities (semidiurnal and ~10-20 days) of the modelled temperature time series agreed with those from the observations and can be explained by changes in water temperature caused by the day-night cycle and the movement of low and high atmospheric pressure systems which vary over periods of 15 days (Mata et al. 2006).

The main flow characteristics, such as the orientation of the axis of total kinetic energy of the high and low frequency signals, are well characterized by the model. As expected, the

low frequency flow is oriented along shore in a south-west north-east direction, and the high frequency signal is oriented roughly across shore (Wolanski and Pickard 1985). In addition the difference in flow orientation observed across sites (i.e., 288° from the East close to Pith reef and 320° form the East close to Chicken reef) is also depicted by the model. The more south-north orientation close to Pith reef is due to topographical forcing; this station is located between a group of reefs to the northwest, and a second group of reefs to the southeast; this topographic landscape steers the south-east flow, directing it along a south-north oriented "channel".

Within the central GBR, the low frequency currents are highly correlated with the along-shore wind component (Wolanski and Pickard, 1985). The effect of the winds on the low frequency currents are well captured by the model. Moreover, such an effect might be the cause of the main difference found between the modelled and observed low frequency currents. The north-west direction of the modelled low frequency flow at Pith Reef from February-March 2006 is induced by the strong south-easterly winds (Figure 3.11). It is possible that the wind field used to force the model overestimates the wind intensity causing intense north-west flows that are weaker and short-lived in the observations.

Chapter 4. The Island Wake Parameter and retention time in the central Great Barrier Reef (GBR)

4.1 Introduction

The vast majority of marine organisms have a planktonic stage during which larvae can be retained close to the source or disperse elsewhere (e.g., Pineda et al. 2007). The degree to which individual reefs retain locally produced larvae throughout their pelagic life determines their potential for self-replenishment (e.g., Cowen and Sponaugle 2009). Hence, estimates of local larval retention time are necessary for management and conservation plans seeking population persistence (e.g., Botsford et al. 2001; Sale et al. 2005; Cowen & Sponaugle 2009; Botsford et al. 2009).

Because of their minute size and long retention time in the plankton, tracking larvae directly and quantifying them over time and space is very difficult (Gaines et al. 2007). Thus, the phenomenon of larval dispersal has been tackled using hydrodynamic models that simulate the transport of water-borne particles. Still, modelling larval transport poses significant challenges. The temporal and spatial scales of mechanisms that drive larval transport vary over orders of magnitude (Legrand et al. 2006; Werner et al. 2007). For instance, low frequency boundary currents are part of basin-wide ocean gyres and determine the main pathway and direction in which larvae are advected (Cowen et al. 2006; Tang et al. 2006). At the other extreme, the interaction of boundary currents with reef topography generates local fronts, horizontal flow convergence and divergence over spatial scales of hundreds of metres, that modify larval distributions (Parslow and Gabric 1989). Thus, modelling efforts, even at individual reefs, need to solve circulation patterns at spatial scales from kilometres to metres requiring extensive computational time.

Model architecture and computational resources have progressed in the last decade (Chassignet et al. 2006), but critical challenges limit the potential of such tools and the

application of computationally intensive approaches. An example of such improvement relevant to the study of larval transport is the development of unstructured grids that have fine spatial resolution in shallow waters and coarse spatial resolution in oceanic waters; this type of grid reduces substantially computational time (Chen et al. 2006). Nevertheless, comprehensive oceanographic data sets are required to implement and validate any hydrodynamic model. In particular, data from different locations are necessary in order to test whether circulation patterns reproduced by the model are congruent with observations at all the temporal and spatial scales relevant to larval transport. Similarly, simultaneous time series of oceanic and atmospheric variables are necessary to define the forcing of the model, and precise bathymetry is essential. Thus, data availability constrains the quality of model outputs, and the regions where hydrodynamic models can be implemented. Therefore, investigation of simpler methods to approximate particle retention has the potential to facilitate modeling larval transport, especially where more detailed alternatives are unavailable.

Close to reefs, the interaction of the flow with the bathymetry provokes horizontal velocity shear, inducing the formation of reef-scale circulation features such as lee reef eddies. Modelling and observational studies have shown that lee eddies play a key role in larval transport. For instance, Oliver and Willis (1987) observed coral spawn slicks associated with eddies behind reefs. Similarly, in the vicinity of One Tree Island, high concentrations of pre-settlement fishes were found in locations where eddies were known to form while low concentrations occurred at locations where eddies were absent (Burgess et al. 2007). Lee reef eddies can recirculate particles and prolong retention (Sponaugle et al. 2002) but can also intensify flow and accelerate particle flushing, particularly for particles that travel along the edge of the eddy (Sandulescu et al. 2006). Eddy life-span and stability are also important determinants of the time particles can be retained. While remaining adjacent to the reef, long lived eddies have the potential to recirculate and bring particles back to the reef over longer periods of time than short lived eddies. However, if eddies detach and are advected

downstream, particles trapped within the eddy would also be flushed away from the reef. Thus, the formation and persistence of lee eddies has an important effect on particle transport.

The wake or flow structure past an obstacle, such as the formation and stability of an eddy, is controlled by a balance of destabilising inertial forces and stabilising frictional forces (Tomczack 1988). In steady flows, the wake can be classified by its form at equilibrium, that is, once sufficient time for the wake to fully develop and for any disturbance to dissipate has passed. At least for isolated obstacles, accurate parameterization of the forces' balance in the wake is a powerful tool to predict the form of the wake at equilibrium (Zulberti 2010). This parameterization in shallow waters is given by The Island Wake Parameter (Tomczak 1988); specifically, values close to unity indicate lee eddies that form and persist, values larger than unity indicate that eddies form and dissipate, and values smaller than unity indicate laminar flow where eddies are absent (Wolanski et al. 1984; Barton 2001). In Chapter 2, the Island Wake Parameter was shown to be adequate to capture the flow dynamics behind isolated, idealized reefs under simplified circulation regimes. The circulation regimes that were tested consisted of constant unidirectional flow or the combination of a constant unidirectional flow plus a perpendicular cyclic flow that resembled tidal currents. Different flow magnitudes (0.1 – 0.7 ms^{1}) and simple reef morphologies (rectangles, triangles and horse-shoe shaped) were implemented. More importantly, the Island Wake Parameter explained a large percentage of variability in particle retention across reefs and circulation regimes.

Real oceanic flows, however, differ in important ways from those considered in Chapter 2. Real flows are never perfectly periodic; for instance, temporal fluctuations of tidal currents can be disturbed by changes on direction of the low frequency flow, under this circumstance there is no guarantee that the wake will fully develop or that residual disturbances will dissipate; consequently parameterization of the wake flow structure at equilibrium, given by the Island Wake Parameter, might not reflect the actual characteristics of

the flow past reefs. In addition, the presence of secondary obstacles, and their positions relative to the obstacle on which the flow first impinges, has the potential to modify wake dynamics and thus alter their relationship with the Island Wake Parameter. For instance, Strykowski and Sreenivasan (1990) used flume experiments and flow visualization techniques to show that eddy shedding behind cylinders can be altered or suppressed by the presence of a second smaller cylinder in the near wake of the main cylinder (see Bao and Tao 2013 for a similar example). In particular, Caldeira and Sangra (2012) placed a system of "islands" into numerical and experimental channels to study the complexity of an archipelago wake. Their study found that neighboring islands can induce asymmetry in the wake flow and destabilize eddies. This or similar configurations can happen in the ocean where reefs might have a smooth downstream slope, or may occur in close proximity as part of a reef matrix or a reef chain. Therefore, the formation and detachment of eddies behind reefs within complex bathymetry may not occur as predicted by the Island Wake Parameter. The extent to which the Island Wake Parameter can predict the characteristics of flow past real reefs under realistic non-stationary circulation regimes, complex bathymetries, and arrangements of multiple reefs is consequently unclear. Any breakdown in the Island Wake Parameter's characterization of the flow regime could potentially erode its relationship with retention times, relative to the idealized cases considered in Chapter 2.

Here, we assess how well the Island Wake Parameter characterizes the absence and presence of lee eddies and their stability for circulation patterns that represent the kind of complexity observed in the ocean close to reefs. Furthermore, we investigate whether the relation between the Island Wake Parameter and mean retention time that prevails across idealized reefs, under the influence of simplified circulation regimes, holds under these more realistic scenarios; specifically, for non isolated reefs along the Central part of the Great Barrier Reef (CGBR). Circulation patterns during the coral spawning season and consequent lee reef eddy prevalence along the Central Great Barrier Reef are characterized. My findings show that

the Island Wake Parameter qualitatively captures the flow structure past reefs and relates to mean retention as predicted for ideal reefs under stationary flows. However, the wake flow structure and mean retention times obtained from the simulations show that lee reef eddies are commonly dissipated within hours, limiting their potential to enhance self recruitment of larvae that take few days to acquire competence to settle.

4.2 Methods

4.2.1 Simulations

The 3D Sparse Hydrodynamic Ocean Code (SHOC) was used to simulate the circulation and simultaneous particle transport in the Central Region of the Great Barrier Reef, this region encompasses 19 middle and offshore reefs with different sizes and morphologies (Figure 4.1). Some of these reefs are relatively isolated; for instance, Keeper, Helix, Grub and Centipede have no reefs within ~10 km or more downstream, well beyond the distance at which they might directly interfere with wake eddy dynamics. Conversely, Dip, Yankee and Bowl reefs are within few km from each other and interspersed other, smaller reefs.

Continuous release simulations were conducted by seeding 120 particles per hour, for 10 days, uniformly between the surface and 5 metres below, on top of 10 reefs (see Figure 4.1). Reefs with different sizes (~ 1.5 -5 km wide) from the middle and outer shelf were included. 3D velocity fields and particle position were recorded every hour and 30 minutes respectively for the whole time period. Circulation is expected to change over time; hence a continuous release allows depicting the effect of such variation on particle transport and was chosen over simulating an instantaneous particle release. Similarly, running simulations for two different events permits capturing a wider range of circulation regimes in the area; thus, two independent simulations were started at different dates. Simulations were performed for times when coral broadcast spawning occurs. For inshore reefs this usually takes place a few nights after the full moon in October, whereas outer shelf reefs spawn during November and

December (GBRMPA, 2006). Since the study region comprises both middle and outer shelf reefs, we simulated two different events releasing particles 5 days after the full or new moon, on October 22/2005, and December 06/2005 respectively.

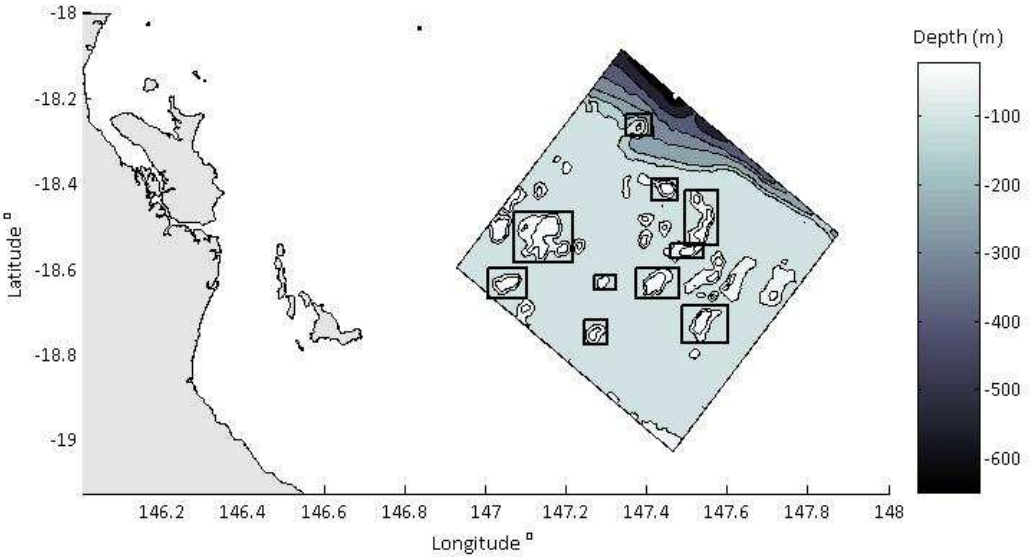

Figure 4.1. Study area showing the north-east Australian coastline and the bathymetry of the model domain. Reefs are shown in white; the black squares delimit reefs at which particles were seeded for the continuous release simulations.

4.2.2 Hydrodynamic model and grid characteristics

The model was previously validated for the CGBR (see Chapter 3). Briefly, it was forced through four open boundaries with current velocity outputs of coarser resolution simulations and through the surface with sea surface temperature, pressure, sea level elevation, wind velocities and weather variables to account for heat flux (see Chapter 3). The model grid is rectangular and oriented along shore, the velocity outputs are in a normal and tangential direction relative to the grid orientation. When necessary, these components were rotated into geographical north-south east-west components. The eastern boundary of the domain reaches the continental platform where the sea floor drops to approximately 760 metres. Hence, 36 vertical layers were implemented, with resolution increasing approximately as a negative exponential from the sea floor to surface (from 70 m at the bottom to 0.65 m close to the surface). Lee reef eddy dimensions are known to be on the order of reef size. The utilized

horizontal spatial resolution (280 m) provided five measurements (grid cells) behind the smallest reef inside the domain, providing sufficient resolution to depict the formation of eddies. In order to parameterize flow structure at smaller scales, particles were advected by the velocity explicitly solved by the model plus a random diffusion velocity proportional to the diffusion coefficient relevant to spatial scales smaller than the horizontal grid size; in this case 0.134 m^2s^{-1} (Okubo 1971).

4.2.3 Island Wake Parameter

Analogous to the Reynolds number, the Island Wake Parameter is used as a measure of turbulence of the flow past obstacles in shallow waters and is given by the ratio of inertial to frictional forces (Tomczak 1988). Close to reefs, friction caused by the shallow bottom provokes strong velocity shear across depth inducing vertical momentum transfer. Thus, the terms relevant to friction in this environment are depth and the vertical diffusion coefficient. The velocity at which the current approaches a reef and the reef's width are in turn, the inertial relevant terms. Thus, the Island Wake Parameter, described as the ratio between inertial to frictional forces in this environment, is given by:

$$I = \frac{VH^2}{WK_z} \qquad \text{eq. 4.1}$$

Where *V* is the velocity upstream of the reef, *H* is the water depth, *W* is the width or size of the reef perpendicular to the main flow, and K_z is the vertical turbulent diffusion coefficient. The terms that constitute I are not constant. *V* and K_z vary over space and time; similarly, *H* is not uniform over and around the reef, and *W* might differ on the order of 10s of metres depending on the direction of the prevailing current. Nevertheless, on the CGBR, currents normally flow along-shore (Black et al. 1990), thus, the dimension of the reef perpendicular to the coastline was deemed the most appropriate choice for *W*. With the same reasoning, the along-shore component of velocity upstream of the reef was used to compute *V*. The temporal and depth (6-40m) mean of this component was calculated to obtain a single value for *V*. The vertical

turbulent diffusion coefficient was first chosen equal to the background vertical diffusion (K_b) following the method described in Chapter 2. Finally, *H* was calculated as the mean depth found downstream the reef in the region were eddies could form. Temporal means were calculated over the time each particle remained close to the reef; thus, an Island Wake Parameter value was first obtained for each particle at each reef. A single I value for each reef was then obtained calculating the mean across particles.

Visual examination of the velocity fields was conducted in order to investigate if the Island Wake Parameter represents the characteristics of the flow behind reefs as theory describes: the life-span and number of eddies formed in the lee of the reef were quantified at each reef and event. Furthermore, I was calculated for every time step and the mean across times when eddies were absent or present was computed for each reef and event to corroborate that I values are consistent with the quality of the flow structure (presence/absence of eddies) past individual reefs across events or diverse circulation patterns.

4.2.4 Retention time

Particles can be entrained in an eddy, recirculate within it, and be brought back towards the reef. Similarly, tidal currents can advect particles back to the reef after reversal. Thus, particle retention was measured as the time it took a particle to be advected outside a 'retention area' around the reef within which circulation features could displace the particles back to the reef. Observational and modelling studies have shown that lee eddies can be as large as twice the size of the reef's side perpendicular to the incoming flow (Wolanski et. al. 1984; Burgess et al. 2007). Retention area was delimited by counting 16 grid cells (the extent of the largest observed eddy) to the north, south, east and west of each reef edge. This is equivalent to approximately 4.5 km. Only tidal currents of 0.21 ms^{-1} or stronger could advect particles for larger distances after 6 hours (before reversal). Tidal currents are rarely this

strong over a six hour period and results show that their magnitude was slower (see results, currents section). Thus, 16 grid cells suffice to encompass an area where particles can be advected back to the reef. In order to investigate how the presence of eddies influences particle transport, particles with long and short retention time (larger/shorter than the mean +- one standard deviation) were identified for each reef. Snapshots of the depth-averaged (5-45m) horizontal velocity field and particle position were created for the period of time the particles remained close to the reef. These revealed the trajectories of particles with short and long retention time.

4.2.5 Island Wake Parameter and Retention time relationship

A power law function modified by an offset term given by:

$$R = aI^b + c \qquad \text{eq. 4.2}$$

Where *R* denotes mean retention time, I is the Island Wake Parameter and *a*, *b* and c are regression parameters, was found to describe well the relationship between I and retention time for idealized reef shapes under simple and stationary circulation regimes with and without the presence of tidal flows (Chapter 2). To investigate if such a relationship prevails despite the complex morphology of real reefs and temporal circulation variability, regression analysis between the Island Wake Parameter and retention across reefs and spawning events was first performed by fitting this function.

For all regressions, the existence of parameter *c*, or a minimum retention time as *I* increases was tested by comparing regressions with *c* fixed at zero, and using a likelihood ratio test to choose between the two models. Regression analysis was first performed for each event separately. Secondly, regression analysis was conducted with the data pooled across events and a likelihood ratio test was used to discern if there was significant support for variation between events in the functional relationship between the Island Wake Parameter and mean retention time.

Island Wake Parameter values found in the present study are larger than those obtained for idealized reefs (see Results section). Thus, pooling the data from both studies allows evaluating the relationship between I and mean retention time over a wider range of flow regimes. Moreover, it allows testing if the relationship between the Island Wake Parameter and mean retention for idealized reefs under simplified circulation regimes persist for real reefs under realistic circulation patterns. Regressions were then performed combining data from both chapters. Tidal currents are present and intense during both events investigated in this chapter. Therefore, only data from idealized reefs that were under the influence of unidirectional plus tidal flows were first included in the regression analysis. A likelihood ratio test was used to determine if a single, or separate models, explained better the variability in the data.

Given the structure of the regression residuals, and because there is no physical theory to specifically support the modified power law (eq.4.2), data were also fitted using a generalized additive model. This allows obtaining a relationship between the Island Wake Parameter and mean retention time without constraining it to a peculiar functional form. Akaike's Information Criterion (*AIC*) was used for model selection between the modified power law fit and the general additive model fits. Finally, as with the power law regressions in Chapter 2, the results from the present chapter and all the idealized reefs (including those under unidirectional flows) were pooled to determine if a single generalized additive model (favoured over the modified power law fit, see Results) could approximate retention time across the entire set of simulations.

4.2.6 Currents and Wind

To elucidate circulation patterns in the region and their variability, velocity time series spanning the whole simulation period (10 days) were analysed independently for each event (October and December). First, to identify and compare flow intensity and orientation representative of each event, time series at 81 locations evenly distributed inside the domain and at 3 different depths (1.8, 33 and 96 metres) were used. A principal component analysis following Emery and Thomson (2001) was performed to obtain velocity time series along an axis that captures most of the temporal variance at each location. The temporal mean of the current magnitude along the principal axis and the axis orientation were then averaged across space for each depth and event. This provided a mean current magnitude and main orientation of the flow at each depth and for each event. To investigate possible mechanisms inducing prevalent current patterns, variability ellipses of wind velocity time series were computed independently for each event.

In order to quantify the variability of the current orientation over time, time series upstream of each reef inside the domain (19) and at 3 different depths (1.8, 33 and 96 metres) were used. Current variability ellipses, that is, the axis that accounts for most of the temporal variance, and the orthogonal axis, were calculated for each reef across depths, following Emery and Thomson (2001). The temporal variation of the flow orientation was then quantified with the ellipses eccentricity values. When the eccentricity is near 1 there is little temporal variation of the flow direction; oppositely, eccentricity values close to zero imply large temporal variation on the flow's orientation. The ellipses eccentricity is given by:

$$\sqrt{1 - \frac{vp^2}{up^2}} \qquad \text{eq.5.3}$$

where *up* and *vp* are the length of the semi major and semi minor axis of the ellipses, respectively. The principal component analysis was performed on the total, low frequency and high frequency velocity signals. These signals were separated using a Lanczos filter and a cut

off frequency of 1/24 hr^{-1}. The current variability ellipses were obtained from the total velocity signal.

4.2.7 Island Wake Parameter Values along the Great Barrier Reef (GBR)

The range and frequency of occurrence of Island Wake Parameter values along the GBR were roughly estimated to elucidate the potential for larval retention by lee reef eddies in the region. The width (*W*) of the reefs was measured as the upstream side perpendicular to the direction of the main flow; this in turn was considered to approach the reef from the south-east or north-west for reefs that were located to the north and south of ~ 18° S latitude respectively. Approximately at this latitude, water from the Coral Sea reaches the continental platform and along-shore currents to the north and south originate (e.g., Church 1987; Brinkman 2001). The vertical turbulent diffusion coefficient (*Kz*) was substituted by the background vertical diffusion as described in Chapter 2, depth (*H*) was set to 20, 50 or 100 metres depending if the reef was in the inner, middle or outer shelf and current magnitudes (*V*) of 0.1 and 0.7 ms^{-1} were used to estimate I over a range of current velocities observed along the GBR (e.g., Wolanski and Pickard 1985; Church 1987). To capture a wide range of possible *I* values, five reefs from each section of the GBR (11 as classified by the reef monitoring program of the Australian Institute of Marine Science AIMS) were used encompassing different sizes (e.g. from 0.37 – 5.6 km) and reef locations (inner, middle and outer shelf). Once I values were obtained, associated retention times were calculated using the appropriate regression model to describe the relationship between the Island Wake Parameter and mean retention time.

4.3 Results

4.3.1 The Island Wake Parameter, wake flow characteristics and retention time

I values obtained across reefs and events have orders of magnitude between 10^1 and 10^5 (Table 4.1); these indicate the occurrence of wake flows with the presence of unstable eddies and agree with the velocity fields obtained from the simulations. All I values are at least an order of magnitude larger than unity and, as predicted, none of the generated eddies persisted throughout the simulation period. Similarly, I values calculated over periods of time when eddies were present were always smaller than those obtained when eddies were absent, and in most cases significantly different (Figure 4.2). All eddies eventually detached and dissipated. Nevertheless, some discrepancies with theory were found. Very large I values, which theoretically represent the rapid repeated formation and detachment of eddies, were found to associate with no eddy formation. In addition, the magnitude of I values associated with the formation of eddies did not show a clear relation with the number of eddies or their lifespan across reefs. Theory predicts that wakes with stable eddies associate with Island Wake Parameter values close to unity. Conversely, if eddies are detached and advected downstream, allowing the formation of new eddies, the Island Wake Parameter is larger than unity. Thus, we expected larger Island Wake Parameter values to indicate a faster rate of eddy formation and detachment; over the same time period, this implies the formation of more eddies with a shorter lifespan. This pattern was not observed consistently across reefs. Amongst reefs that developed lee eddies, Dip and Yankee had some of the largest Island Wake Parameter values. However, rapid formation of eddies as predicted by the corresponding I values was not observed at these reefs; instead, very few eddies consolidated. In addition, the life-span of eddies formed behind reefs with large Island Wake Parameter values (e.g. 2 and 4 hours for Yankee reef) was not always shorter than the life-span of eddies formed behind reefs with smaller Island Wake Parameter values (e.g. 3.2 and 7.9 hours for Centipede reef). Nevertheless, the lifespan of eddies varied accordingly with the magnitude of I values at most

(4 out of 6) of the individual reefs across events (see values in Table 4.2). Pair-wise comparisons across events for reefs where eddies formed showed that larger Island Wake Parameter values generally corresponded to shorter eddy life-spans. For instance, at John Brewer the mean eddy life span is shorter and I is larger in October (1.5 hours and 34 respectively) than in December (2.1 hours and 11 respectively).

Table 4.1. Island Wake Parameter (I) values (ascending order), number of eddies, mean lifespan of eddies and mean retention time for each reef and event.

I	Eddies Mean lifespan (hours)	Number of eddies	Average time when eddies were present (hours)	Mean retention time (days)	Reef O – October D – December
11	2	12	24	0.86	Fore and After (D)
20	4	14	56	0.81	Fore and After (O)
32	2.1	16	33.6	0.74	John Brewer (D)
32	7.9	33	260.7	0.87	Centipede (O)
34	1.5	4	6	0.50	John Brewer (O)
65	3.2	21	67.2	0.74	Centipede (D)
68	2.8	5	20	0.85	Bowl (O)
161	2	5	10	0.56	Dip (D)
111	21.5	20	430	1.09	Grub (O)
155	2.9	34	98.6	0.63	Grub (D)
220	2.8	5	14	0.64	Dip (O)
343	-	-		0.73	Keeper (O)
361	-	-		0.52	Bowl (D)
385	4	2	8	0.80	Yankee (O)
392	-	-		0.37	Helix (O)
482	-	-		0.47	Keeper (D)
542	-	-		0.38	Helix (D)
1330	2	3	6	0.51	Yankee (D)
19709	3.3	3	9.9	0.45	Myrmidon (O)
79328	-	-		0.16	Myrmidon (D)

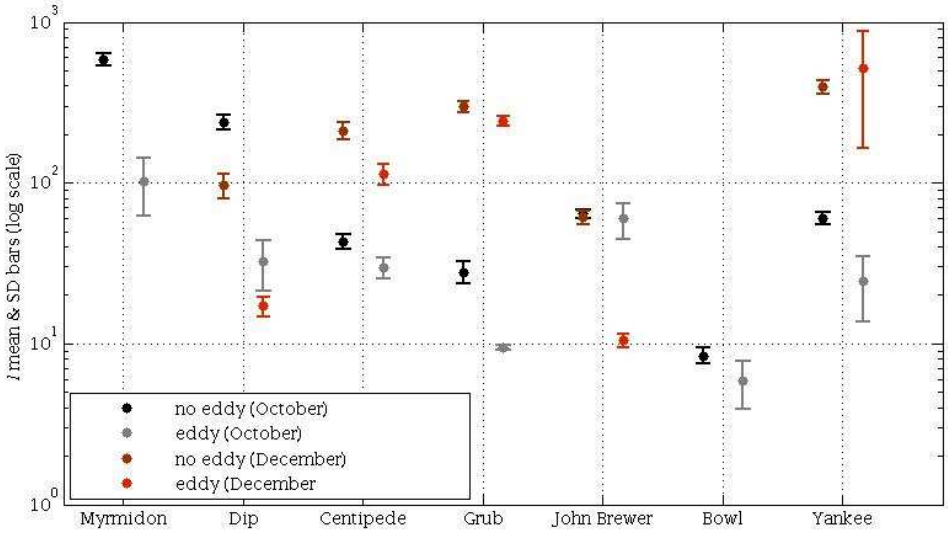

Figure 4.2. I mean value and standard error bars when eddies are present (dark tones) and absent (light tones) for each reef (along the x axis) and event (red colors for December and grey colors for October).

Table 4.2. Mean lifespan of eddies (hours) and Island Wake Parameter (I) for reefs that developed lee eddies during both events. Pairs (across events) where the larger Island Wake Parameter (I) value corresponds to the shorter mean lifespan of eddies are in bold.

Reef	October		December	
	Mean lifespan of eddies (hours)	*I*	Mean lifespan of eddies (hours)	*I*
Fore and After	4	20	2	11
John Brewer	**1.5**	**34**	**2.1**	**32**
Centipede	**7.9**	**32**	**3.2**	**65**
Dip	2.8	220	2	161
Grub	**21.5**	**111**	**2.9**	**155**
Yankee	**4**	**385**	**2**	**1330**

Mean retention times obtained from the simulations varied from 0.16 to 1.09 days. Generally, longer retention times occurred during October when flows were less intense and Island Wake Parameter values were smaller at most of the reefs. The wake flow structure clearly affected particle paths and consequent retention time. Trajectories of particles that had large retention times always showed entrainment in an eddy or eddy pair and consequent recirculation. Conversely, those particles with short retention times showed relatively straight trajectories, or followed one side of the outer edge of the eddy, without becoming entrained in the eddy or otherwise recirculating (Figure 4.3). Furthermore, eddies that prevail for longer

have the potential to avoid particle flushing while they remain attached to the reef. Hence differences in eddy duration relate to retention time variation among wakes where unstable eddies form. For instance, the longest retention time was provoked by eddies with a mean life-span of 0.87 days formed at Grub reef during October. At the same reef, eddies dissipated within 0.087 days during December and retention time was almost halved. Even though eddies formed at most of the reefs, their life span was rarely longer than 0.17 days. The potential of lee eddies to prolong retention time was often diminished by fluctuations of the incoming flow that caused eddy detachment. Indeed, harmonic analysis showed that tidal currents explained a large percentage of the variability of the flow during December and that they were quite intense during both events (see magnitude values in Table 4.3). Thus, the detachment of eddies after tidal reversal was common and mean retention times were shorter than a day.

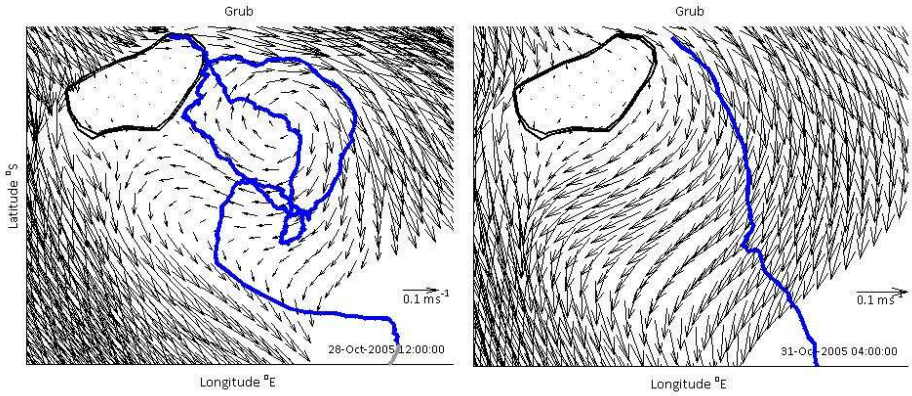

Figure 4.3. Top view snapshots of the horizontal velocity field (arrows) and particle trajectory (blue line). The particle was seeded 5.4 and 0.09 days before the snapshot for the left and right hand panels respectively.

Table 4.3. Temporal and spatial (across latitude and longitude) mean and standard deviation of the flow magnitude and orientation along the principal axis. Spatial (across latitude and longitude) mean of the percentage of the current variance explained by tides. Results for different depths and spawning events are presented.

Events	Depth	Original			Low frequency		High frequency	
		Mean magnitude (ms^{-1})	Mean orientation (degrees from the east)	Mean % of current variance explained by tides	Mean magnitude (ms^{-1})	Mean orientation (degrees from the east)	Mean magnitude (ms^{-1})	Mean orientation (degrees from the east)
October	Surface	0.40 +- 0.10	266.79 +- 13.7	9.46	0.35 +- 0.09	268.62 +- 13.8	0.07 +- 0.02	69.42 +- 13.7
	Mid depth	0.22 +- 0.09	264.43 +- 30.6	9.01	0.19 +- 0.08	264.52 +- 30.4	0.04 +- 0.02	64.74 +- 30.2
	Bottom	0.08 +- 0.04	300.06 +- 48.4	2.54	0.06 +- 0.03	292.12 +- 47.7	0.01 +- 0.01	92.07 +- 47.3
December	Surface	0.82 +- 0.32	318.43 +- 12.1	49.19	0.70 +- 0.27	317.78 +- 12.2	0.16 +- 0.05	16.38 +- 12.2
	Mid depth	0.54 +- 0.32	312.21 +- 22.2	48.79	0.46 +- 0.28	311.93 +- 22.3	0.12 +- 0.05	10.69 +- 22.4
	Bottom	0.28 +- 0.16	324.36 +- 25.4	36.85	0.24 +- 0.14	324.30 +- 24.9	0.06 +- 0.02	25.82 +- 26.4

4.3.2 Island Wake Parameter and Retention time relationship

The relationship between I and mean retention time was not statistically significant for October. Conversely, regressions for December, and for the data pooled across events, were statistically significant, explaining 89 and 48 % of the variability in the data respectively (Table 4.4). In all cases likelihood ratio tests showed no significant support for the inclusion of an asymptote parameter *c*. In addition, the likelihood ratio test supports the pooled model (Figure 4.4, purple line) in which a single set of regression parameters describes the relationship across events (G = 4.0864, $X^2_{(3,0.05)}$ = 7.815, P = 0.25).

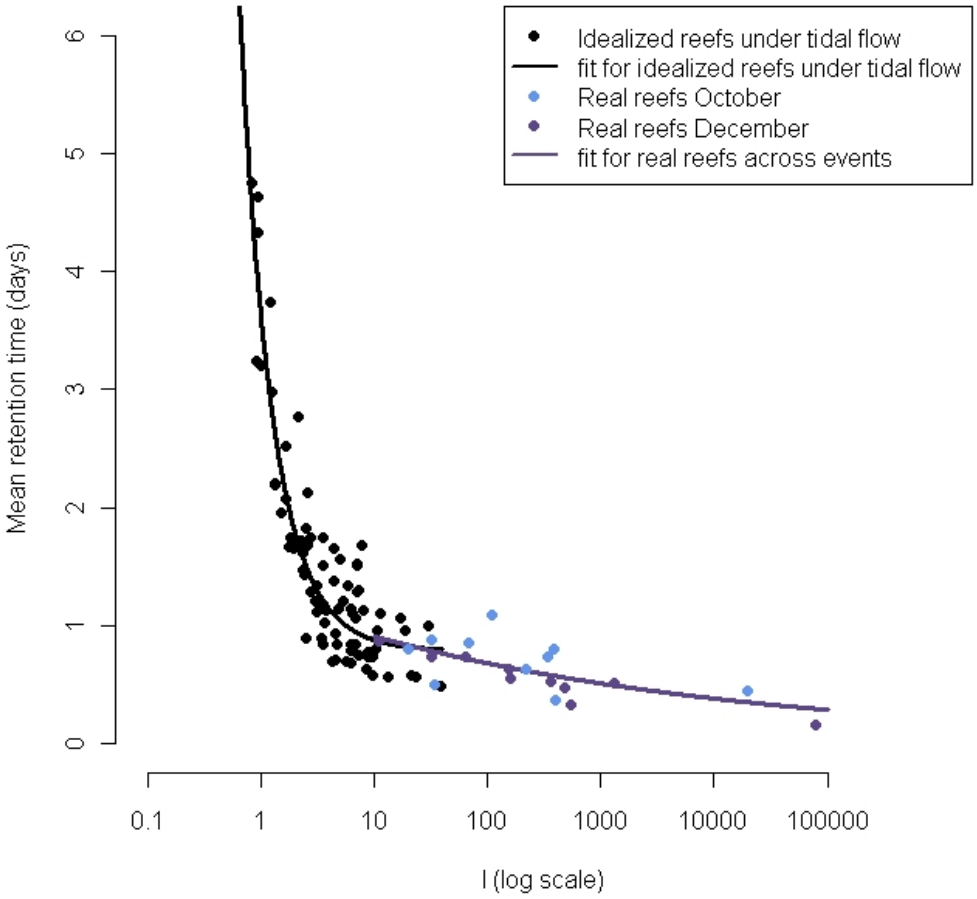

Figure 4.4. Relationship between the Island Wake Parameter (I) and mean retention time for idealized reefs under the influence of tidal flows simulated in Chapter 2 (black dots) and for reefs along the Central GBR simulated in this chapter (purple dots). Different purple tones are used to differentiate between the October and December events. The lines are the regressions for the idealized reefs (black) and the reefs along the Central GBR (purple).

Table 4.4. Regression parameters with 95% confidence bounds, coefficient of determination (R^2), *F* statistic, *P* values for regression models between Island Wake Parameter (I) and mean retention time for each event and events pooled together.

Event	G	a (95% cb)	-b (95% cb)	R^2	*F*	*P* value
October	0.0534	1.06	0.077	0.22	0.92	0.4424
		(0.34 – 1.76)	(-0.06 – 0.21)			
December	0.6198	1.34	0.16	0.89	28.11	0.00045
		(0.99 – 1.68)	(0.11 – 0.22)			
Pooled	0.4825	1.22	0.12	0.48	7.50	0.0046
		(0.77 – 1.66)	(0.05 – 0.20)			

The pooled regression is favoured over separated regressions (G = 4.0864, $X^2_{(3,0.05)}$ = 7.815, P=0.25)

The relationship between the Island Wake Parameter and mean retention time found for idealized reefs under simplified flows (Chapter 2) shows that, when lee eddies detach and dissipate, retention times vary between 0.27 and 1.1 days (see the distribution of symbols for I>10 in Figure 2.7 from Chapter 2). In agreement with this finding, results from the present chapter show that retention times associated with the formation of unstable eddies or no eddies have similar magnitudes (0.16 - 1.09 days). Tidal currents were intense during both events simulated in this study, reaching magnitudes of 0.07 and 0.16 ms^{-1}. The regression for idealized reefs under the influence of tides is significant and explains 84% of the variability in retention time (Table 4.5, Figure 4.4, black line). Although this data set spreads over different ranges of I values than the data set for reefs in the CGBR, they overlap between Island Wake Parameter values of 10 – 40. More importantly, the regressions between the Island Wake Parameter and mean retention time, obtained separately for each group of data, coincide where the ranges of I values overlap. This suggests that each data set describes a different range of a single underlying relationship between the Island Wake Parameter and mean retention time. In fact, the regression obtained when data from idealized reefs under tidal flow and data from the present study are pooled is also significant, explains 85% of the variability in retention time, and is favoured by the likelihood ratio test over separate models for the idealized and realistic reefs (G = 3.4384, $X^2_{(3,0.05)}$=7.815, P=0.328, Table 4.5).

Model selection for the power law regressions obtained for idealized reefs under tidal flows and CGBR reefs implies the existence of a minimum retention time (i.e., a non-zero parameter c); however, for I>10 most of the points lay under the fitted line for this model (Table 4.5, Figure 4.5, grey solid line). In contrast, the generalized additive model describing the relationship between mean retention time and the Island Wake Parameter, fitted to the same data, implies that retention continues to decrease even for I values larger than 10 (Figure 4.5, grey dashed line). The residual variation is more well-behaved for the generalized additive model than for the power law fit, particularly for I>10. Accordingly, model selection

indicates that the generalized additive model describes significantly better the relationship between the Island Wake Parameter and mean retention time ($AIC_{\text{gam fit}} = 71.45 < AIC_{\text{modified power law fit}} = 72.92$). This suggests that the support of asymptote parameter *c* found for the power law fit is a consequence of restricting the functional form of the response to a power law function, and that the existence of a minimum retention time is spurious, i.e. a systematic deviation of the "true" underlying relationship between mean retention time and the Island Wake Parameter and that allowed by the modified power law (eq. 4.2).

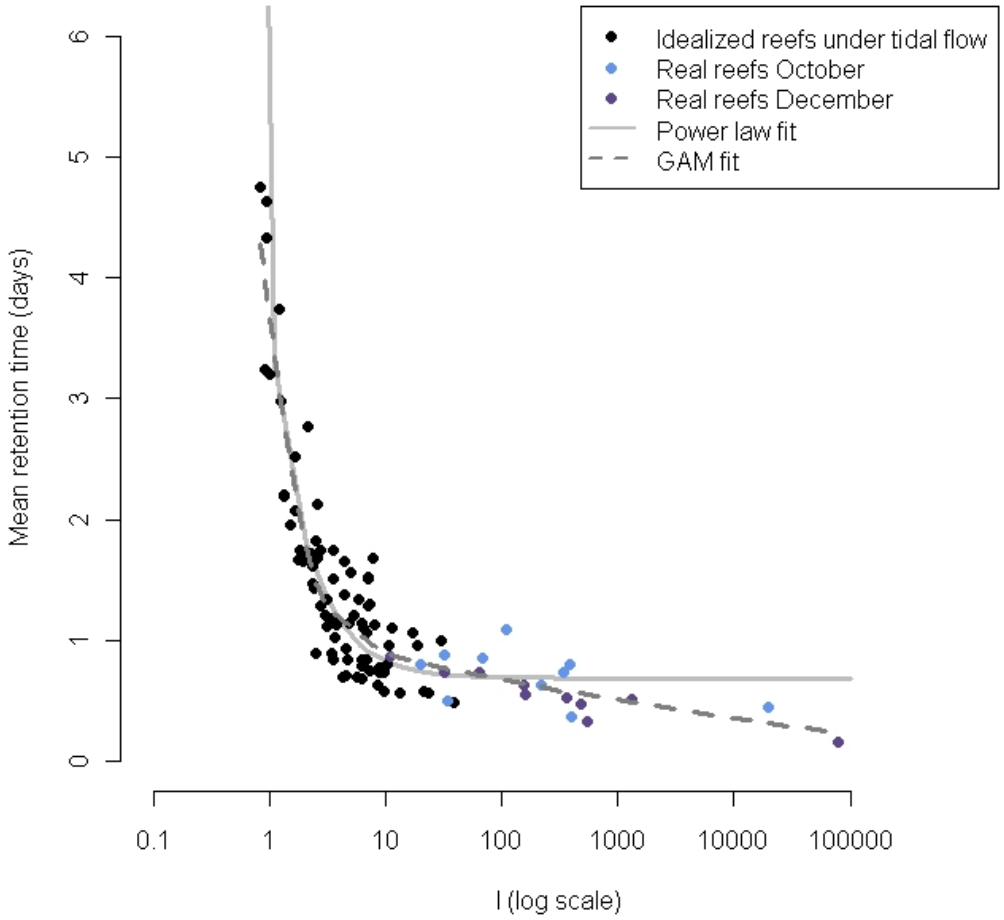

Figure 4.5. Relationship between the Island Wake Parameter (I) and mean retention time for idealized reefs under the influence of tidal flows simulated in Chapter 2 (black dots) and for reefs along the Central GBR simulated in this chapter (purple dots) pooled together. Different purple tones are used to differentiate between the October and December events. The solid line is the parametric fit and the dash line is the GAM fit.

Table 4.5. Regression parameters with 95% confidence bounds, coefficient of determination (R^2), *F* statistic, *P* values for regression models between the Island Wake Parameter (I) and mean retention time for idealized reefs under the influence of tidal flows (data from Chapter 2), for CGBR reefs under realistic circulation regimes (data from this Chapter), and both data sets pooled together.

Data									
Chapter 2		Chapter 3							
Circulation regime	Reef shape	Events	*G*	a (95% cb)	-b (95% cb)	c (95% cb)	R^2	*F*	*P*
Tidal	All	-	27.90	2.84 (2.55 – 3.14)	1.50 (1.17 – 1.83)	0.81 (0.64 – 1.00)	0.84	133.82	<0.001
-	-	October, December	0.4825	1.22 (0.77 – 1.66)	0.12 (0.05 – 0.20)	NA	0.48	7.50	0.0046
Tidal	All	October, December	54.89	2.95 (2.70 – 3.20)	1.33 (1.11 – 1.54)	0.70 (0.57 – 0.82)	0.85	182.96	<0.001

A single regression is favoured for the tidal idealized and data from the present study pooled together over the separate models ($G = 3.4384$, $X^2_{(3,0.05)} = 7.815$, $P = 0.328$).

The regression obtained with a generalized additive model when pooling data from the present study and all data from idealized reefs (including those under unidirectional flow) was also significant (Table 4.6). The presence of tidal flows can prolong the time it takes a particle to be flushed by inducing flow reversals over short periods of time (on the order of hours). Conversely, unidirectional or low frequency flows displace particles in a constant direction over larger periods of time. Hence, retention time decreases faster when flow is unidirectional than when strong tidal flows are present. Thus, the regression obtained for idealized reefs under the influence of unidirectional flows decays more rapidly than that obtained for reefs under tidal flows (Figure 4.6). Consequently, the likelihood test supports the use of separate general additive models for flows with and without tides ($AIC_{separate} = 247.23 < AIC_{pooled} = 275.48$, Table 4.5, Figure 4.6).

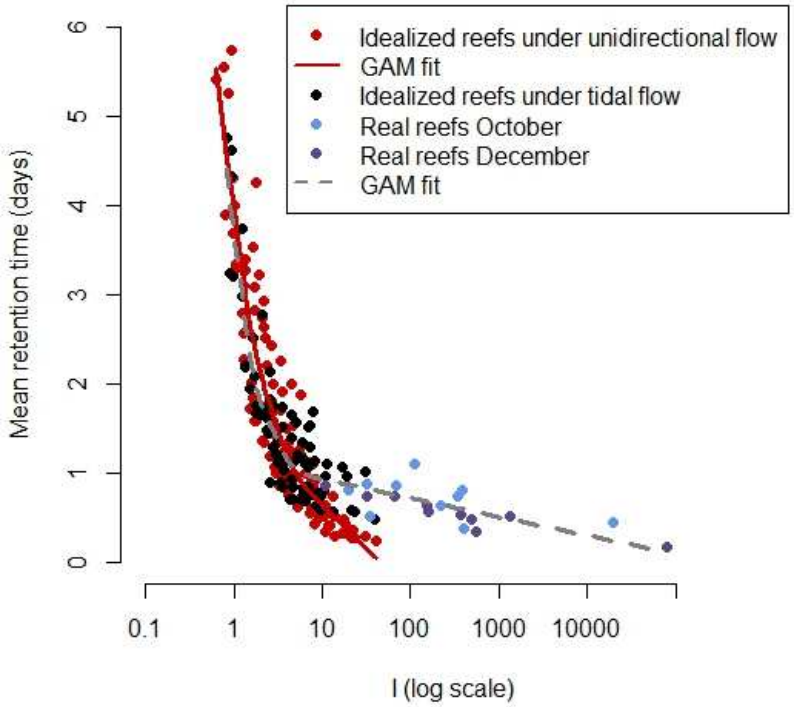

Figure 4.6. GAM fits for the relationship between the Island Wake Parameter (I) and mean retention time for idealized reefs under the influence of unidirectional flows (red line), for idealized and CGBR reefs under the influence of tidal flows and realistic circulation regimes respectively (dashed grey line). Idealized reefs under unidirectional flow are represented by the red dots, idealized reefs under tidal flows are represented by the black dots, CGBR reefs are represented by the purple dots (light tone for October and dark tone for December).

Table 4.6. Coefficient of determination (R^2), *F* statistic, *P* values and Akaike Information Criterion (*AIC*) for the general additive regression models (GAM) between the Island Wake Parameter (I) and mean retention time for idealized reefs under unidirectional flow, for idealized reefs under tidal flow and CGBR reefs under realistic circulation regimes pooled together, and for all data (idealized reefs under unidirectional and tidal flows and CGBR reefs) combined.

Data						
Chapter 2		Chapter 3				
Circulation Regime	Reef shape	Events	R^2	*F*	*P*	*AIC*
Unidirectional	All	-	0.83	124.2	<0.001	175.78
Tidal	All	October, December	0.86	120.3	<0.001	71.45
Unidirectional, Tidal	All	October, December	0.83	208.9	<0.001	275.48

Separated regressions for the idealized reefs under unidirectional flow and the idealized reefs under tidal flow pooled with the CGBR reefs under realistic circulation regime are favoured over the regression for all data pooled ($AIC_{separate}$ = 247.23 < AIC_{pooled} model = 275.48, G = 14.12, $X^2_{(6,0.05)}$ = 12.59, P = 0.028)

4.3.2 Currents and Wind

The current principal component analysis shows that, during October, the current direction showed variability over space, flowing towards the south or south-west between 264 – 300 degrees from the east (Table 4.3). A change in direction over depth is evident across the study area (Figure 4.7, left hand panel). Conversely, during December the currents flow along the coastline towards the south-east at approximately 318 degrees from the east (Table 4.3). These currents are coherent across the domain and showed little variation with depth except for the southern region in the domain (Figure 4.7, right hand panel). Differences in current orientation and vertical shear across events are likely related to changes of the wind field. The wind intensity was similar across events; however, the direction from which it blew and its temporal variation changed considerably. During October the strong east component of the wind velocity (see Figure 4.8), deflected the currents from the usual south-east direction along the coast to a south or south-west direction, weakening their intensity and allowing for longer retention times. Conversely, the consistent north-east direction of the wind during December, (see Figure 4.8) strengthened the south-east flowing currents; consequently, currents were well defined, fast, and retention times shorter.

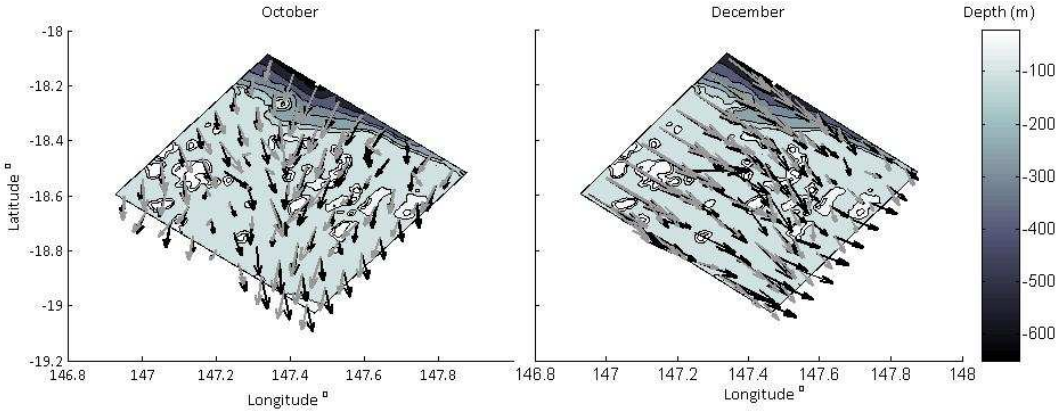

Figure 4.7. Top view of the spatial structure of the current principal component of the total velocity signal for October (left hand panel), and December (right hand panel). The arrows indicate the main current direction and intensity relative to depth. Black colour corresponds to the 1.8 m currents and grey colour corresponds to the 33 m currents

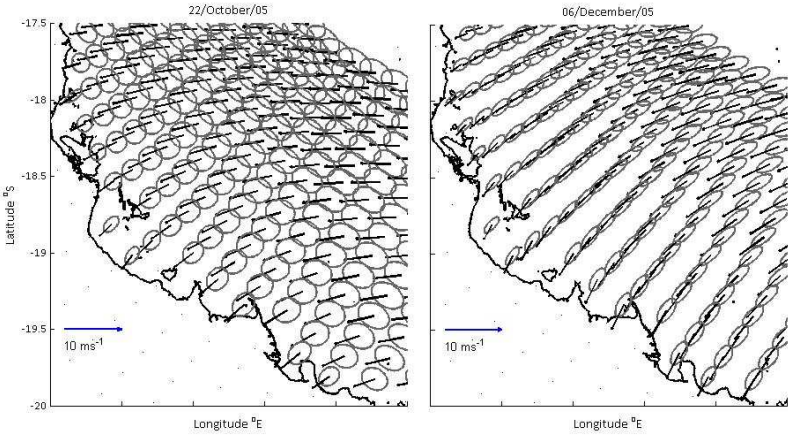

Figure 4.8. Monthly wind velocity variability ellipses and mean velocity (arrow) for October (left hand panel) and December (right hand panel).

Currents were stronger during December than October, reaching mean surface magnitudes of 0.82 and 0.4 ms^{-1} respectively. Surface tidal currents have mean values of 0.16 ms^{-1} in December, and 0.07 ms^{-1} in October (Table 4.3). These magnitudes corresponded to strong currents observed along the Great Barrier Reef (e.g. Wolanski and Pickard 1985; Griffin et al. 1987; Church 1987; Black et al. 1990). The current variability ellipses analysis showed that temporal variability in the flow direction is larger during October than in December at most of the reefs (see eccentricity values in Table 4.7). The harmonic analysis showed that tides explain around 50% of the flow variation during December, but only a maximum of 9% during October (Table 4.3).

Table 4.7. Spatial (over depth) mean and standard deviation of the ellipses eccentricity at each reef and event. The reefs were particles were seeded are in bold.

Reef	Mean ellipses eccentricity +- SD	
	October 22	December 06
Myrmidon	**0.94 +- 0.050**	**0.91 +- 0.096**
Faraday	0.88 +- 0.052	0.86 +- 0.018
Aral	0.90 +- 0.072	0.95 +- 0.017
Hopkins	0.90 +- 0.050	0.96 +- 0.012
Helix	**0.84 +- 0.061**	**0.94 +- 0.016**
Dip	**0.70 +- 0.137**	**0.92 +- 0.029**
Keeper	**0.87 +- 0.060**	**0.95 +- 0.023**
Fore and After	**0.92 +- 0.035**	**0.98 +- 0.008**
Grub	**0.72 +- 0.111**	**0.91 +- 0.029**
Backnumbers	0.92 +- 0.040	0.96 +- 0.016

Continuation Table 4.7

Reef	Mean ellipses eccentricity +- SD	
	October 22	December 06
Centipede	0.93 +- 0.070	0.93 +- 0.043
Fork	0.93 +- 0.019	0.91 +- 0.023
John Brewer	**0.89 +- 0.059**	**0.93 +- 0.023**
Bowl	**0.90 +-0.097**	**0.82 +- 0.057**
Knife	0.69 +- 0.222	0.87 +- 0.036
Lodestone	0.97 +- 0.012	0.93 +- 0.021
Wheeler	0.96 +- 0.037	0.78 +- 0.109
Yankee	**0.85 +- 0.086**	**0.94 +- 0.024**
Cup	0.78 +- 0.157	0.97 +- 0.014

4.3.3 Distribution of Island Wake Parameter values along the Great Barrier Reef (GBR)

For fast mean flow magnitudes (0.7ms^{-1}) all *I* values are larger than 10. When the mean flow is weak (0.1ms^{-1}), few reefs have I values on the order of unity (Figure 4.9). This indicates that stable lee eddies are not commonly formed in the lee of reefs in the GBR. Furthermore, retention times calculated for these I values using the general additive model obtained for idealized reefs under tidal flows and CGBR reefs indicates that the retention time provoked by lee-eddies at reefs along the GBR are rarely longer than a day. In fact, the maximum retention time found was 4 days, and this had only one occurrence.

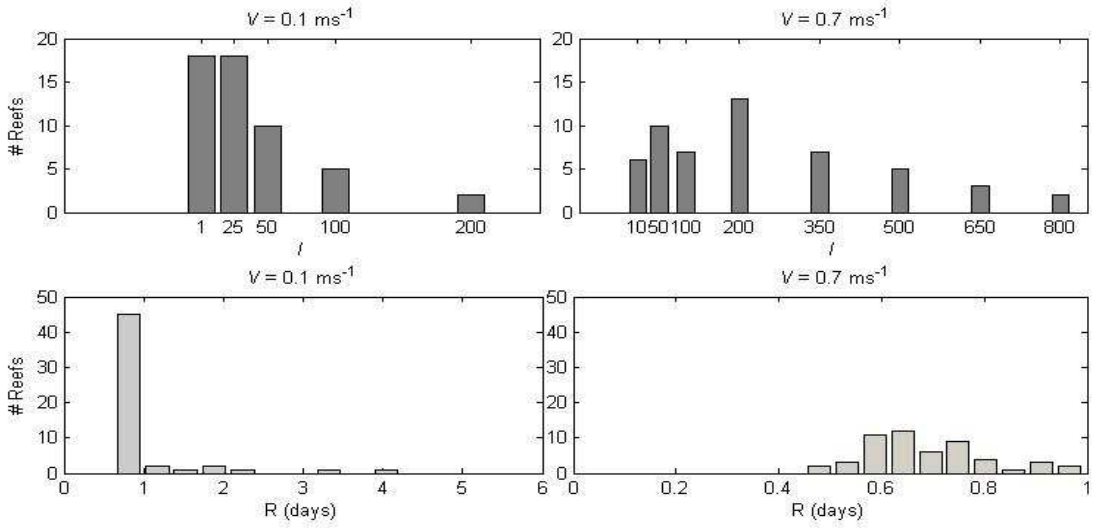

Figure 4.9. Frequency distribution of I (top panels) and associated mean retention times (bottom panels) for reefs along the GBR and velocities of 0.1 ms^{-1} (left hand panels) and 0.7ms^{-1} (left hand panels). The mean retention times were calculated with the GAM model obtained for the idealized and CGBR reefs under tidal flows and realistic circulation regimes pooled together.

4.4 Discussion

4.4.1 Island Wake Parameter and Retention time

This study shows that complex topography limits the potential of the Island Wake Parameter to characterize the wake dynamics. An increase in the Island Wake Parameter only coincides with the formation of more eddies amongst reefs that are relatively isolated. Conversely, reefs that have a 'secondary' reef downstream, such as Yankee and Dip, only developed a few lee-eddies despite having large Island Wake Parameter values. This finding is in agreement with flume and numerical experiment studies which found that the presence of downstream obstacles within a region relative to the main obstacle, and to the main flow, may provoke the diffusion of vorticity and avoid the development of eddies (e.g. Gerrard 1966, Strykowski and Sreenivasan 1990). With respect to particle retention, however, the Island Wake Parameter relates parsimoniously with mean retention time across reefs. In addition, for any given bathymetry (i.e. around a given reef), the Island Wake Parameter does characterize differences in wake flow quality over time, even under realistic non-stationary circulation regimes that prevent the wake flow from reaching an equilibrium state. Specifically, the Island Wake Parameter was consistently smaller when eddies formed and correlates with changes in mean eddy life-span caused by flow variation at individual reefs. In turn, the presence of eddies and their duration influences the time particles remain close to a reef. Consequently, changes in the Island Wake Parameter relate to changes in mean retention time any given reef across circulation regimes.

When we combined the simulations from this chapter with those from chapter 2, strong support for using different models when tidal flows are included and excluded was found. This suggests that the relationship between the Island Wake Parameter and mean retention time is affected by the presence and absence of tidal flows, which in turn promote eddy detachment from the reef. This effect was not significant when idealized reefs were

considered alone (Chapter 2) presumably because of the shorter range of Island Wake Parameters included in the regressions.

Although eddies play a key role in particle transport, they are not the only factor determining retention time. This is evidenced by different retention times found across reefs where lee eddies never developed. Black et al. (1990) found that the concentration of particles close to reefs decays exponentially at a rate that depends principally on free stream current and reef dimensions, increasing with the former and decreasing with the latter; and secondarily, amongst other factors, on shelf depth. The Island Wake Parameter incorporates these variables and relates to them similarly, (i.e., it is proportional to velocity and inversely proportional to reef width). The fact that retention time tends to decrease as the Island Wake Parameter increases for reefs where eddies are absent, suggests that flow velocity, reef width, and depth downstream the reef are crucial in determining not only lee eddy dynamics, but circulation patterns that dictate larval retention or flushing close to reefs. Consequently, differences in mean retention time that are not necessarily induced by the formation of eddies may be captured implicitly by the Island Wake Parameter. Moreover, although the Island Wake Parameter did not discern consistently between eddy dynamics in the wake of non isolated reefs, its relationship with retention time prevailed. Indeed, within reefs that developed eddies, larger Island Wake Parameters values did not necessarily correspond with the constant formation of shorter life span eddies, but they did correspond to shorter retention times. For any given reef, lee eddies are more likely to detach as the flow velocity increases. Both factors, strong currents, and the continuous formation and quick detachment of eddies, would flush particles quickly and provoke short mean retention times. Even though the formation of eddies was suppressed at non isolated reefs, strong currents prevailed; as a result, Island Wake Parameter values were large and, despite not corresponding with the continuous generation of short lived eddies, they did correspond to short mean retention times.

Results from the present study reveal that the longest lived eddies formed behind two of the widest reefs and were associated with the longest mean retention times. This finding agrees with previous studies, which conclude that the probability of retaining larvae increases with reef size (Black et al. 1990). In accordance with studies that demonstrate the suppression of eddy formation and shedding behind obstacles that are not isolated (e.g. Strykowsky and Sreenivanasan, 1990, Parezanovic and Cadot 2012, Bao and Tao 2013), more eddies developed behind reefs where the downstream region is free of topographic mounts. This finding supports the hypothesis of population self-replenishment at isolated islands due to the recirculation of locally produced larvae in lee eddies (Barton 1998; Swearer et al. 1999), provided that tidal currents are not dominant or strong (in which case rapid detachment and dissipation of eddies occurs).

4.4.2 Circulation patterns and particle retention along the Central GBR

Particle flushing occurred more rapidly in December, when the currents were oriented along-shore and were coherent with depth, than in October, when currents were oriented south at the surface and south-west at depth (Table 4.3, figure 4.7). Variation of the current orientation across events is likely to be dictated by the wind direction and the latitude at which the North Caledonian Jet (NCJ), the southern ramification of the Southern Equatorial Current (SEC), approached the continent during each event. It is known that the NCJ impinges upon the continental platform around 18°S latitude (e.g. Gourdeau et al. 2008; Choukroun et. al. 2010), but the exact location at which it veers and gives rise to the Eastern Australian Current (EAC) varies (e.g., Church 1987; Brinkman 2001). Results suggest that during December the NCJ reached the continent north of the modelled region, so the EAC was well defined within the study area and currents were flowing along the coast throughout the water column. Conversely, during October the NCJ may have reached the continent approximately at the same latitude as the modelled region, so the currents were weaker and oriented more

southerly, rather than being aligned with the coastline. In addition, the direction and variability of the wind field across events contributed to similar patterns (i.e., differences in current magnitude and vertical shear). These mechanisms (i.e., NCJ intrusion and wind field), would also have influenced the magnitude of the currents and their orientation over depth; weak currents and vertical shear, such as occurred during October, facilitates the formation of longer lived eddies, which in turn would prolong retention times. Conversely, the fast coherent currents that prevailed in December shortened eddy durations and consequently retention times.

4.4.3 Implications for dispersal

Oceanic circulation is driven by different forcing agents such as wind, atmospheric pressure gradients, sea level change, differences in water density, etc. The variety of mechanisms causing water movement and their interaction induces large temporal and spatial variability in the flow. Results from this study indicate that the occurrence of stable lee-reef eddies under these conditions is rare. Rough estimates of I values for reefs spread throughout the GBR suggest likewise. Unstable eddies may delay particle flushing; however, their potential to prolong retention is limited by their life-span which seems to be reduced to less than a day when tidal currents are strong. The majority of marine organisms produce larvae that develop for hours-months before becoming competent to settle; the duration of the pelagic stage depends on the organism and their reproductive mode. Fish larvae commonly take weeks to months to develop before being able to settle (e.g., Wellington and Victor 1989; Leis 1991), while the majority of invertebrates such as sponges or corals develop within hours or days (e.g., Babcock and Heyward 1986; Maldonado and Young 1999; Hadfield et al. 2001). The time it takes for larvae to develop before settling depends on the reproductive mode. For instance, larvae from fish with pelagic eggs (released into the water column) generally spend more time in the plankton (30-78 days, Jones et al. 2009) than larvae from fish with demersal eggs (laid

on the substrate until they hatch) which can be ready to settle within 9-30 days (Jones et. al. 2009). Similarly, coral brooders have internal fertilization and hatch larvae that have started developing and can achieve competence immediately or within days (e.g., Best and Resing 1987; Baird 2001). In contrast, coral spawners' larvae are fertilized and develop in the water column; as a result, average time to acquire competence is typically about a week (Connolly and Baird 2010). This implies that lee-reef eddies do not have the potential to retain any but the fastest developing larvae (<1 day), thereby reducing genetic differentiation of populations between reefs.

Various studies regarding the dispersal of corals suggest that self-recruitment at individual reefs can be high for populations of brooding corals, but is also supplemented by occasional longer dispersal over tens of kilometres (Jones et al. 2009). For instance, a study by van Oppen et al. (2008), revealed that although GBR populations of the brooding coral *Seriatopora hystrix* are mostly self-seeded and some are highly isolated, a considerable amount of sexual larvae has been exchanged among reefs separated by 10s to 100s of kms. In contrast, populations of broadcast-spawning corals show low levels of genetic variation among reefs. Ayre and Hughes (2000) found moderate to high levels of gene flow along the whole GBR for four different species of coral spawners. Similarly, Smith-Keune and van Oppen (2006), found high levels of gene flow between populations in the North and Central GBR for the spawning coral *Acropora millepora*. In agreement with these results, the mean retention times obtained in this study for reefs of the CGBR indicate that a significant proportion of larvae can be retained up to a day, which implies that a significant proportion of brooders could settle at the natal reef. In contrast, in most cases, the overwhelming majority of the larvae from broadcast-spawning corals would drift away from the natal reef before achieving competence to settle, restricting their recruitment to downstream reefs, ensuring gene flow and retarding genetic differentiation. A study on the population genetic structure of a brooding sponge species (*Rhopaloeides odorabile*) along the CGBR provides results of dispersal patterns that can

be explained by the retention times at individual reefs found in the present study. Mean retention times found in this study were both shorter and longer than the typical time to competence of this sponge (12 hours, Whalan et al. 2008a). In addition, the main flow direction was different for each event. Hence, different dispersal outcomes, i.e., along shore dispersal, across shore dispersal, and self-recruitment, can occur for *Rhopaloeides odorabile* resulting in a pattern of genetic patchiness as observed by Whalan et al. (2008b). Specifically, the absence of genetic differentiation between inner and mid shelf populations of this sponge (Whalan et al. 2008b) can be explained by events of across shelf transport of larvae such as that observed during October when the currents had a predominant south-west direction and retention times at all reefs were shorter than maximum retention times recorded for this species (60 hours, Whalan et al. 2008a). Nevertheless, Whalan et al. (2008b) detected some restrictions to gene flow among some reefs (e.g., reefs of the Lynch complex). Although our study area does not include this reef, its dimensions are similar to those of reefs with the highest retention times (i.e., Centipede, Grub). This suggests that sites from this reef can experience high percentages of self recruitment and contribute to the genetic differentiation found by pair-wise comparisons (Whalan et al. 2008b).

In summary, the mean retention times found in the present study suggest that populations of species which achieve competence to settle quickly (within 1 day) are likely to show some genetic differentiation amongst reefs, but can maintain gene flow through dispersal during events when currents are strong. A small proportion of larvae that require days to develop can experience self-recruitment at specific reefs. For instance, 1% of the particles are retained for more than 4 days during the October event at Centipede and Grub reefs; similarly, maximum retention times larger than 5 days were found at 6 reefs in October and 1 reef in December. Nevertheless, most of these larvae would be advected to downstream reefs before reaching a competent state, explaining the higher levels of gene flow observed across reefs of the CGBR for broadcast-spawning corals.

Empirical studies of fish dispersal show evidence for ecologically significant levels of self-recruitment at the scale of individual reefs or reef clusters for a range of species (Jones et al. 2009). For organisms that acquire competence quickly, such as coral brooders, self-recruitment can be allowed by circulation features, such as eddies. However, larvae that take weeks to months to develop, such as reef fish larvae, would not be retained by eddies throughout their pelagic life. This suggests that other mechanisms, such as swimming behaviour, might play an important role on larval retention and dispersal patterns. In the next chapter of the thesis the effect of swimming activity and interaction with circulation features such as lee eddies on larval retention at individual reefs is investigated.

Chapter 5. The effect of larval swimming behaviour and lee-reef eddies on larval supply

5.1 Introduction

Research on population genetic structure, as well as studies conducting larval tagging and recapture of settlers, have shown that a significant proportion of reef fish with different life traits (i.e. pelagic larval duration [PLD], reproductive mode) can recruit back to their natal reef, or to within tens of kilometres from where they hatched or were released. For instance, Jones et al. (2005) found 15-60% self-recruitment for a population of *Pomacentrus amboinensis* at Lizard Island in the Great Barrier Reef (GBR). Similarly, Harrison et al. (2012) used parentage analysis (i.e. , assigning larvae to their parents through their genetic signature), and found that approximately 7% and 20% of *Plectropomus maculatus* and *Lutjanus carponotatus* experienced self-recruitment, respectively, and an additional 4-20 % dispersed within an area of 1000km^2 (i.e., over linear distances of ~30km). This shows that substantial recruitment close to the area where larvae are released occurs.

Researchers have proposed mechanisms to explain the occurrence of short dispersal or larval retention that leads to self-recruitment. Sponaugle et al. (2002) concludes that any departure from unidirectional or depth uniform flow can provide an opportunity for larval retention. For instance, in environments with vertically stratified circulation, transport of larvae that exhibit vertical migration yields dispersal patterns different from those of passive larvae (e.g., Paris and Cowen 2004, Paris et al. 2007) and can result in higher proportions of larvae arriving to settlement grounds. However, favourable vertical stratification (i.e., currents with varying directions over depth) does not always occur. Dispersal can also be restricted by larval orientation coupled with strong horizontal swimming (Staaterman et al. 2012); however, the extent to which this mechanism can contribute to larval retention has received little attention. Most modelling studies of larval transport invoke processes that explain the distribution of larvae observed in the field, particularly diurnal and ontogenetic vertical

migration (Paris and Cowen 2004). More importantly, those studies that underpin the effect of swimming towards a target often consider that larvae settle if they are within a distance from the reef where they can sense it by smelling or hearing its presence (e.g., Wolanski et al. 1997; Cowen et al. 2006) but only one study has modelled explicitly the transport of larvae within this sensory zone and the settlement habitat (Staaterman et al. 2012). Thus, further studies are necessary to estimate more accurately the potential of horizontal swimming behavior to modify dispersal.

Reef fish larvae have sensorial and behavioural capabilities that allow them to modify their dispersal by recognizing the environment and performing oriented navigation (e.g., Kingsford et al. 2002; Gerlach 2007). In addition, laboratory studies have shown that fish larvae can swim at speeds of the same order of magnitude as currents measured in reef systems (Fisher 2005). Nevertheless, larval distribution is strongly influenced by circulation patterns; indeed, fish larval distribution has been associated not only with larval behaviour, but also with specific circulation features and their interaction. For instance, during an observational study, Burgess et al. (2007) found higher pre-settlement larval concentrations in locations where eddies are known to form close to reefs in the southern Great Barrier Reef (GBR). Similarly, Staaterman et al. (2012) showed that orientation behaviour can increase self-recruitment, and decrease dispersal distances; however the likelihood of settlement depends on the ambient current conditions. For instance, at locations where the circulation was mainly unidirectional, orientation was crucial for increasing probability of settlement. Conversely, at locations where a mesoscale gyre was present, the orientation had much smaller effects. Finally, outcomes from simulations of larval transport show better agreement with observed larval distributions when larval behaviour is invoked (e.g., Wolanski et al. 1997; Gerlach et al. 2006; Sponaugle et al. 2012). These findings indicate that fish dispersal is driven by the interaction of larval behaviour and circulation.

Although fish larvae have the capability to swim, this activity incurs an energetic cost and plays a major part in their energy budget (Brett and Groves 1979). If swimming episodes exhaust energy stores, they can be detrimental for larval growth and survival (Stobutzki 1997). Therefore, the potential to influence dispersal by swimming activity maybe limited or costly, and swimming strategies that enhance successful arrival to suitable habitat are likely to be constrained to those that exploit the currents encountered by larvae. Consistent with this, Armsworth (2001) used an analytical model to examine the effect of different swimming behaviours on energy consumption, and found that optimal trajectories involve larvae using the velocity field in their favour. For instance, the most energetically efficient strategies consisted of swimming upstream of the reef, followed by riding alongshore currents, or swimming vertically to reach boundary layers where currents are slower. Nevertheless, swimming behaviours that strategically take advantage of beneficial circulation structures have rarely been implemented in biophysical models in order to examine their effect on larval dispersal patterns. Furthermore, the extent to which energy consumption due to swimming performance during dispersal affects larval survival has been largely neglected. This is particularly important since food availability for larval fish can be scarce (MacKenzie et al. 1990) limiting the opportunity to replenish energy storages.

This chapter focuses on the interaction between horizontal swimming behaviour and reef scale circulation (~300m). Specifically, it investigates how this interaction affects larval retention at individual reefs by tracking larvae within the reef proximity. Previous models that implement swimming behaviour do not investigate larval transport at such spatial scales and only Staaterman et al. 2012 has explored larval trajectories within the region at distances on the order of km or less from the reef. In addition, this chapter considers energy expenditure caused by the swimming performance of fish larvae. Some studies of active larval transport take mortality into account, but they rarely focus on the effect on survivorship of energy used

for swimming. My approach is to examine the effect on larval retention close to reefs of horizontal swimming, energy expenditure caused by swimming, and reef eddies in isolation. An idealized setting with a single reef is used to facilitate interpretation of future work exploring these mechanisms in more realistic environments.

The interaction of currents with reefs normally forms lee eddies that can retain larvae while the eddies persist. Results from Chapter 2 showed that stable lee-eddies can produce mean retention times of passive larvae of up to approximately 6 days. However, when tidal currents are strong, their oscillating nature provokes the detachment and downstream advection or dissipation of these eddies. Thus, mean retention times are reduced considerably, in some cases to less than a day. Similarly, results from Chapter 4 indicate that in regions where tidal currents are intense (e.g., in the central Great Barrier Reef), the life span of lee-eddies is often on the order of hours. Therefore, it is unlikely that lee-reef eddies retain fish larvae over time frames sufficient to account for self-recruitment (i.e., weeks-months) in the absence of swimming. Nevertheless, if larvae swim towards areas where such eddies form, they potentially could exploit these features to remain close to a reef.

This study examines the effects of lee-eddies with different durations, swimming behaviour with and without exhaustion due to energy depletion by swimming activity, and their interaction on the supply of larvae to reefs. Specifically, it investigates if eddies facilitate the arrival of larvae to reefs, and if fish larvae that engage in swimming activity can exploit the presence of lee-eddies to increase the probability of retention or arrival to suitable settlement habitat relative to larvae retained in a scenario without eddies. In addition, the energy expenditure associated with swimming performance is considered to determine when it is sufficient to cause larvae to become exhausted. Two extreme scenarios are considered. The first assumes that, while swimming, larvae consume their energy reserves until they are

depleted. A second assumes that larvae can feed enough to replenish the energy used to swim and do not become exhausted.

5.2 Methods

5.2.1 Hydrodynamic model and grid

Larval transport simulations were conducted using the Sparse Hydrodynamic Ocean Code (SHOC), a finite difference model based on the three-dimensional equations of momentum. This model contains a Lagrangian particle tracking algorithm that permitted recording the positions of larvae throughout the simulation period, and that was modified to incorporate swimming behaviour (Appendix 2). A common grid of approximately 30 km^2, nine depth layers, and the presence of a reef located in the centre was generated and used for all the simulations. Similar to the grid utilized in Chapter 2, the vertical resolution changed with depth, going from 0.5 m at the surface to 5 m at the bottom. A higher resolution at the surface allows solving accurately the interaction of the flow with the reef surface (2-10 metres deep). The horizontal spatial resolution was approximately 300 m and was sufficient to solve explicitly the structure of the circulation at the reef-scale, particularly the formation of lee-eddies. Designing a grid with an idealized reef facilitates generating specific circulation scenarios with the presence of stable and unstable eddies, and therefore, allows testing the effect of eddy dynamics on larval transport. Nevertheless, a reef from the central Great Barrier Reef (i.e., Grub) was used as a model to assign dimensions to the idealized reef used for the simulations. Specifically, this reef is approximately 5km wide in the direction perpendicular to the direction of the dominant current, 3 km long, and rises from 70 m to 2-10 m deep. Similarly, the life-span of unstable eddies reproduced for the simulations were in agreement with those obtained for eddies formed downstream of reefs in the central GBR (Chapter 4), when circulation regimes similar to those modelled in Chapter 4 were imposed.

5.2.2 Circulation scenarios and boundary forcing

The grid was oriented in a 'North-South' 'East-West' direction and had four open boundaries through which the model was forced. The reef was located in the centre of the grid and the boundaries were far enough (41-45 grid cells) from the reef edge to ensure no effect of the boundaries in the region where particle transport was explored (reef vicinity). Forcing conditions similar to Chapter 2 were utilized; unidirectional constant flows at the north and south boundaries, which produce flows that resemble a low frequency current such as the Eastern Australian Current, and sea level time series at the east and west boundaries to reproduce perpendicular tidal flows. This condition, i.e. low frequency current and perpendicular tidal flows, is particularly common along the GBR (Wolanski and Pickard 1985). Furthermore, results from Chapter 4 demonstrate that eddies form downstream of reefs along the GBR, where such flow conditions prevail. The sea level time series were synthetically generated as the sum of diurnal and semidiurnal harmonics. These boundary conditions were combined to achieve velocities of approximately 0.2 ms^{-1} within the domain, which correspond to weak or mean currents observed close to reefs within the GBR lagoon (Wolanski and Pickard 1985), and to produce three different circulation scenarios: one where eddies are absent, a second with unstable eddies with life-spans of 2-6 hours, which is the common duration of lee eddies formed in the central GBR (see Chapter 4, Table 4.1), and a third with stable eddies.

5.2.3 Larval behaviour, swimming speed model and energy depletion model

Simulations were conducted for passive larvae, and for active larvae. Vertical swimming can increase the potential of swimming behavior on larval retention, particularly if implemented to exploit boundary layers or stratified circulation. However, this study focuses on the effect of oriented horizontal swimming where the exploited circulation structures are lee reef eddies. Moreover, results from chapter 4 indicate that lee eddies that formed behind reefs along the Central Great Barrier Reef were often coherent with depth, thus, approaching a

reef from downstream would be similar at any depth throughout most of the water column, once a larva is on the vicinity of the eddy. Therefore, larvae were set to swim horizontally. All larvae were advected by the 3D velocity field explicitly solved by the hydrodynamic model plus a random diffusion velocity. The diffusion velocity was determined by drawing a random number from a Gaussian distribution with mean zero and standard deviation equal to the diffusion coefficient that represents circulation at smaller spatial scales than the grid size (that is, 0.09 m^2s^{-1}: Okubo 1971). The same approach was taken in Chapters 2 and 4 to simulate the transport of particles and parameterize flow structure at smaller scales than the model gird.

Passive larvae did not have any behaviour and were only advected by oceanographic currents, whereas active larvae were advected by the ocean currents plus a swimming horizontal velocity. For this purpose, swimming velocity fields were constructed using the swimming orientation angle and the swimming speed. The swimming orientation changed over the horizontal space and was kept constant over time. The swimming speed changed over time within regions where swimming behavior was invoked, and was set to zero within regions where swimming behavior ceased. The rationale used to determine swimming orientation, regions where swimming ceased, and the method to compute speed over time is described below. Larvae were released randomly across depths and active larvae displayed the same horizontal swimming behaviour regardless of their vertical position.

Field studies have identified ambient reef sound as a navigational cue for fish larvae (Tolimieri et al. 2004). Sound is potentially useful for controlling fish behavior because it travels rapidly (ca. 1500 m/s) in water, attenuates slowly, and provides navigational information regardless of the position of larvae with respect to the reef (i.e., upstream or downstream) (Popper and Carlson 1998). Therefore, fish larvae were considered capable of sensing a reef by hearing and set to swim if they were within a distance of approximately 5km in any direction from the reef edge. This distance is somewhat arbitrary but was kept constant throughout simulations and lies within the range of distances (1-10km) selected by studies of

active larval transport that implement larval navigation (e.g., Wolanski et al. 1997; James et al. 2002). In addition, Staaterman et al. (2012) found that the most advantageous orientation cue operates over distances of 1-5km.

Assuming that fish larvae can hear the presence of a reef, within a 5km distance from the reef edge, larvae were set to swim horizontally towards the closest edge of the reef depending on its horizontal position at every time step. Those larvae that reached the reef from upstream were allowed to swim past the reef into a downstream region; this permits larvae to remain close to settlement grounds and avoid predation which is likely higher on the reef (e.g., Irisson et al. 2004).

In addition, larvae were set to stop swimming if they were within the region where eddies normally form. This is a reasonable assumption because this region is downstream of the reef, as a result the water would have a specific chemical signature that, according to laboratory studies which have tested fish larvae olfactory capabilities (e.g., Atema et al. 2002; Gerlach et al. 2007), can be recognized by the larvae. The region where eddies (stable and unstable) normally formed was previously identified from the velocity fields obtained with simulations of all circulation scenarios (see Figure 5.1 for a diagram) and used to determine the region where larvae would cease swimming and construct the swimming velocity fields used to advect active larvae.

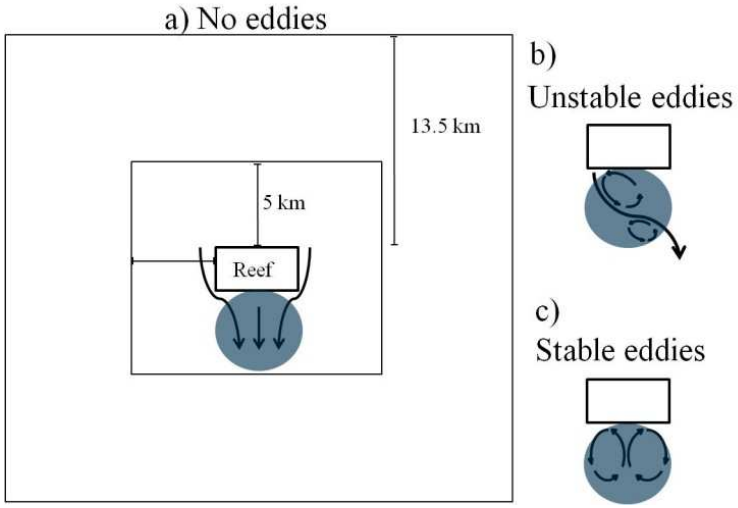

Figure 5.1 Top view diagram of: a) the grid setting for the larval transport simulations exemplifying the circulation scenario without eddies; b) circulation scenario with unstable eddies, and c) the circulation scenario with stable eddies. In panel a) the outer square delimits the simulation domain; the inner square delimits the region where active larvae swam. In all panels the blue region represents the area within which swimming behaviour ceased.

Studies have clearly shown that the speed at which fish larvae are able to swim changes as larvae develop (e.g., Clark et al. 2005). Therefore, the swimming speed was set to change as larvae aged following an empirically-calibrated model proposed by Fisher (2005; cf. Staaterman et al. 2012, who used Fisher's equations in their dispersal model as well). This model describes changes in maximum swimming speed (*S*) as fish length (*L*) increases, according to:

$$S(L) = 10^{((L_n)*log_{10}(S_{sett}-S_{hatch}))} + S_{hatch} \quad \text{eq. 5.1}$$

S_{sett} is swimming speed at settlement, S_{hatch} is the swimming speed at hatching, and L_n is the normalized length given by:

$$L_n(t) = [log_{10}(L(t) - L_{hatch})/log_{10}(L_{sett} - L_{hatch})] \quad \text{eq. 5.2}$$

L_{hatch} is the length at hatching, L_{sett} is the length at settlement, and *L(t)* is a vector that represents the length over time of fish larvae with a constant growth rate (Fisher 2005), computed as:

$$L(t) = ((L_{sett} - L_{hatch})/LD * t) + L_{hatch} \quad \text{eq. 5.3}$$

LD is larval duration. S_{hatch} was obtained from an empirical relationship between S_{hatch} and L_{hatch} presented in Figure 2 of Fisher (2005):

$$S_{hatch} = 1.24 * L_{hatch} - 1.20 \qquad \text{eq. 5.4}$$

S_{sett} was extracted from Figure 1 of Fisher (2005) which shows the mean and SE of swimming speed of late stage larvae. The rest of the data necessary to compute *S* was retrieved directly from Fisher (2005). All the data necessary to compute *S* is summarized in Table 5.1, and Figure 5.2 shows how swimming velocity changes with age and thus length for different fish families. For the simulations in this chapter, I selected data from the family *Lutjanidae*; this family includes commercially important fishery species on the GBR (Mapstone et al. 2004).

Table 5.1. Data used to compute Swimming speed as larvae age, *S(L)* gathered from Fisher (2005).

	Lutjanidae	Acanthuridae	Apogonidae	Chaetodontidae	Lethrinidae
Length at hatching L_{hatch} (cm)	2.1	1.7	2.6	1.5	1.6
Length at settlement L_{sett} (cm)	27.7	29.4	12.6	19.8	21.8
Larval duration LD (days)	36	64	22.5	33.6	35.8
Swimming speed at hatching S_{hatch} (cms^{-1})	1.40	0.91	2.02	0.66	0.78
Swimming speed at settlement S_{sett} (cms^{-1})	52	61	20	34	40

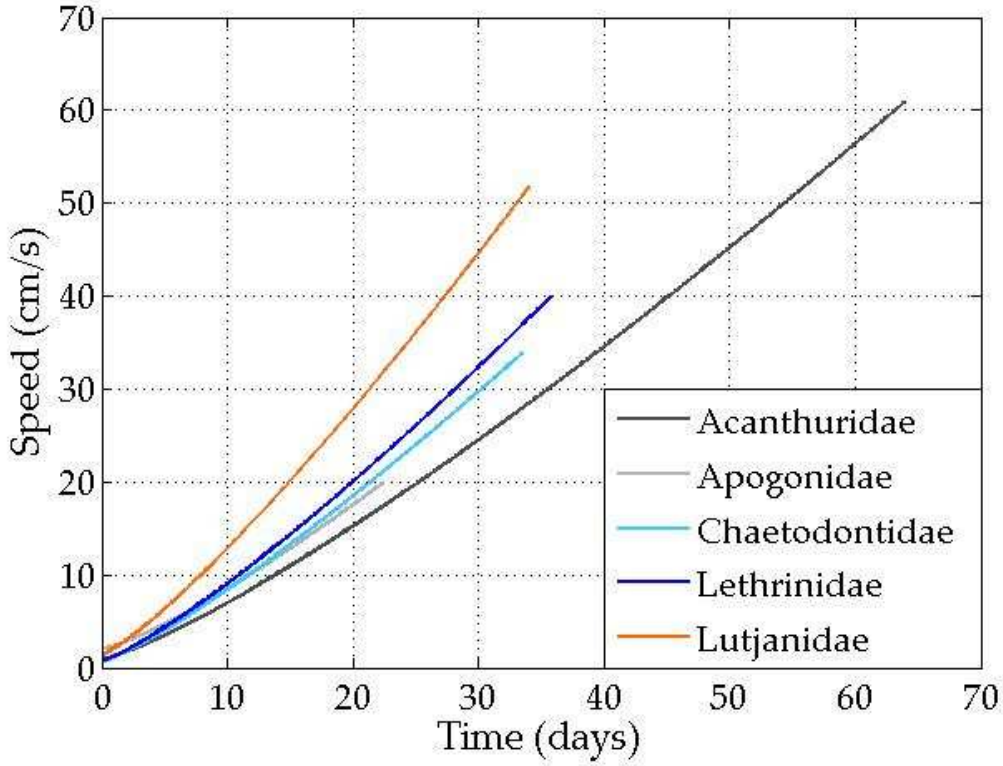

Figure 5.2. Swimming speed as larvae age for different fish families computed using eq. 5.1 and data presented in Table 5.1.

Locomotion is energetically expensive for fishes (Brett and Groves 1979; Beamish 1978). Therefore, larvae can deplete their energy reserves due to swimming activity and become exhausted. Studies of fish larvae swimming activity have shown that swimming endurance depends upon food availability (Fisher and Bellwood 2001). In addition, Stobutzki (1997) showed that different energy sources such as proteins, carbohydrates and lipids are utilized by reef fish larvae that perform swimming activity, and that initial levels of energy reserves correlate with distance swum. Thus, swimming activity incurs an energetic cost and can only be sustained if energy reserves are available (Stobutzki 1997). In turn, energy reserves are determined by food availability and ingestion rates. Kerrigan (1994) examined the effect of food supply on the deposition of energy reserves of juvenile fish and found a considerable difference between the lipid content of fully fed and starved fish. In the ocean, food availability and ingestion vary substantially depending upon hydrodynamic conditions that regulate

primary productivity, determine plankton densities, and influence rates of prey encounter. For instance, upwelling systems can generate blooms of plankton distributed in high density patches; this increases food availability and facilitates feeding success (Legget and Deblois 1994). However, as micro-turbulence associated with upwelling events increases, prey capture success decreases (MacKenzie and Kiorboe 2000).

Results from studies quantifying food requirements of fish larvae for survival show that the minimum plankton densities needed to subsist vary broadly depending upon the species. Houde (1978) reviewed these results and concluded that food concentrations that would ensure significant survival and growth occur in coastal and sometimes in oceanic waters. However, reported values of plankton densities close to reefs are typically low. For instance, Hamner et al. (1988) found densities between 0.27 and 5.80 μgl^{-1} at Davis reef in the GBR; and Meekan et al. (2003) found densities of 26.77 and 74 μgl^{-1} at Ningaloo reef, Western Australia, for summer periods when conditions for upwelling events were rare and common respectively. Moreover, ingestion rates increase steeply with food density until ~185 μgl^{-1}, therefore, densities reported at locations along the GBR are well below those associated with maximum ingestion rates (i.e., satiation: MacKenzie et al. 1990). Similarly, for juveniles of *Pomacentrus amboinensis*, a reef fish, food availability appears to limit growth in shallow and deep habitats (Jones 1986). Hence, in oligotrophic ecosystems, such as reefs, it is likely for food supplies to be below the minimum required for fish larvae to maintain energy reserves.

In order to account for energy expenditure due to swimming during dispersal, two cases that considered extreme probabilities of energy replenishment were simulated in this study. The first case considered that larvae encountered and ingested enough food to restock the energy utilized for swimming. A second case considered that larvae encountered only enough food to provision basal metabolism and growth, relied entirely on their initial energy reserves to swim, and would not survive if the energy spent swimming exhausted their energy

Fisher and Bellwood (2002) provided an empirically derived relationship between the time unfed larvae could swim before becoming exhausted (t_e):

$$log_{10}(t_e) = -2.95 * log_{10}(S) + c \quad \text{eq. 5.5}$$

where t_e is time to exhaustion, *S* is swimming speed and *c* is a constant whose value depends on the fish family. Fisher and Bellwood (2001) found that swimming endurance of *Amphriprion melanopus* depended upon feeding; this indicates that exhaustion is determined by depletion of energy reserves, so I assumed that time to exhaustion is inversely proportional to the rate of depletion of energy reserves. In turn, if energy reserves are depleted and there is absence of sufficient food (as my second case considers) larvae would die. Therefore, time to exhaustion represents the time larvae can sustain swimming behavior before depleting their energy reserves and dying. Hence, if larvae reached swam over a period of time equivalent to the exhaustion time it was considered to die. The value of *c* was obtained by rearranging equation (5.5) and substituting data from a study by Stobutzki and Bellwood (1997), who reported the times several fish larvae from the Lutjanidae family endured swimming at 0.135 ms^{-1}. These data, and corresponding *c* values, are summarized in Table 5.2, and the shape of the relationship between time to exhaustion and swimming speed is shown in Figure 5.3. The maximum and minimum values of *c* correspond to larvae that swam the longest and the shortest times before becoming exhausted respectively, while the average corresponds to the average time that larvae could sustain swimming activity before becoming exhausted (Stobutzki and Bellwood 1997).

Table 5.2. Data for swimming endurance of Lutjanidae fish larvae from Stobutzki and Bellwood (1997) and corresponding *c* values computed using equation (5.5)

	Endurance (hours)	$c = 2.95 * log_{10}(S) + log_{10}(te)$
Minimum	25.9	2.40
Average	156.95	3.19
Maximum	288.5	3.45

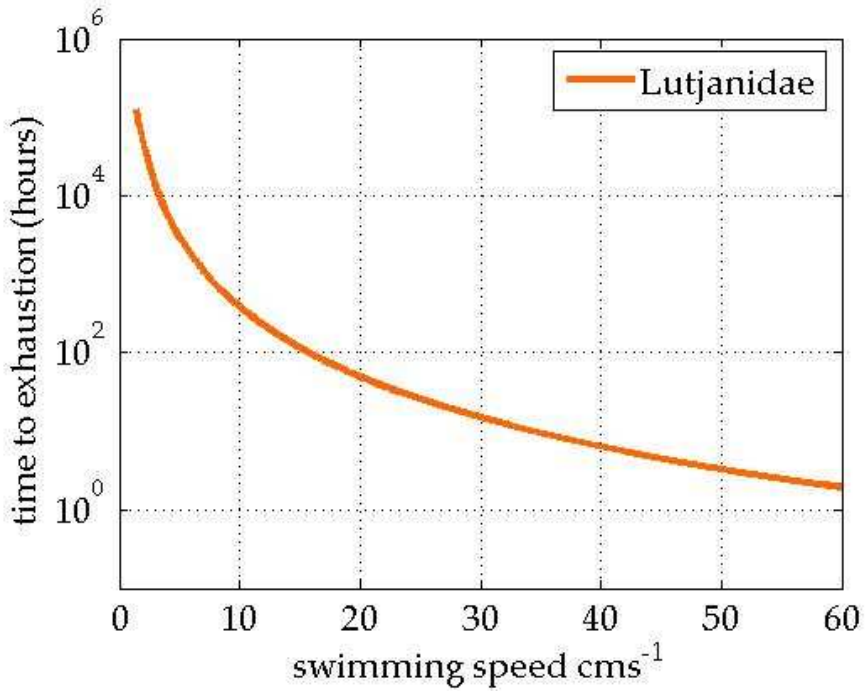

Figure 5.3. Time to exhaustion as a function of swimming speed for fish larvae of the family *Lutjanidae* computed using eq 5.5 and *c* average value from Table 5.2.

All larvae were followed through time thus a time series of swimming speed was obtained for each larva. The proportion of initial energy reserves expended swimming was computed hourly, according to eq.6 for each of the values of *c* presented in Table 5.2. In this manner, variability of individuals within the Lutjanidae is considered. Once cumulative energy expended reached 100% of energy reserves, larvae were considered to be exhausted. All calculations of energy expenditure used to discern which larvae became exhausted were run offline, that is, from outputs of active particle tracking over the whole simulation period.

5.2.4 Larval release and retention

For each simulation, a distance of 5 km from the edge of the reef was used to delimit a square that encompassed the reef within which particles would be released; 10,000 virtual passive or active larvae were randomly released anywhere inside this larger square, and randomly distributed in the vertical through the water column. By releasing larvae in such manner we simulated a situation where larvae were advected into the reef surroundings (i.e.

within the large square) at different stages of their pelagic life, specifically at 6, 12, 18, 24 and 30 days old, hereafter referred to as age of release. In addition, simulations releasing larvae on top of the reef at age 0 were also conducted to investigate self-recruitment, where self-recruitment indicates the percentage of larvae that remains at its reef source relative to the total amount of larvae released at the same reef. Simulations were run for a duration equivalent to the pelagic larval duration (PLD), lutjanids larval duration varies among species within a range of about 15-48 days (Lindeman et al. 2000). I chose an intermediate value of 36 days for my simulations. For all simulations, the 3D position of each larva was recorded hourly for the duration of the simulation, or until the larva exhausted its energy reserves. Larvae were designated as "retained" if they were within the region where eddies normally form at the end of the simulation (i.e., day 36). This area was selected because if eddies are present larvae can recirculate and be brought back to the reef; the same region was used for the circulation scenario without eddies to have a consistent measure of retention throughout scenarios. Moreover, this area extends to approximately 5km from the reef; given the swimming capabilities of Lutjanid reef fish larvae at the end of their planktonic life (~0.55ms^{-1}), such distances can be covered within 4 hours even against currents of 0.2 ms^{-1}. Similarly, the distance swam by fish larvae of different families, at an average speed, extends to tens of kilometres (Figure 6 from Stobutzki and Bellwood 1997). The percentage of retained larvae was quantified separately for every age of arrival to the reef and each circulation scenario.

5.2.5 Analysis

The percentage of retained larvae, passive or active, was computed for each circulation scenario (i.e., no eddies, stable eddies and unstable eddies), and for each age of release. For active larvae, the percentage of retained larvae was also computed for each case regarding energy expenditure due to swimming (i.e., with and without exhaustion, Figure 5.4). Comparison of such values allowed quantifying the potential of: 1) eddies with different

dynamics, 2) horizontal swimming behaviour with and without assuming energy expenditure, and 3) the interaction of eddies (stable and unstable) with horizontal swimming behavior, with and without assuming energy expenditure, to enhance: 1) self-recruitment (the percentage of larvae released at age 0 that recruits at the source reef), and 2) retention of larvae released at the age of 6 days or older. In addition, the time spent swimming when eddies are absent, unstable, and stable was quantified to elucidate if the presence of eddies diminishes the time larvae needs to swim to remain close to a reef preventing the consumption of energy reserves. In other words, it allows assessing the potential for larvae to exploit eddies in order to remain close to the reef and avoid the depletion of energy reserves caused by constant swimming associated with different swimming strategies.

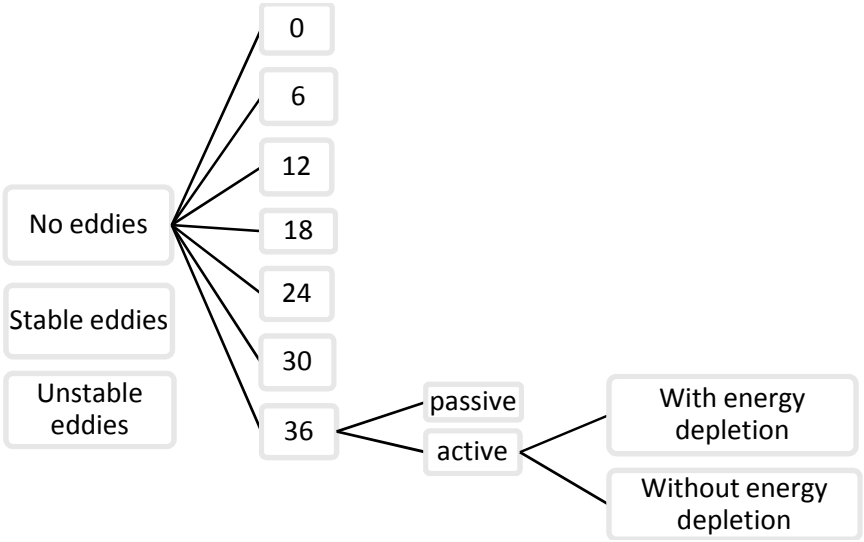

Figure 5.4 Diagram of a hierarchical structure for the simulation factors; first column: circulation regimes, second column: age of larvae at release, third column: behaviour, fourth column: energy consideration.

5.3 Results

5.3.1 Effect of eddies, passive larvae

The presence of stable eddies had a large effect on the retention of late-stage passive larvae. When eddies are absent (black line in Figure 5.5a), larvae do not remain close to the

reef regardless of the age of larvae when they are released. When eddies are unstable (blue line Figure 5.5a), 0.8-3% of the larvae are retained, depending upon the age of release. Finally, when eddies are stable (red line Figure 5.5a), 0.6-9% of the larvae are retained.

5.3.2 Effect of swimming behaviour

When energy consumption was considered, three different values of *c* (eq. 5.5, Table 5.2), associated with different swimming endurance across organisms, were utilized to compute the amount of spent energy and discern which larvae survived. However, the change in energy consumption and larval survival associated with different *c* values was negligible (~0.1% of larvae). Therefore, only the results obtained with the average *c* are presented and discussed.

In contrast to the fate of passive larvae, orientation and horizontal swimming behaviour allows a significantly larger proportion of larvae to arrive to the reef and remain close to it, even in the absence of eddies. However, the probability that active larvae remain close to the reef is highly sensitive to energetic considerations. When energy consumption is considered, no larvae are retained when they are released within the first 18 days of age, and even for larvae released at the age of 30 days retention is only 6% (Figure 5.5c, black line). In contrast, when assuming that larvae can feed to replace the energy spent swimming, retention is extremely high. Approximately 100% of larvae are retained close to the reef when they are released at an age of 18 days onwards, close to 95% of the larvae released at an age of 6-12 days are retained, and self-recruitment occurs for 63% of the larvae (Figure 5.5b, black line).

5.3.3 Effect of swimming behaviour in the presence of eddies

The proportion of retained larvae is considerably larger when, eddies are present and horizontal swimming behaviour also takes place. When full replenishment of energy reserves is assumed, the presence of unstable and stable eddies increases the proportion of active larvae

that self-recruit by 10% and 26% respectively, relative to the no eddy case (Figure 5.5b). In contrast, if cumulative depletion of energy reserves is assumed, self-recruitment only occurs if stable eddies are present. Overall, the percentage of retained active larvae is considerably larger when eddies are stable (26-81%, red line in Figure 5.5c) than when eddies are unstable (0-15%, blue line in Figure 5.5c). These are much larger than the proportions of passive larvae arriving to the reef under the same circulation scenarios (0.3-9%, depending on the age of release: Figure 5.5a).

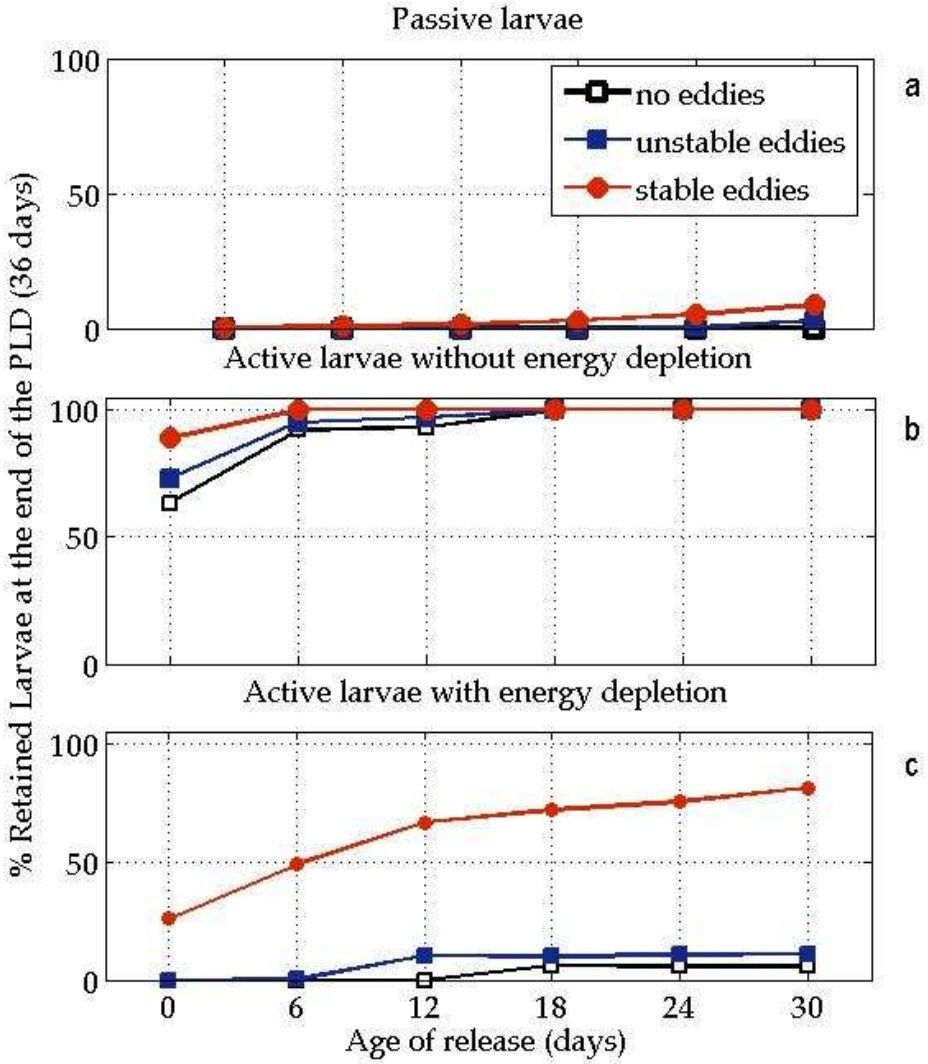

Figure 5.5. Percentage of larvae retained at each age of release (i.e. the larval age assumed when larvae where first placed in the model domain 5 km from the reef) and circulation scenario (i.e. no eddies, stable eddies and unstable eddies) for: a) passive larvae b) active larvae without considering energy depletion, and c) active larvae when energy depletion was considered.

The proportion of time spent swimming, relative to the time spent in the plankton, is longest when eddies are absent, intermediate when eddies are unstable, and shortest when eddies are stable. Because larval swimming capabilities develop with age, older larvae maintain their position with shorter bouts of swimming than young larvae. As a result, the time larvae spend swimming, relative to the time spent in the plankton, also decreases with age. There are strong differences between the three circulation scenarios (i.e., no eddies, unstable eddies and stable eddies: Figure 5.6), except for those between no eddies and stable eddies for larvae released at 30 days of age.

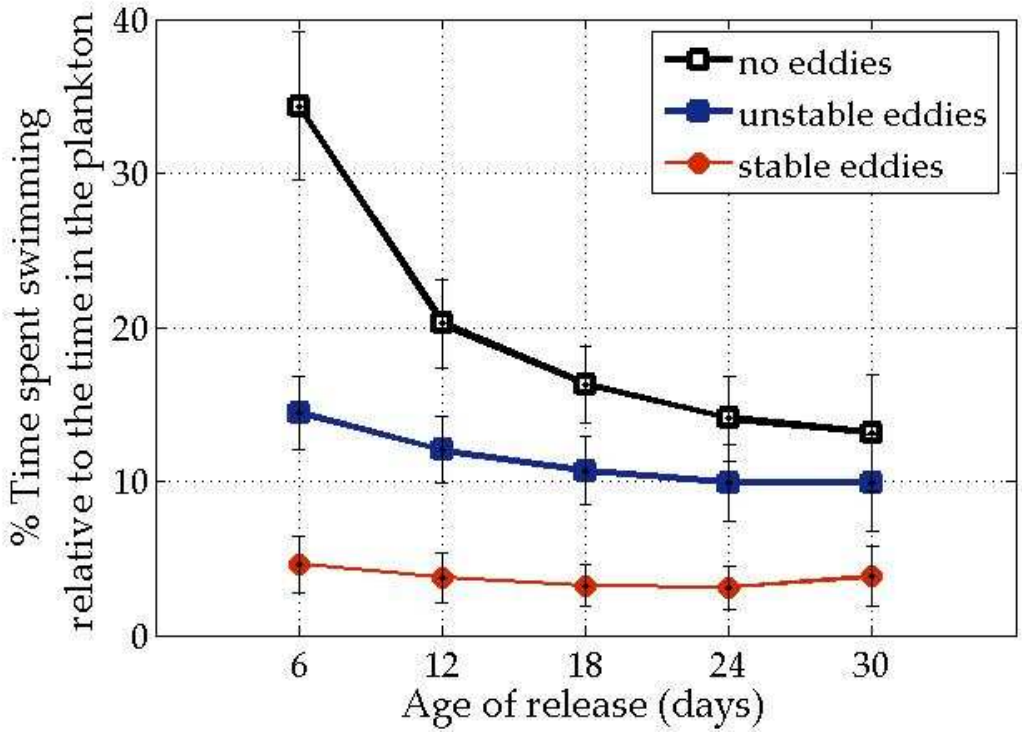

Figure 5.6. Mean +- SD of time spent swimming relative to the time spent in the plankton for different larval ages at the time of release and circulation scenarios when energy consumption was considered.

5.4 Discussion

This study shows that oriented horizontal swimming facilitates larvae staying close to suitable habitat for settlement. However, the extent to which horizontal swimming can modify dispersal by facilitating self-recruitment, or retention of larvae advected into a reef's

proximity, varies considerably depending on the extent to which larvae can replenish energy consumed by swimming bouts. In addition, the presence and duration of lee eddies play a key role by recirculating larvae, reducing larval swimming time and allowing larvae to avoid exhaustion. This chapter confirms that the presence of lee-eddies does not suffice to retain passive larvae over time scales of weeks, even if eddies are stable. Only active larvae that engaged in oriented horizontal swimming were retained at the source reef, and only when long-lived eddies were present, or energy reserves were assumed to be replenished.

5.4.1 Energetic considerations

The increase in retention due to swimming activity varies substantially depending upon energetic considerations. This is apparent from the large disparity between the proportion of retained larvae when energy depletion is not considered (Figure 5.5b) and the proportion retained when depletion of energy reserves occurs (Figure 5.5c), particularly in the absence of eddies (black lines). This result highlights the need to account for energy expenditure due to swimming strategies implemented in biophysical models that investigate dispersal patterns, and for estimating likely rates of energy acquisition in the field.

Swimming has been recognized to play a crucial role in fish energy budgets because the energy required for maintenance is comparatively low relative to that required for locomotion (Brett and Groves 1979). Concurrently, swimming capabilities of reef fish larvae, such as the duration they can swim, depends upon energy reserves. For instance, fish larvae with higher levels of lipids and carbohydrates can swim longer distances (Stobutzki 1997). Similarly, Fisher and Bellwood (2001) found that swimming endurance of late-stage *Amphripion melanopus* larvae depends considerably on food ingestion. Specifically, they found that fed larvae almost doubled the average distance they could swim, relative to unfed larvae. These studies indicate that energy reserves, food availability and consumption will constrain the capability of fish larvae to swim and modify their dispersal.

A study by Spounaugle et al. (2009) shows that, for a common coral reef fish (*Thalassoma bifasciatum*) gut fullness is significantly related to prey abundance across Florida straits between USA and Bahamas, suggesting that larval feeding rates are highly sensitive to changes in food availability over realistic ranges. In turn, spatially heterogeneous distribution of food has the potential to substantially influence larval growth and survival or coral reef fish larvae (Sponaugle et al. 2009). Therefore, ingestion rates of fish larvae can result in a gradient of possible realizations from none to full replenishment of energy reserves. If larvae are able to feed enough to maintain energy reserves during their development, horizontal swimming behaviour has the potential to modify considerably dispersal patterns, by augmenting larval retention close to reefs, 5.5. Nevertheless, the planktonic larval stage is highly vulnerable to predation and starvation (Llopiz and Cowen 2009). This study does not consider predation and estimates of retained larvae could be overestimated. If the risk of predation is similar across the simulated scenarios, relative differences in larval retention amongst them would remain robust. Eddies associate with vertical water movements that typically induce nutrient input; this eventually produces local population growth at each trophic level and ultimately attracts predators (Bakun, 2006). Therefore, regions where eddies form are likely to have a larger risk of predation compared to regions where eddies do not form. Differences in predator abundance between regions where eddies are stable or unstable might be more subtle. As a consequence, the greater number of retained larvae when eddies are stable compared to unstable is likely to be similar regardless of predation. Conversely, differences in predation could decrease the extent to which eddies increase larval retention. Results from this chapter show that even when energy depletion caused by swimming activity and consequent mortality is considered, the presence of stable eddies may allow for self-recruitment. However, regions where eddies form are often productive and may consequently have large predator abundances. The extent to which high predation risk constrains the enhancement of larval retention caused by eddies warrants further investigation.

One of the primary causes of high mortality rates and survival in the pelagic zone is starvation (Job and Bellwood 2007). In addition, differences in body composition between well fed laboratory raised larvae and wild larvae are significant. For instance, Kerrigan (19944) found a 3.5 fold difference in total lipid between fully fed and field fish larvae of *Pomacentrus amboinensis*: the lipid content of the field fish was similar to starved fish. This strongly suggests that reef fish larvae rely heavily on energy reserves throughout their planktonic life. If so, this chapter results suggest that swimming behaviour is likely to substantially increase the retention close to a reef of late stage larvae, but is likely to have much smaller effects on recruitment at the source reef (Figure 5.5 panel c).

5.4.2 Effect of eddies and swimming behaviour

Connectivity is influenced by larval behaviour and circulation regimes (e.g., Paris et al. 2007). This study illustrates how the interplay of horizontal swimming behaviour and lee-eddies determine larval transport in the proximity of reefs. Even though this study implemented swimming capabilities and pelagic larval duration of the family Lutjanidae, the results are likely broadly indicative of patterns of larval retention arising from the interaction of behaviour and lee-eddies. Although other fish families do have somewhat stronger or weaker swimming capabilities than Lutjanids, the order of magnitude of their swimming speeds are comparable, particularly during the early stages of development (Figure 5.2). Variation in orientation (among larvae or over time) was not considered (e.g. through biased random walks). Such variation could influence the extent to which larvae modify their transport through swimming behavior. Since larvae were set to orient constantly towards the reef in the simulations presented here, incorporating such variability would reduce the efficiency of the swimming strategy and the amount of larvae remaining close to the reef would diminish, potentially increasing the importance of physical recirculation processes such

as lee reef eddies. Nevertheless, variability in larval energy expenditure due to swimming is implicitly considered through the implementation of different *c* values in equation 5.5, and would likely have effects similar to those of variation in orientation (which would essentially extend the time and energy required to swim to the reef or swim to maintain position near the reef). This analysis showed small effects of swimming efficiency. This suggests that variation in swimming orientation, unless very large, would be unlikely to substantially alter the results of this chapter.

The presence of unstable and stable eddies allows passive larvae close to the final phase of their pelagic life to stay close to a reef. However, if larvae are advected close to a reef early in their development, only very stable eddies would allow recirculation of passive larvae long enough to retain them until they are ready to settle. Thus, when eddies are unstable or absent, swimming performance is crucial to remain close to the reef for periods of time longer than a week (Figure 5.5a). Conversely, when larvae are active, the presence of eddies even with short life-spans facilitates larval retention at any stage of arrival. When exhaustion does not occur, swimming behaviour by itself induces significant retention of larvae. Nevertheless, the presence of unstable and stable eddies markedly increases the retention of early stage larvae and consequently self-recruitment (Figure 5.5b). When energy consumption is considered, the proportion of larvae advected close to the reef that are ultimately retained is larger when eddies are present than when they are absent, for most of the larval ages of arrival (Figure 5.5 panel c). Similarly, the time larvae swim is significantly shorter when eddies are present (Figure 5.6) suggesting that eddies recirculate larvae, keeping them close to the reef, and reducing energy depletion due to swimming activity. Moreover, stable eddies are necessary for self-recruitment to occur. Thus, oceanographic and biological processes can promote retention of larvae close to a reef once they are advected in their vicinity at some

point of their pelagic life, but a combination of both factors seems necessary for self-recruitment to occur if larvae depend on their initial energy reserves.

Studies of population structure of reef fish indicate that considerable recruitment occurs within tens of kilometres, suggesting that larvae have the ability to actively restrict their dispersal. Biophysical models have shown that larval vertical migration reduces larval export where there is vertical stratification (e.g., Paris and Cowen 2004, Paris et al. 2007). Theoretical studies have shown that exploiting boundary layers can also facilitate returning to a reef (e.g., Armsworth, 2000). Nevertheless, if flow vertical stratification is not favourable, vertical migration might not result in retention. Similarly, close to offshore reefs with a steep shelf drop, reef fish larvae might not be able to reach the bottom and exploit slow currents associated with boundary layers. This study shows that horizontal swimming, and its interaction with lee eddies, are alternative mechanisms by which larvae can remain close to suitable habitat particularly if food availability is high enough for fish to replenish, at least partially, their energy reserves. Along the Central GBR, tidal flows are dominant and lee-reef eddies detach from the reef with tidal reversals, therefore, eddies are commonly unstable, prevailing only for a few hours (see results Chapter 3). Under this circulation regime, swimming behaviour is crucial to remain close to a reef for periods on the order of weeks, and a significant proportion of the larvae advected close to reefs can be expected to remain within suitable habitat and achieve settlement. This mechanism can contribute to dispersal over shorter distances than those predicted solely by circulation patterns if larvae are advected close to suitable habitat particularly later on their pelagic stage.

The proportion of larvae retained when eddies are absent, and when swimming depletes energy reserves (black line, Figure 5.5c), shows that larvae remain close to the reef only if they arrive relatively late in larval life. This suggests that larvae are most likely to benefit from swimming once they can swim faster than the currents encountered (for these simulations at 0.22 and 0.20ms^{-1} respectively). Therefore, if the probability of encountering

suitable habitat for settlement is similar throughout the pelagic life, and circulation features that promote retention are absent, the onset of swimming behaviour is likely to be beneficial principally after larvae can swim at speeds that match those of the flow, and not necessarily at earlier life stages. In contrast, when eddies are present, active larvae that arrives earlier in life can be retained, and the proportion of retained larvae increases monotonically with age of arrival (see blue and red lines in Figure 5.5c). This suggests that the benefit from the onset of early or late swimming behaviour depends upon the probability of encountering downstream habitat, circulation regimes favourable for retention, or currents that are slower than larval swimming speed.

This study highlights the need to account for energetic cost when considering that larvae engage in swimming behaviour to achieve settlement. It also suggests that when implementing behaviour using a sensory zone, the percentage of larvae that are likely to settle successfully, if found within such a zone, depends upon the presence and duration of lee eddies, as well as the age of arrival into this zone. Finally, it suggests that early onset of swimming behaviour does not necessarily maximize settlement. Rather, the most beneficial time to start swimming is likely to depend on the reef landscape (i.e., the probability of finding suitable habitat downstream), the strength of swimming ability relative to dominant currents in the environment, the presence and lifespan of lee reef eddies, and the availability of food.

Chapter 6. General Discussion

This thesis uses a 3D hydrodynamic model to investigate mechanisms driving larval transport close to reefs and demonstrates that lee-reef eddies play a crucial role in larval transport in this environment. Specifically, the absence, presence and dynamics of lee-reef eddies determine the retention of passive larvae close to reefs and contribute to the retention of active larvae. In addition, the results presented here demonstrate that the Island Wake Parameter captures the qualitative nature of the flow downstream of reefs. Although the Island Wake Parameter predicted eddy dynamics accurately only on isolated reefs, it appears to capture particularly well the characteristics of the flow that are relevant for particle transport regardless of complex topography. Consequently, the Island Wake Parameter is strongly related to retention time, and a calibrated relationship can be used as a tractable and simple method to approximate mean retention time of passive larvae close to reefs. Finally, this thesis strongly suggests that the potential for swimming behavior to modify dispersal patterns depends largely upon food availability for larvae and therefore the probability to replenish energy reserves.

6.1 Lee-reef eddies dictate passive larval retention

Chapters 2 and 4 of this thesis elucidate the effect of lee-reef eddies on larval transport by quantifying retention times of passive larvae close to reefs due to lee-reef eddies with different dynamics. Observational and modelling studies have suggested that lee-reef eddies influence larval distribution (e.g., Oliver and Willis 1987; Black et al. 1993), and such eddies have been proposed as a physical mechanism by which larvae can remain close to suitable habitat for settlement (e.g., Sponaugle 2002). However, the extent to which lee-reef eddies modify larval transport by enhancing retention has not been quantified explicitly in previous work. This thesis clarifies the potential of lee-reef eddies with a gradient of eddy life spans, from stable to unstable, induced by the interaction of low frequency and tidal flows

with the bathymetry close to reefs, to affect retention time of passive larvae close to reefs, and consequently, to allow self-recruitment or facilitate arrival to suitable habitat.

Chapter 2 shows that stable lee-eddies, which can form downstream of isolated wide reefs under the influence of weak flows with low frequency variability, cause retention times sufficient to promote moderate to substantial levels of self-recruitment for organisms that disperse passively for a period of hours to few days before acquiring competence to settle. Thus, it supports the hypothesis that lee-eddies can allow some species to self-recruit on oceanic islands or isolated reefs whose dimensions and flow structure facilitate relatively long-lived eddies (Swearer et al. 1999). Nevertheless, Chapter 4 makes evident that complex bathymetry, or the presence of reefs in the near wake of other reefs, hampers eddy consolidation. In addition, at places where tidal currents are dominant or fast, such as those occurring along the central GBR, eddies are short-lived, and mean retention times are shorter than the time the majority of marine organisms larvae take to acquire competence to settle. Thus, lee-eddies have a limited potential to self-recruit in such circumstances, particularly for species that develop over weeks or months.

Collectively, these results highlight the importance of accounting for reef-scale flow structure when quantifying larval transport, show that the potential of lee-reef eddies to promote self-recruitment depends largely upon their lifespan, recognize the probability of eddies with specific life-spans to form at reefs along the central GBR, and elucidate the likelihood for self-recruitment versus downstream dispersal to occur in this region. However, lee eddies are not the only physical mechanisms that can facilitate larval retention close to reefs. In regions where reefs are highly aggregated, such as the Swains in the southern GBR, eddies are unlikely to develop due to topographical constraints; nevertheless, flushing is poor because currents are deflected and directed away from the high density reef matrix and retention times can be long enough to facilitate recruitment (Andutta et al. 2012).

6.2 The Island Wake Parameter, eddy dynamics and passive larval retention time

This thesis applies a tool commonly used in fluid mechanics (i.e., non-dimensional numbers) to address questions regarding larval retention. The quality of flows can be captured with non-dimensional numbers that contrast the forces acting upon it. A well known example is the Reynolds number, which expresses the ratio of inertial to frictional forces as an indicator of the degree of flow turbulence. Analogous to this number, the Island Wake Parameter describes the characteristics of flow past obstacles in shallow waters. The order of magnitude of the Island Wake Parameter indicates whether eddies are expected to form downstream of obstacles, and, if so, how frequently they form, and how long they prevail.

Chapter 2 shows, for the first time, that the Island Wake Parameter characterizes adequately the quality of flow past isolated reefs with a variety of shapes and sizes, under the influence of unidirectional low frequency flow and perpendicular tidal flow. Moreover, it shows that the Island Wake Parameter relates significantly with passive larval retention times. Chapter 4 shows that, in environments with convoluted bathymetry and under more complex flows, such as those occurring at reefs along the central GBR, the Island Wake Parameter allows distinguishing between the absence and presence of eddies but does not relate to mean frequencies of eddy detachment. Nevertheless, the relationship between the Island Wake Parameter and mean retention times is significant for reefs under these more realistic circulation regimes. Moreover, this relationship is common to the realistic flow regime and the stationary flows and idealized reef shapes considered in Chapter 2. This suggests that the Island Wake Parameter incorporates the variables that determine flow characteristics relevant to larval transport sufficiently well to provide the basis for a first-order estimate of retention time.

Because the Island Wake Parameter did not discern between the frequencies of eddy formation amongst reefs I explored if the Strouhal number, which considers explicitly the frequency of eddy detachment (Levi 1983), could explain a larger percentage of the variability

in mean retention time than the Island Wake Parameter. However, due to complex topography, and the non-stationary nature of the flow, the frequency at which eddies form behind reefs was variable, and the Strouhal number, computed with the mean frequency of eddy formation did not relate significantly with mean retention time (results not shown). This suggests that the Island Wake Parameter depicts better the characteristics of a non-stationary flow that drive larval transport than those indicated by the Strouhal number.

Eddies formed behind reefs along the central GBR become detached and dissipate quickly. Consequently, the Island Wake Parameters values in this region are always large (10^1-10^5). Thus the relationship between the Island Wake Parameter and the time passive larvae are retained could only be examined for Island Wake Parameter values larger than 10. The formation of long-lived, stable eddies might occur downstream of wider reefs than those present in the model domain, or when low frequency, or tidal currents are weaker than those occurring during the two spawning events investigated in Chapter 4. Calculating the Island Wake Parameter and associated mean retention times in regions where, or at times when, stable eddies form would therefore complement the results of Chapter 4. Particularly, it would allow testing if Island Wake Parameter values on the order of unity are associated with stable or long-lived eddies even for non-stationary realistic circulation regimes, and also if the steep change in retention time observed for idealized reefs associated with the transition of Island Wake Parameter values from 1 to 10 also occurs for real reefs under realistic circulation regimes.

The circulation setting examined for idealized reefs and for reefs along the central GBR consists of low frequency flows and perpendicular tidal flows which tend to induce the detachment and dissipation of lee-eddies. Many reef systems are distributed along boundary currents; however, tidal currents are not always perpendicular to the low frequency flow. As a result, lee-eddies might prevail after tidal reversals. Therefore, the occurrence of longer-lived

eddies might be more common elsewhere, and retention times induced by lee-eddies close to reefs could be longer than those occurring most commonly along the central GBR.

6.3 Alternative method to estimate mean retention times of passive larvae

This thesis shows that reef-scale flow structure plays a crucial role in larval transport. Thus, hydrodynamic models used to investigate larval dispersal in reefs need to implement a reef-scale spatial resolution, or an adequate parameterization of the flow at such scales. Models with high spatial resolution require large computational resources. The parameterization of sub-grid flow can be used to reduce computational time and is often attained by implementing advection-diffusion approximations (e.g., Paris and Cowen 2004; Marinone et al. 2008). However, diffusion is highly variable in space and time (Visser 1997). Hence, this approach requires model architecture flexibility and involves extensive calibration. In addition, comprehensive oceanographic and atmospheric data sets are necessary to force and validate any hydrodynamic model (e.g., Rothstein et al. 2006). This thesis provides an alternative method to approximate passive larval or water-born particle retention close to reefs that considers the reef-scale flow structure and overcomes difficulties associated with the use of hydrodynamic models.

Black et al. (1990) found that the number of retained particles close to a reef decreases exponentially at a rate determined by the water volume that flows over the reef. In turn, they parameterized the water volume in terms of the speed of the tidal-cycle average residual current downstream the reef, the free stream current speed, and reef dimensions. The authors formulated an analytical solution to estimate the decline of the number of particles retained around reefs, and tested it against outcomes of a 2D hydrodynamic model. The relationship between retention time and oceanographic or geo-morphological variables of the analytical solution proposed by Black et al. (1990) are similar to those implied by the relationship between the Island Wake Parameter and mean retention time found in this thesis. For

instance, in both equations, retention time decreases with current velocity and increases with the reef dimension perpendicular to the main direction of the flow. However, the method developed in this thesis focused on the effect of lee-reef eddies on retention using the Island Wake Parameter as an indicator of eddy dynamics, and was developed and tested considering 3D flow dynamics. Conversely, the analytical formula postulated by Black et al. (1990), is based on the water volume exchange, used residual currents (i.e., the temporal average over a tidal cycle of velocities downstream the reef) and considered a well-mixed vertically homogenous environment. The absence of vertical stratification is common on shelf waters under strong winds (Brinkman et al. 2001). However, close to offshore reefs, where the platform drops, vertical stratification can prevail during upwelling events (Luick et al. 2007) or under calmed weather conditions. In addition, lee eddies induce regions of upwelling and downwelling which in turn strengthen the eddy and affect their duration (Bakun 2006). Although both methods yield similar retention times close to reefs depending upon flow velocity and reef dimensions, Black et al.'s (1990) formula requires more data collection to estimate retention times than those needed to compute the Island Wake Parameter and associated mean retention times. Specifically, the Black et al. (1990) formula includes the magnitude of a residual current, so more than one velocity time series is likely to be necessary to choose a magnitude representative of the flow structure downstream of the reef. In contrast, the Island Wake Parameter is designed to capture the dynamics of the flow downstream of the reef from a single velocity time series upstream the reef, along with reef width and depth. Moreover, because the relationship between the Island Wake Parameter and retention times has been calibrated considering 3D dynamics in this thesis, this approximation is likely to be appropriate even in environments where vertical stratification is present or where regions of upwelling and downwelling occur.

6.4 Lee-reef eddies contributing to active larval retention

Population genetic structure and tagging and recapture studies of reef fish evidence that self-recruitment or dispersal occurs between reefs within tens of kilometres. The fifth Chapter of this thesis investigates mechanisms that allow this dispersal pattern to emerge. It shows that the interaction of lee-reef eddies and horizontal swimming behaviour enhances retention of larvae in suitable habitat. Thus, it is possible that orientation towards reefs and recirculation caused by eddies allows larvae in early stages of their development to remain close to reefs near the source until ready to settle. However, the presence of eddies and horizontal swimming can only induce substantial self-recruitment if lee-reef eddies are stable, or if fish larvae can feed sufficiently to replace the energy spent on swimming. These results suggest that energy expenditure caused by swimming performance during the planktonic stage constrains the potential for swimming behaviour to modify dispersal. Hence, it supports the hypothesis that fish larvae implementing swimming strategies which exploit favourable currents are more likely to reach suitable habitat than those that do not benefit from the circulation patterns. More comprehensive empirical data on energy expenditure caused by swimming, and energy replenishment by feeding of fish larvae, are therefore necessary to calibrate models of fish larvae energy budgets in the wild. Such energy budgets can then be used to quantify more accurately the potential effect of swimming behaviour on larval dispersal.

This thesis examined the combined effect of eddies and larval swimming behaviour in larval retention at individual reefs. Simulations of active larval transport along a reef system would be the next step to elucidate how the investigated swimming strategies would modify the shape, width and magnitude of larval dispersal kernels. For instance, results from Chapter 5 suggest that swimming behaviour can produce the largest proportions of larval retention if its onset occurs when larvae are able to swim at speeds that overcome the encountered currents. If this is a strategy implemented by reef fish larvae, the maximum of their dispersal

kernel would occur somewhere between the source reef and the distance passive larvae would have been advected by the end of their planktonic life. The likelihood of this or similar patterns in larval dispersal kernels emerging from the interaction between eddy dynamics and swimming behaviour can be examined by simulating and comparing the transport of active larvae performing swimming behaviour at different stages of their development.

References

Andrews JC and Furnas MJ (1986) Subsurface intrusions of Coral Sea Water into the Central Great Barrier Reef I, Structures and shelf-scale dynamics, Continental Shelf Research, vol. 6, pp. 491-514.

Andutta FP, Kingsford MJ and Wolanski E (2012) Sticky water enables the retention of larvae in a reef mosaic, Estuarine Coastal and Shelf Science, vol. 101, pp. 54-63.

Armsworth PR (2000) Modelling the swimming response of late stage larval reef fish to different stimuli, Marine and Ecology Progress Series, vol. 195, pp. 231-247.

Armsworth PR (2001) Directed Motion in the Sea: Efficient Swimming by Reef Fish Larvae, Journal of Theoretical Biology, vol.210, pp. 81-91.

Atema J, Kingsford M and Gerlach G (2002) Larval reef fish could use odour for detection, retention and orientation to reefs, Marine Ecological Progress Series, vol. 241, pp. 151-160.

Ayre DJ and Hughes TP (2000) Genotypic diversity and gene flow in brooding and spawning corals along the Great Barrier Reef, Australia. Evolution vol. 54, no. 5, pp. 1590-1605.

Babcock RC and Heyward AJ (1986) Larval development of certain gamete-spawning scleractinian corals, Coral Reefs, vol. 5, pp. 111-116.

Baird AH (2001) 'The ecology of coral larvae: settlement patterns, habitat selection and the length of the larval phase', PhD thesis, James Cook University, Australia.

Bakun A (2006) Fronts and eddies as key structures in the habitat of marine fish larvae: opportunity, adaptive response and competitive advantage, Scientia Marina, vol. 70S2, pp. 105-122.

Bao Y, Tao J (2013) The passive control of wake flow behind a circular cylinder by parallel dual plates. Journal of Fluids and Structures, vol. 37, pp. 201-219.

Barton ED, Aristegui J, Tett P, Canton M, Garcia-Braun J, Hernandez-Leon S, Nykjaer L, Almeida C, Almunia J, Ballesteros S, Basterretxea G, Escanez J, Garcia-Weill L, Hernandez-Guerra A, Lopez-Laatzen F, Molina R, Montero F, Navarro-Perez E, Rodriguez JM, Van Lenning K, Velez H, and Wild K (1998) The transition zone of the Canary Current upwelling region, Progress in Oceanography, vol. 41, pp.455-504.

Barton ED (2001) Island wakes, in: *Encyclopedia of Ocean Sciences*, Elsevier, pp. 1397-1403.

Bellwood DR, Hughes TP, Folke C and Nystrom M (2004) Confronting the coral reef crisis, Nature, vol. 429, no. 24, pp. 827-833.

Beamish FWH (1978) 'Swimming capacity', in Hoar WS, Randall DJ (eds.) *Fish Physiology*, Vol VII Academic Press, London, pp. 101-189.

Best BA and Resing JM (1987) Active settlement of coral planulae: the effects of flow and swimming behaviour on local recruitment. American Zoologist vol. 27, no.4, pp:103A.

Black KP, Gay SL (1987) Eddy formation in unsteady flows, Journal of Geophysical Research vol.92 no.C9, pp. 9514-9522.

Black KP, Gay SL and Andrews J (1990) Residence times of neutrally-buoyant matter such as larvae, sewage or nutrients on coral reefs, Coral Reefs, vol. 9, pp. 105-114.

Black KP (1993) The relative importance of local retention and inter-reef dispersal of neutrally buoyant material on coral reefs, Coral Reefs, vol. 12, pp. 43-53.

Blaise S, Deleersnijder E, White L and Remacle JF (2007) Influence of the turbulence closure scheme on the finite-element simulation of the upwelling in the wake of a shallow-water island, Continental Shelf Research, vol. 27, pp. 2329-2345.

Blowes S and Connolly RS (2012) Risk spreading, connectivity, and optimal reserve spacing, Ecological Applications, vol. 22, no.1, pp. 311-321.

Botsford LW, Hastings A and Gaines SD (2001) Dependence of sustainability on the configuration of marine reserves and larval dispersal distance, Ecology Letters, vol. 4, pp. 144-150.

Botsford LW, White JW, Coffroth MA, Paris CB, Planes S, Shearer TL, Thorrold SR and Jones GP (2009) Connectivity and resilience of coral reef metapopulations in marine protected areas: matching empirical efforts to predictive needs, Coral Reefs, vol. 28, pp. 327-337.

Bradbury IR and Snelgrove PVR (2001) Contrasting larval transport in demersal fish and benthic invertebrates: the roles of behaviour and advective processes in determining spatial pattern, Canadian Journal of Fisheries and Aquatic Science vol. 58, pp.811-823.

Brassington GB, Pugh T, Spillman C, Schulz E, Beggs H, Schiller A and Oke P (2007) BLUElink Development of operational oceanography and servicing in Australia, Journal of Research and Practice in Information Technology , vol. 39, no. 2, pp. 151-164.

Bricker JD and Nakayama A (2007) Estimation of far-field horizontal and vertical turbulent diffusion coefficients from the concentration field of a wastewater plume near the Akashi Strait, Environmental Fluid Mechanics, vol. 71, pp. 1-22.

Brinkman R, Wolanski E, Deleersnijder E, McAllister F and Skirving W (2001) Oceanic Inflow from the Coral Sea into the Great Barrier Reef, Estuarine Coastal and Shelf Science, vol. 54, pp. 655-668.

Brett JR and Groves TD (1979) 'Physiological energetics', in Hoar WS, Randall DJ (eds.) *Fish Physiology*, Vol VII Academic Press London pp. 279-361.

Brothers EB, Williams DMcB and Sale PF (1983) Length of larval life in twelve families of fishes at "One Tree Lagoon" Great Barrier Reef, Australia, Marine Biology, vol. 76, pp.319-324.

Burchard HK, Peterson O and Rippeth TP (1998) Comparing the performance of the Mellor-Yamada and the k-ε two equation turbulence models, Journal of Geophysical Research, vol. 103, no. C5, pp. 10543-10554.

Burgess SC, Kingsford MJ and Black KP (2007) Influence of tidal eddies and wind on the distribution of presettlement fishes around One Tree Island, Great Barrier Reef. Marine Ecology Progress Series, vol. 341, pp.233-242.

Caldeira RMA and Sangra P (2012) Complex geophysical wake flows. Ocean Dynamics, vol 62, pp.683-700.

Cartwright DE and Ray RD (1990) Oceanic tides from Geosat altimetry, Journal of Geophysical Research vol. 95, no. C3, pp. 3069-3090.

Chassignet EP, Hurlburt HE, Smedstad OM, Halliwell GR, Wallcraft A, Metzger EJ, Blanton BO, Lozano C, Rao DB, Hogan PJ and Srinivasan A (2006) Generalized Vertical Coordinates, for eddy-resolving global and coastal ocean forecast, Oceanography, vol. 19, no. 1, pp. 118-129.

Chen C, Beardsley R and Cowles G (2006) An Unstructured-grid, finite Volume coastal Ocean Model (FVCOM) System, Oceanography, vol. 19, no. 1, pp. 78-89.

Chia F-S, Buckland-Nicks J and Young CM (1984) Locomotion of marine invertebrate larvae: a review, Canadian Journal of Zoology, vol.62, pp. 1205-1222.

Choukroun S, Ridd PV, Brinkman R and McKinna LIW (2010) On the surface circulation in the western Coral Sea and residence times in the Great Barrier Reef, Journal of Geophysical Research, vol. 115, no. C6, pp. C06013.

Church JA (1987) East Australian Current Adjacent to the Great Barrier Reef, Australian Journal of Marine and Freshwater Research, vol. 38, pp., 671-683.

Church JA and Boland FM (1983) A permanent undercurrent adjacent to the Great Barrier Reef, Journal of Physical Oceanography, vol. 13, pp. 1747-1749.

Clark DL, Leis JM, Hay AC and Trnski T (2005) Swimming ontogeny of larvae of four temperate marine fishes, Marine Progress Ecology Series, vol. 292, pp. 287-300.

Condie SA, Loneragan NR and Die DJ (1999) Modelling the recruitment of tiger prawns *Penaeus esculentus* and *P. semisulcatus* to nursery grounds in the Gulf of Carpentaria, northern Australia: implications for assessing stock-recruitment relationships, Marine Ecology Progress Series, vol.178, pp. 55-68.

Condie SA and Andrewartha JR (2008) Circulation and connectivity on the Australian North West Shelf, Continental Shelf Research, vol. 28, pp. 1724-1739.

Condie SA, Hepburn M and Mansbridge J (2012) Modelling and visualisation of connectivity on the Great Barrier Reef, *Proceedings of the 12th International Coral Reef Symposium*, Cairns, Australia, pp. 325-326.

Connolly SR, Baird AH (2010) Estimating dispersal potential for marine larvae: dynamic models applied to scleractinian corals, Ecology, vol. 91, no.12, pp. 3572-3583.

Cowen RK, Paris CB and Srinivasan A (2006) Scaling of connectivity in marine populations, Science, vol.311, no. 5760, pp. 522-527.

Cowen RK and Sponaugle S (2009) Larval Dispersal and Marine Population Connectivity, Annual Review of Marine Science, vol. 1, pp. 443-466.

Cresswell GR and Greig MA (1978) Currents and Water Properties in the North-central Great Barrier Reef during the South-east Trade Wind Season, Australian Journal of Marine Freshwater Research, vol. 29, pp. 345-353.

Done TJ (1982) Patterns in the distribution of coral communities across the central Great Barrier Reef, Coral Reefs, vol.1, pp. 95-107.

Dong C, McWilliams JC (2007) A numerical study of island wakes in the Southern California Bight, Continental Shelf Research, vol. 27, pp. 1233-1248.

Duchon CE (1979) Lanczos Filtering in One and Two dimensions, Journal of Applied Meteorology, Vol 18, pp. 1016-1022.

Emery WJ and Thomson RE (2001) Data Analysis Methods in Physical Oceanography, 2nd edition, Amsterdam, Elsevier Science.

Fisher R and Bellwood DR (2001) Effects of feeding in the sustained swimming abilities of late-stage larval *Amhirion melanopus*, Coral Reefs, vol. 20, pp. 151-154.

Fisher R and Bellwood DR (2002) The influence of swimming speed on sustained swimming performance of late-stage ref fish larvae, Marine Biology, vol. 140, pp. 801-807.

Fisher R and Wilson SK (2004) Maximum sustainable swimming speeds of late-stage larva of nine species of reef fishes, Journal of Experimental Marine Biology and Ecology, vol. 312, pp. 171-186.

Fisher R (2005) Swimming speeds of larval coral reef fishes: impacts on self-recruitment and dispersal, Marine Ecology Progress Series, vol 285, pp. 223-232.

Foster NL, Paris CB, Kool JT, Baums IB, Stevens JR, Sanchez JA, Bastidas C, Agudelo C, Bush P, Day O, Ferrari R, Gonzalez P, Gore S, Guppy R, McCartney MA, McCoy C, Mendes J, Srinivasan A, Steiner S, Vermeij M, Weils E and Mumby P (2012) Connectivity of Caribbean coral populations: complementary insights from empirical modelled gene flow, Molecular Ecology, vol. 21, pp. 1144-1157.

Gaines SD, Gaylord B, Gerber LR, Hastings A, Kinlan A (2007) Connecting Places, The Ecological consequences of dispersal in the sea, Oceanography, vol 20, no. 3, pp. 90-99.

GBRMPA Great Barrier Reef Marine Park Authority, Protecting the Great Barrier Reef World Heritage Area, viewed 17 September 2012, <http://www.gbrmpa.gov.au/__data/assets/pdf_file/0006/7593/gbrmpa_WorldHeritage_brochure.pdf

GBRMPA Great Barrier Reef Marine Park Authority (2006) Coral Spawning, Fact sheet No. 20, viewed 17 September 2012, http://www.gbrmpa.gov.au/__data/assets/pdf_file/0016/5290/20-coral-spawning-2006.pdf

Gerlach G, Atema J, Kingsford M, Black KP and Miller-Sims V (2007) Smelling home can prevent dispersal of reef fish larvae. Proceedings of the National Academy of Science USA, vol. 104, no. 3, pp. 858-863.

Gerrard JH (1966) The mechanics of the formation region of vortices behind bluff bodies. Journal of Fluid Mechanics, vol. 25, part 2, pp 401-413.

Glimour JP, Smith LD and Brinkman R (2009) Biannual spawning, rapid larval development and evidence of self-seeding for scelaractinian corals at an isolated system of reefs, Marine Biology, vol.156, pp. 1297-1309.

Gordeau L, Kessler WS, Davis RE, Sherman J, Maes C and Kestenare E (2008) Zonal jets entering the coral sea, Journal of Physical Oceanography, vol. 38, no.3, pp. 715-725.

Griffies SM, Pacanowski RC and Rosati A (2004) A technical guide to MOM4, GFDL Ocean Group Technical Report No. 5 NOAA/ Geophysical Fluid Dynamics Laboratory, 371 pp.

Griffin DA, Middleton JH and Bode L (1987) The tidal and longer-period circulation of Capricornia, Southern Great Barrier Reef, Australian Journal of Marine and Freshwater Research, vol.38, pp. 461-474.

Hadfield MG Carpizo-Iruarte E, del Carmen K and Nedved BT (2001) Metamorphic Convergence in Marine Invertebrate Larvae, American Zoologist, vol. 41, no. 5, pp. 1123-1131.

Hamner WM, Jones MS, Carleton JH, Hauri IR, Williams DMcB (1988) Zooplankton, planktivorous fish, and water currents on a windward reef face: Great Barrier Reef, Australia, Bulletin of Marine Science, vol. 42, no. 3, pp. 459-479.

Harrison PL, Babcock RC, Gordon DB, Oliver JK, Wallace CC and Willis BL (1984) Mass Spawning in Tropical Reef Corals, Science, vol 223, no 4641, pp. 1186-1189.

Harrison HB, Williamson DH, Evans RD, Almany GR, Thorrold SR, Russ GR, Feldheim KA, van Herwerden L, Planes S, Srinivasan M, Berumen ML and Jones GP (2012) Larval Export from Marine Reserves and the Recruitment Benefit for Fish and Fisheries, Current Biology vol. 22, pp. 1023-1028.

Hellberg ME, Burton RS, Neigel JE and Palumbi SR, (2002) Genetic assessment of connectivity among marine populations, Bulletin of Marine Science, vol. 70 SUPPL. 1, pp.273-290.

Herzfeld M and Waring JP (2012) *SHOC, Sparse Hydrodynamic Ocean Code V4150 User Manual*, CSIRO Marine Research, viewed 14 September 2012, <http://www.emg.cmar.csiro.au/www/en/emg/software/EMS/hydrodynamics.html>

Herzfeld M, Andrewartha J and Sakov P (2010a) Modelling the physical oceanography of the D'Entrecasteaux Channel and the Huon Estuary, south-eastern Tasmania, Marine and Freshwater Research, vol. 61, pp. 568-586.

Herzfeld M, Waring JP, Parslow J, Margvelashvili N, Sakov P and Andrewartha J (2010b) *SHOC, Sparse Hydrodynamic Ocean Code V1632 Scientific Manual*, CSIRO Marine Research, viewed 14 September 2012, <http://www.emg.cmar.csiro.au/www/en/emg/software/EMS/hydrodynamics.html>

Houde ED (1978) Critical food concentrations for larvae of three species of subtropical marine fishes, Bulletin of Marine Science, vol. 28, no. 32, pp. 395-411.

Irisson J-O, LeVan A, De Lara M and Planes S (2004) Strategies and trajectories of coral reef fish larvae optimizing self-recruitment, Journal of Theoretical Biology vol. 227, pp.205-218.

James MK, Armsworth PR, Mason LB and Bode L (2002) The structure of reef fish metapopulations: modelling larval dispersal and retention patterns. Proceedings of the Royal Society London B Biological Sciences vol. 269, no.1505, pp. 2079-2086.

Job S, Bellwood B (2007) Ultraviolet photosensitivity and feeding in larval and juvenile coral reef fishes, Marine Biology, vol. 151, pp 495-503.

Jones GP (1986) Food availability affects growth in a coral reef fish, Oecologia, vol. 70, pp. 136-139.

Jones GP, Milicich MJ, Emslie MJ and Lunow C (1999) Self-recruitment in a coral reef population Letters to Nature, vol. 402 , no. 6763, pp. 802-804.

Jones GP, Almany GR, Russ GR, Sale PF, Steneck RS, van Oppen MJH and Willis B (2009) Larval retention and connectivity among populations of coral and reef fishes: history, advance and challenges, Coral Reefs, vol. 28, pp. 307-325.

Kerrigan BA (1994) Post-settlement growth and body composition in relations to food availability in a juvenile tropical reef fish, Marine Ecology Progress Series, vol. 111, pp. 7-15.

Kingsford MJ, Leis JM, Shanks A, Lindeman KC, Morgan SG and Pineda J (2002) Sensory environments, larval abilities and local self-recruitment, Bulletin of Marine Science, vol.70, SUPPL. 1, pp.309-340.

Kool JT, Paris CB, Andrefouet S and Cowen RK (2010) Complex migration and the development of genetic structure in subdivide populations: an example from Caribbean coral reef ecosystems, Ecography vol. 35, pp. 597-606.

Lambechts J, Hanert E, Deleersnijder, Bernard PE, Legat V, Remacle JF and Wolanski E (2008) A multi-scale model of the hydrodynamics of the whole Great Barrier Reef, Estuarine Coastal and Shelf Science, vol. 79, pp. 143-151.

Large WG and Pond S (1981) Open ocean momentum flux measurements in moderate to strong winds, Journal of Physical Oceanography, vol.11, pp. 324-336.

Leggett WC and Deblois E (1994) Recruitment in marine fishes: is it regulated by starvation and predation in the egg and larval stages? Netherlands Journal of Sea Research, vol 32, no.2 pp. 119-134.

Legrand S, Deleersnijder E, Hanert E, Legat V and Wolanski E (2006) High resolution, unstructured meshes for hydrodynamic models of the Great Barrier Reef, Australia, Estuarine Coastal and Shelf Science vol. 68, pp. 36-46.

Leis JM (2006) Are larvae of demersal fishes plankton or nekton? Advances in Marine Biology, vol.51, pp.57-141.

Leis JM (1991) 'The pelagic stage of reef fishes: the larval biology of coral reef fishes', in PF Sale (ed.) *The ecology of fishes on coral reefs*. Academic Press, London, pp. 183-230.

Levi E (1983) A universal Strouhal Law, Journal of Engineering Mechanics, vol. 109, no. 3, pp 718-727.

Leys SP and Degnan BM (2001) Cytological basis of photoresponsive behaviour in a sponge larva, Biological Bulletin, vol. 201, no. 3, pp. 323-338.

Llopiz JK and Cowen RK (2009) Variability in the trophic role of coral reef fish larvae in the oceanic plankton, Marine Ecology Progress Series, vol. 381, pp 259-272.

Luick JL, Mason L, Hardy T and Furnas M (2007) Circulation in the Great Barrier Reef Lagoon using numerical tracers and in situ data, Continental Shelf Research, vol. 27, pp. 757-778.

MacKenzie BR, Leggett WC and Peters RH (1990) Estimating larval fish ingestion rates: can laboratory derived values be reliably extrapolated to the wild? Marine Ecology Progress Series, vol. 67, pp. 209-225.

MacKenzie BR and Kiorboe T (2000) Larval fish feeding and turbulence: A case for the downside, Limnology and Oceanography, vol. 45, no.1, pp. 1-10.

Maldonado M and Young CM (1999) Effects of duration of larval life on postlarval stages of demosponge *Sigmadocia caerulea*, Journal of Experimental Marine Biology and Ecology, vol. 232, pp. 9-21.

Mapstone BD, Davies CR, Little LR, Punt AE, Smith ADM, Pantus F, Lou DC, Williams AJ,Jones A, Ayling AM, Russ GR and McDonald AD (2004) The Effects of line fishing on the Great Barrier Reef and Evaluations of Alternative potential management strategies, CRC Reef Research Centre Technical Report No 52. CRC Reef Research Centre, Townsville, Australia.

Marinone SG (2006) A numerical simulation of the two- and three-dimensional Lagrangian circulation in the northern Gulf of California, Estuarine Coastal and Shelf Science vol. 68, pp. 93-100.

Marinone SG, Ulloa MJ, Pares-Sierra A, Lavin MF and Cudney-Bueno R (2008) Connectivity in the northern Gulf of California from particle tracking in a three-dimensional numerical model, Journal of Marine Systems, vol. 71, pp. 19-158.

Mata MM, Wijffels S, Church JA and Tomczak M (2006) Statistical description of the East Australian Current low-frequency variability from the WOCE PCM3 array, Marine and Freshwater Research, vol. 57, pp. 273-290.

Meekan MG, Carleton JH, McKinnon AD, Flynn K and Furnas M (2003) What determines the growth of tropical reef fish larvae in the plankton: food or temperature? Marine Ecology Progress Series, vol. 256, pp. 193-204.

Moum JN, Caldwell DR and Stabeno PJ (1988) Mixing and intrusions in a rotating cold-core feature off Cape Blanco, Oregon , Journal of Physical Oceanography, vol. 18, pp. 823-833.

Nahas EL, Jackson G, Pattiaratchi CB and Ivey GN (2003) Hydrodynamic modelling of snapper *Pagrus auratus* egg and larval dispersal in Shark Bay, Western Australia: reproductive isolation at a fine spatial scale, Marine Ecology Progress Series vol. 265, pp. 213-226.

Neill SP and Elliott AJ (2004) Observations and simulations of an unsteady island wake in the Firth of Forth, Scotland, Ocean Dynamics, vol.54, pp. 324-332.

Nozawa Y and Harrison PL (2008) Temporal patterns of larval settlement and survivorship of two broadcast-spawning acroporid corals, Marine Biology, vol. 155, pp. 347-351.

Oliver JK and Willis BL (1987) Coral-spawn slicks in the Great Barrier Reef: preliminary observations, Marine Biology, vol. 94, pp. 521-529.

Oke PR, Brassington G, Griffin DA and Schiller A (2008) The Bluelink ocean data assimilation system (BODAS), Ocean Modelling, vol. 21, pp. 46-70.

Okubo A (1971) Oceanic diffusion diagrams, Deep-Sea Research, vol. 18, pp. 789-802.

Paris CB and Cowen RK (2004) Direct evidence of a biophysical retention mechanism for coral reef fish larvae, Limnology and Oceanography, vol. 49, pp. 1964-1979.

Paris CB, Cowen RK, Claro R and Lindeman C (2005) Larval transport pathways from Cuban snapper (Lutjanidae) spawning aggregations based on biophysical modelling, Marine Ecological Progress Series, vol. 296, pp.93-106.

Paris CB, Cherubin LM and Cowen RK (2007) Surfing, spinning or diving from reef to reef: effects on population connectivity, Marine Ecology Progress Series, vol. 347, pp. 285-300.

Parslow JS and Gabric AJ (1989) Advection, dispersal and plankton Patchiness on the Great Barrier Reef, Australian Journal of Marine and Freshwater Research vol. 40, pp. 403-419.

Parslow JS, Herzfeld M, Hunter JR, Andrewartha JR, Sakov P and Waring J (2001) Mathematical modelling of the dispersal and fate of CES discharge from the Boyer Mill in the Upper Derwent Estuary: Results of Part B, final report CSIRO Division of Marine Research, Hobart, TAS 189 pp

Pattiaratchi C, James A and Collins M (1986) Island wakes and headland eddies: A comparison between remotely sensed data and laboratory experiments, Journal of Geophysical Research, vol. 92, no. C1, pp. 783-794.

Parezanovic V, Cadot O (2012) Experimental sensitivity analysis of the global properties of a two-dimensional turbulent wake, Journal of Fluid Mechanics, vol. 693, pp 115-149.

Pickard GL, Donguy JR, Henin C and Rougerie F (1977) A review of the physical oceanography of the Great Barrier Reef and Western Coral Sea, Australian Institute of Marine Science Monograph Series, vol. 2, 135pp.

Pineda J, Hare JA and Sponaugle S (2007) Larval Transport and Dispersal in the Coastal Ocean and Consequences for Population Connectivity, Oceanography, vol. 20, no. 3, pp. 22-39.

Popper AN, Carlson TJ (1998) Application of Sound and Other Stimuli to Control Fish Behavior, Transactions of the American Fisheries Society, vol. 127, no 5, pp 673-707.

Puri K, Dietachmayer GS, Mills GA, Davidson NE, Bowen RA and Logan LW (1998) The new BMRC Limited Area Prediction System, LAPS, Australian Meteorology Magazzine, vol. 47, pp. 203-223.

Raymond WH and Kuo HL (1984) A radiation boundary condition for multidimensional flows, Quarterly Journal of the Royal Meteorological Society, vol. 110, pp. 535-551.

Ridgway KR and Dunn JR (2003) Mesoscale structure of the mean East Australian Current System and its relationship with topography, vol. 56, pp. 189-222.

Roberts CM (1997) Connectivity and management of Caribbean coral reefs, Science, New Series, vol. 278, no. 5342, pp. 1454-1457.

Rothstein LM, Cullen JJ, Abbott M, Chassignet EP, Denman K, Doney SC, Ducklow H, Fennel K, Follows M, Haidvogel D, Hoffman E, Karl DM, Kindle J, Lima I, Maltrud M, McClain C, McGillicuddy D, Olascoaga MJ, Spitz Y, Wiggert J and Yoder J (2006) Modelling Ocean Ecosystems the paradigm program, Oceanography, vol. 19, no. 1, pp. 22-51.

Russ GR, Alcala AC, Maypa AP, Calumpong HP and White AT, (2004) Marine Reserve Benefits local Fisheries, Ecological Applications, vol. 14, no.2, pp.597-606.

Sale PF (1991) Ecology of coral reef fishes, in: Sale PF(ed.) *The ecology of fishes on coral reefs*. Academic press, San Diego, pp.3-15.

Sale PF, Cowen RK, Danilowicz BS, Jones GP, Kritzer JP, Lindeman KC, Planes S, Polunin VCN, Russ GR, Sadovy JY and Steneck RS (2005) Critical science gaps impede use of no-take fishery reserves, Trends in Ecology & Evolution vol. 20, pp. 74-80.

Salomon Y, Connolly SR and Bode L (2010) Effect of asymmetric dispersal on the coexistence of competing species, Ecology Letters, vol. 13, pp. 432-441.

Sandulescu M, Hernandez-Garcia E, Lopez C, and Feudel U (2006) Kinematic studies of transport across an island wake, with application to the Canary Islands, Tellus Series A, Dynamic Meteorology and Oceanography, vol. 58A, pp. 605-615.

Scully-Power PD (1973) Coral Sea flow budgets in winter, Australian Journal of Marine and Freshwater Research, vol. 24, pp 203-215.

Signell RP and Geyer WR (1991) Transient eddy formation around headlands, Journal of Geophysical Research, vol. 96, no. C2, pp. 2561-2575.

Smagorinksy J (1963) General circulation experiments with the primitive equations, I The basic experiment Monthly Weather Review, vol. 91, pp. 99-164.

Smith-Keune C and van Oppen M (2006) Genetic structure of a reef-building coral from thermally distinct environments on the Great Barrier Reef, Coral Reefs, vol. 25, pp. 493-502.

Sponaugle S, Cowen RK, Shanks A, Morgan SG, Leis JM, Pineda J, Boehlert GW, Kingsford MJ, Lindeman KC, Grimes C and Munro JL (2002) Predicting self-recruitment in marine populations: biophysical correlates and mechanisms, Bulletin of Marine Science, vol.70, SUPPL. 1, pp. 341-375.

Sponaugle S, Llopiz JK, Havel LN and Rankin TL (2009) Spatial variation in larval growth and gut fullness in a coral reef fish, Marine Ecology Progress Series, vol. 383, pp 239-249.

Sponaugle S, Paris C, Walter KD, Kourafalou V, D'Alessandro E (2012) Observed and modeled larval settlement of a reef fish to the Florida Keys, Marine Ecology Progress Series, vol. 453, pp 201-212.

Staaterman E, Paris CB and Helgers J (2012) Orientation behaviour in fish larvae: A missing piece to Hjort's critical period hypothesis, Journal of Theoretical Biology, vol. 304, pp. 188-196.

Steneck RS (2006) Staying connected in a turbulent world, Science vol. 311, no. 5760, pp. 480-481.

Stobutzki IC (1997) Energetic cost of sustained swimming in the late pelagic stages of reef fishes, Marine Ecology Progress Series, vol. 152, pp. 249-259.

Stobutzki IC and Bellwood DR (1997) Sustained swimming abilities of the late pelagic stages of coral reef fishes, Marine Ecology Progress Series, vol. 149, pp. 35-41.

Strathmann RR, Hughes TR, Kuris AM, Lindeman KC, Morgan SG, Pandolfi JM and Warner RR (2002) Evolution of local recruitment and its consequences for marine populations, Bulletin of Marine Science vol.70, SUPPL. 1, pp,377-396.

Strykowsky PJ, Sreenivasan KR (1990) On the formation and suppression of vortex shedding at low Reynolds numbers, Journal of Fluid Mechanics, vol. 218, pp 71-107.

Suppiah R (1992) The Australian summer monsoon: a review, Progress in Physical Geography vol. 16, no. 3, pp. 283-318.

Swearer SE, Caselle JE, Lea DW and Warner RR, 1999, Larval retention and recruitment in an island population of a coral reef fish, Nature, vol. 402, no. 6763, pp. 799-802.

Swearer SE, Shima JS, Helberg ME, Thorrold SR, Jones GP, Robertson DR, Morgan SG, Selkoe KA, Ruiz GM and Warner RR (2002) Evidence of self-recruitment in demersal marine populations. Bulletin of Marine Science, vol. 70, SUPPL. 1, pp. 251-271.

Tang L, Sheng J, Hatcher BG and Sale PF (2006) Numerical study of circulation, dispersion, and hydrodynamic connectivity of surface waters on the Belize shelf, Journal of Geophysical Research, vol. 111, no.C01003, pp. 1-18.

Taylor G (1954) The dispersion of matter in turbulent flow through a pipe, Proceeding Royal Society A. Mathematical and Physical sciences, vol. 223, no. 1155, pp. 446-468.

Tolimieri N, Haine O, Jeffs A, McCauley R and Montgomery J (2004) Directional orientation of pomacentrid larvae to ambient reef sound, Coral Reefs, vol. 23, pp. 184-191.

Tomczak M (1988) Island wakes in deep and shallow water, Journal of Geophysical Research vol. 93, no.C5 pp. 5153-5154.

Valiela I (1995) Marine Ecological Processes, 2nd Edition, Springer, New York.

Van Leer B (1979) Towards the ultimate conservative difference scheme. V: a second order sequel to Godanov's method. Journal of Computational Physics, vol. 32, pp. 101-136.

van Oppen MJH and Gates RD (2006) Conservation genetics and the resilience of reef-building corals, Molecular Ecology, vol. 15, pp.3863-3883.

van Oppen M, Lutz A, De'ath G, Peplow and Kininmonth S (2008) Genetic Traces of Recent Long-Distance Dispersal in a Predominantly Self-Recruiting Coral

Victor B (1986) Duration of the planktonic larval stage of one hundred species of pacific and atlantic wrasses (family Labridae). Marine Biology. vol.90, no.3, pp. 317-326.

Visser AW (1997) Using random walk models to simulate the vertical distribution of particles in a turbulent water column, Marine Ecology Progress Series vol. 158, pp. 257-281.

Walker SJ (1999) Coupled hydrodynamic and transport models of Port Phillip Bay, a semi-enclosed bay in south-eastern Australia, Marine Freshwater Research, vol. 50, pp. 469-481.

Wellington GM and Victor BC (1989) Planktonic larval duration of one hundred species of Pacific and Atlantic damselfishes (Pomacentridae), Marine Biology, vol. 101, pp. 557-567.

Werner FE, Cowen RK and Paris CB (2007) Coupled Biological and Physical Models Present Capabilities and Necessary Developments for Future Studies of Population Connectivity, Oceanography

Whalan, S, Ettinger-Epstein P and de Nys R (2008a) The effect of temperature on larval pre-settlement duration and metamorphosis for the sponge, *Rhopaloeides odorabile*, Coral Reefs vol. 27, pp. 783-786.

Whalan S, Ettinger-Epstein P, Battershill C and de Nys R (2008b) Larval vertical migration and hierarchical selectivity of settlement in a brooding marine sponge, Marine Ecology Progress Series, vol. 368, pp. 145-154.

White L and Wolanski E (2008) Flow separation and vertical motions in a tidal flow interacting with a shallow-water island, Estuarine Coastal and Shelf Science, vol. 77, pp. 457-466.

Whiteway TG (2009) Australian Bathymetry and Topography Grid, Record 2009/21 GeoCat #67703, Australian Goverment, Geoscience, Australia

Wild-Allen K, Herzfeld M, Thompson PA, Rosebrock U, Parslow J and Volkman JK, (2010) Applied coastal biogeochemical modelling to quantify the environmental impact of fish farm nutrients and inform managers. Journal of Marine Systems, vol. 81, pp. 134-147.

Willis, BL, Oliver JK (1990) Direct tracking of coral larvae: Implications for dispersal studies of planktonic larvae in topographically complex environments, Ophelia vol. 32, pp. 145-162.

Wolanski E and Pickard GL (1985) Long-term observations of currents on the Central Great Barrier Reef continental shelf, Coral Reefs vol. 4, pp. 47-57.

Wolanski E, Hamner WM (1988) Topographically controlled fronts in the ocean and their biological influence, Science vol. 241, no. 4862, pp. 177-181.

Wolanski E, Imberger J and Heron M L (1984) Island wakes in shallow coastal waters, Journal of Geophysical Research, vol. 89, no.C6, pp. 10553-10569.

Wolanski E, Burrage D and King B (1989) Trapping and dispersion of coral eggs around Bowden Reef, Great Barrier Reef, following mass coral spawning, Continental Shelf Research, vol. 9, pp. 479-496.

Wolanski E (1993) Facts and numerical artefacts in modelling the dispersal of Crown-of-thorns Starfish larvae in the Great Barrier Reef, Australian Journal of Marine and Freshwater Research, vol. 44, pp, 427-436.

Wolanski E, Asaeda T, Tanaka A and Deleersnijder E (1996) Three-dimensional island wakes in the field, laboratory experiments and numerical models, Continental Shelf Research, vol. 16, pp. 1437-1452.

Wolanski E, Brinkman R, Spagnol S, McAllister F, Steinberg C, Skirving W and Deleersnijder E (2003) Merging scales in models of water circulation: Perspectives from the Great Barrier Reef, in: Lakhan (ed.) *Advances in coastal modeling*, Elsevier Science, pp. 411-429.

Wolanski E, Doherty P and Carleton J (1997) Directional Swimming of Fish Larvae Determines Connectivity of Fish Populations on the Great Barrier Reef, Naturwissenschaften, vol. 84, pp. 262-268.

Wyrtki K (1962) Geopotential topographies and associated circulation in the western South Pacific, Australian Journal of Marine and Freshwater Research, vol 13. Pp. 89-105.

Zaret TM and Suffern JS (1976) Vertical migration in zooplankton as a predator avoidance mechanism, Limnology and Oceanography, vol. 21, pp. 804-813.

Zulberti A (2010) 'An experimental investigation of island wakes in shallow oscillatory flow', PhD Thesis, The University of Western Australia, Australia.

Appendices

Appendix1

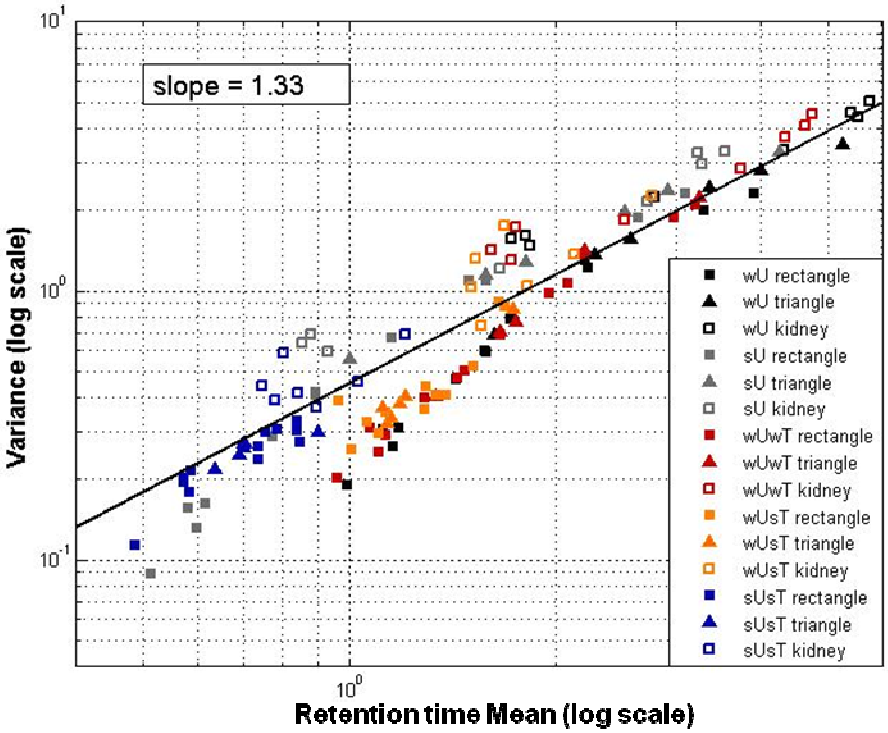

Figure A1.1 Log-transformed mean retention time against variance for all circulation regimes weak unidirectional (*wU*), strong unidirectional (*sU*), weak unidirectional weak tidal (*wUwT*), weak unidirectional strong tidal (*wUsT*), and strong unidirectional strong tidal (*sUsT*). ▲triangular, ■ square/rectangular, and □ kidney shaped reefs.

Table A1.1 Regression parameters with 95% confidence bounds, coefficient of determination (R^2), F statistic, p value and likelihood ratio (G) for the regression models between the Island Wake Parameter (I) and Retention time for different unidirectional flow speeds obtained with the rectangular shaped reefs data. *G*>3.841 indicates statistically significant support for a non-zero value of *c*. *F* statistics indicated that all reported regressions were highly statistically significant (*p*<<0.01 in all cases)

	Velocity (ms^{-1})	G	a (95% cb)	-b (95% cb)	R^2	F	P value
Rectangular reefs	**0.1038**	2.7437	3.18 (2.73 3.63)	0.79 (0.56 1.03)	0.85	22.67	0.0008
	0.1245	2.6573	3.54 (2.92 4.15)	0.90 (0.64 1.15)	0.86	23.94	0.0006
	0.1641	2.4908	4.65 (3.55 5.75)	1.08 (0.80 1.37)	0.89	27.08	0.0004
	0.2020	1.9857	6.07 (4.36 2.92)	1.22 (0.93 1.50)	0.92	29.90	0.0003
	0.3109	0.6866	8.89 (4.92 12.86)	1.27 (0.95 1.60)	0.91	23.71	0.0007
	0.4410	0.1795	9.32 (3.21 15.43)	1.17 (0.78 1.56)	0.86	15.11	0.003
	0.6573	0.0421	11.67 (1.63 21.70)	1.21 (0.77 1.66)	0.84	12.09	0.006

Table A1.2 Regression parameters with 95% confidence bounds, coefficient of determination (R^2), F statistic, p value and likelihood ratio (G) for the regression models between the Island Wake Parameter (I) and Retention time for different flow regimes (with and without tides), obtained with the rectangular shaped reefs data. G>3.841 indicates statistically significant support for a non-zero value of c. F statistics indicated that all reported regressions were highly statistically significant (p<<0.01 in all cases)

	Circulation regime	G	c (95% cb)	a (95% cb)	-b (95% cb)	R^2	F	P value
Rectangular reefs	**wU/sU**	0.046	NA	3.33 (2.89 3.76)	0.77 (0.61 0.94)	0.82	49.46	<0.001
	wUwT	12.77	0.90 (0.60 1.20)	2.42 (2.03 2.82)	1.59 (0.99 2.21)	0.96	98.25	<0.001
	wUsT/sUsT	0.86	NA	2.03 (1.28 2.79)	0.34 (0.16 0.53)	0.40	16.08	<0.001

Table A1.3 Regression parameters with 95% confidence bounds, coefficient of determination (R^2), F statistic, p value and likelihood ratio (G) for the regression models between the Island Wake Parameter (I) and Retention time for different reef shapes (triangular, rectangular and kidney), obtained pooling all flow regimes (*wU, sU, wUwT, wUsT,* and *sUsT*). *G*>3.841 indicates statistically significant support for a non-zero value of *c*. *F* statistics indicated that all reported regressions were highly statistically significant (*p*<<0.01 in all cases)

	Reef Shape	G	c (95% cb)	a (95% cb)	-b (95% cb)	R^2	F	P value
All circulation regimes	**Triangles**	4.20	0.47 (-0.69 1.63)	3.21 (2.02 4.40)	1.15 (0.21 2.08)	0.72	35.25	<0.001
	Rectangles	6.22	0.62 (0.38 0.87)	2.64 (2.30 2.98)	1.11 (0.79 1.42)	0.81	128	<0.001
	Kidneys	4.81	0.47 (-0.29 1.23)	3.60 (2.70 4.50)	1.03 (0.63 1.44)	0.86	111.77	<0.001

Appendix 2, Implementing swimming behaviour into SHOC particle tracking code

Vertical and horizontal particle movements were incorporated into SHOC separately. Vertical movement was already available in SHOC, however it only allowed for particles to sink over time at a constant velocity or at a velocity that depended upon particle size and density, and water density. Two more alternatives were included: 1) to experience diurnal migration, invoking the diurnal settling velocity and providing a single (constant over space and time) maximum velocity (*svel*) and a single (constant over space and time) periodicity (*sper*) of a cosine function that determines the direction of the vertical movement (upwards or downwards, A2.3 section 4.27.5 in SHOC's user manual), and 2) to move vertically as a function of time and space, invoking the filein settling velocity option (A2.3 section 4.27.5 in SHOC's user manual) and providing a file with the vertical speed of a particle at each position over horizontal and vertical space as well as time. This capability was not used in the thesis because Chapters 1,2 and 4 deal with passive larvae, and Chapter 5 focused on the effect of horizontal and not vertical swimming. However, its functionality was tested and proved correct.

The possibility for particles to display horizontal movement was also included; particularly, particles can move at a specific velocity in the east-west (*upt*) and north-south direction *(vpt*) depending on their position horizontal and vertical position (*x,y,z*) and time (*t*). This can now be achieved by invoking the PT_uv_file option (A2.3 section 4.27.6 in SHOC's user manual), and providing files with the east-west and north-south speed of the particle at each position over the horizontal and vertical space as well as time. Finally, the possibility for particles to suffer mortality was also incorporated as a function of time (A2.3 section 4.27.7 of SHOC's user manual).

To incorporate particle behavior I modified the scripts sparse.h, ptrack.h, and pt.c of SHOC's particle tracking algorithm. In sparse.h I added new sparse structures and in ptrack.h I included files for the vertical and horizontal particle velocities. Most of the new coding was done in the script pt.c; in which I programmed: 1) requesting and reading a periodicity (*sper*)

and maximum vertical swimming velocity (*svel*) to determine vertical migration, 2) requesting and reading particle vertical (*wpt*) and horizontal (*upt,vpt*) swimming velocities as a function of time (*t*) and space (*x*,*y*,*z*), 3) considering the particle swimming speeds when particle advection is conducted, 4) requesting and reading mortality percentages as a function of time, and 5) considering particle mortality. The programming I added to SHOC's scripts sparse.h, ptrack.h, and pt.c is shown below (A2.1). User and science manuals of SHOC, as well as its revision history, are provided as pdf documents on internet, these are accessible from: http://www.emg.cmar.csiro.au/www/en/emg/software/EMS/hydrodynamics.html. In A2.2 and A2.3 I provide respectively, the sections from the revision history and the user manual relevant to the inclusion of particle behavior.

A2.1 SHOC's code: my modifications are in red

```
/*****************************************************************
    ENVIRONMENTAL MODELLING SUITE (EMS)

    File: ems/model/hd/include/sparse.h

    Description:
    Primary sparse structures.

    Author(s):
    Mike Herzfeld(MH), CSIRO Marine Research
    Jason Waring(JRW), CSIRO Marine Research

    Revision history:
    16/12/2003 JRW Created

    Copyright:
    Copyright(C) 2003, CSIRO Australia, All rights reserved.
    See COPYRIGHT file for copying, use and redistribution conditions.

    EMS is derived from MECO, sjwlib and other libraries developed by
    Stephen Walker (CSIRO Marine Research) and others.

    $Id: sparse.h,v 1.19 2005/04/04 23:30:29 her127 Exp $
*****************************************************************/

Some code deleted

/*---------------------------------------------------------------*/
/* Master data structure                                         */
/*---------------------------------------------------------------*/

Some code deleted

  /* particle variables */
  double *pt_svel;     /* Settling velocity of the particle */
  double *pt_sper;     /* Settling period of the particle */
  int *svel_type;      /* Type of particle settling */
```

```
  pt_ts_t **wvel_s;    /* Vertical settling for sources */
  pt_ts_t *wvel_i;     /* Vertical settling for initial release */
  pt_ts_t *uvel_i;     /* Horizontal e1 swimming for initial release
*/
  pt_ts_t *vvel_i;     /* Horizontal e2 swimming for initial release
*/
  pt_ts_t *mort_i;     /* Mortality initial release */
```

Some code deleted

```
#endif             /* _SPARSE_H */


/*********************************************************************

    ENVIRONMENTAL MODELLING SUITE (EMS)

    File: ems/lib/include/ptrack.h

    Description:
    Include file for particle tracking routines

    Author(s):
    Jason Waring(JRW), CSIRO Marine Research
    Pavel Sakov(PS), CSIRO Marine Research

    Revision history:
    16/12/2003 JRW Created

    Copyright:
    Copyright(C) 2003, CSIRO Australia, All rights reserved.
    See COPYRIGHT file for copying, use and redistribution conditions.

    EMS is derived from MECO, sjwlib and other libraries developed by
    Stephen Walker (CSIRO Marine Research) and others.

    $Id: ptrack.h,v 1.2 2004/08/17 01:40:51 her127 Exp $

*********************************************************************/

#ifndef _PTRACK_H
#define _PTRACK_H 1

typedef struct {
  double e1;
  double e2;
  double e3;
  short flag;
  int dumpf;
  double age;
  unsigned char out_age;
  double size;
  unsigned char out_size;
  double svel;
  double pt_u_hsv;
  double pt_v_hsv;
} particle_t;

#define PT_ACTIVE 0x001
#define PT_LOST   0x002
#define PT_AGE    0x004
#define PT_SIZE   0x008

int pt_create(char *name, long np, char *t_units, int dumpf);
void pt_read(char *name, int rec, long *np, particle_t **p, double *t,
             char *t_units, int *ndump);
void pt_write(int fid, int rec, double t, long np, particle_t *p);
```

```
#endif                          /* _PTRACK_H */


/*************************************************************************

    ENVIRONMENTAL MODELLING SUITE (EMS)

    File: ems/model/hd/particles/pt.c

    Description:
    particle_t tracking code for meco

    Author(s):
    Mike Herzfeld(MH), CSIRO Marine Research
    Jason Waring(JRW), CSIRO Marine Research
    Paulina Cetina Heredia, JCU

    Revision history:
    16/12/2003 JRW Created

    Copyright:
    Copyright(C) 2003, CSIRO Australia, All rights reserved.
    See COPYRIGHT file for copying, use and redistribution conditions.

    EMS is derived from MECO, sjwlib and other libraries developed by
    Stephen Walker (CSIRO Marine Research) and others.

    $Id: pt.c,v 1.4 2004/09/13 04:26:51 her127 Exp $

*************************************************************************/

#include <stdio.h>
#include <stdlib.h>
#include <string.h>
#include <math.h>
#include <netcdf.h>
#include "hd.h"

#define MAX_COL    127
#define HIST_SCALE 5
#define CONSTANT 2 /*settling velocity tpes*/
#define STOKES   4
#define DIURNAL  8

/* Prototypes */
void particles_to_conc(master_t *master, long np, particle_t *p);
void ptgrid_xytoij(master_t *master, long np, particle_t *p);
void ptgrid_ijtoxy(master_t *master, long np, particle_t *p);
void pt_fit_to_grid(master_t *master, long np, particle_t *p);
void pt_write_at_t(master_t *master, double t);
void pt_move(master_t *master, dump_data_t *dumpdata, particle_t *p,
             double dt, double maxdh);
void pt_set_age(master_t *master, particle_t *p, double dt);
void pt_set_size(master_t *master, particle_t *p, double dt, int n);
void pt_set_svel(master_t *master, particle_t *p, double dt, int n);
void pt_new(master_t *master, long np, particle_t *p);
double time_to_face(master_t *master, double ul, double ur, double f,
                    double *u, double *du);
double pt_step_dist(master_t *master, double u, double du, double dt);
int hd_pt_create(master_t *master, char *name);

Some code deleted

/*-------------------------------------------------------------------
*/
/* particle_t tracking initialisation routine
*/
```

```
/*-----------------------------------------------------------------
*/

Some code deleted

  /* Read the vertical swimming velocity file
*/
  master->wvel_i = NULL;
  sprintf(key, "PT_w_file");
  if(prm_read_char(fp, key, buf)){
    master->wvel_i = (pt_ts_t *)malloc(sizeof(pt_ts_t));
    pt_ts_t *wdata = master->wvel_i;
    wdata->val = NULL;
    wdata->ts = hd_ts_read(master, buf, 0);
    wdata->id = ts_get_index(wdata->ts, fv_get_varname(buf, "wpt",
buf));
    if (wdata->id < 0)
      hd_quit("pt_params_init: The file '%s' does not contain the
settling variable 'wpt' .\n", buf);
    wdata->val = d_alloc_1d(geom->sgsiz);
    memset(wdata->val, 0, geom->sgsiz * sizeof(double));
  }

  /* Read the horizontal swimming velocity file
*/
  master->uvel_i = NULL;
  master->vvel_i = NULL;
  sprintf(key, "PT_uv_file");
  if(prm_read_char(fp, key, buf)){
    master->uvel_i = (pt_ts_t *)malloc(sizeof(pt_ts_t));
    master->vvel_i = (pt_ts_t *)malloc(sizeof(pt_ts_t));
    pt_ts_t *udata = master->uvel_i;
    pt_ts_t *vdata = master->vvel_i;
    udata->val = NULL;
    vdata->val = NULL;
    udata->ts = hd_ts_read(master, buf, 0);
    udata->id = ts_get_index(udata->ts, fv_get_varname(buf, "upt",
buf));
    if (udata->id < 0)
      hd_quit("pt_params_init: The file '%s' does not contain the
settling variable 'upt' .\n", buf);
    udata->val = d_alloc_1d(geom->sgsiz);
    memset(udata->val, 0, geom->sgsiz * sizeof(double));
    vdata->ts = hd_ts_read(master, buf, 0);
    vdata->id = ts_get_index(vdata->ts, fv_get_varname(buf, "vpt",
buf));
    if (vdata->id < 0)
      hd_quit("pt_params_init: The file '%s' does not contain the
settling variable 'vpt' .\n", buf);
    vdata->val = d_alloc_1d(geom->sgsiz);
    memset(vdata->val, 0, geom->sgsiz * sizeof(double));
  }

  /* Reads the mortality file
*/
  master->mort_i = NULL;
  sprintf(key,"PT_mortality_file");
  if(prm_read_char(fp, key, buf)){
    master->mort_i = (pt_ts_t *)malloc(sizeof(pt_ts_t));
    pt_ts_t *wdata = master->mort_i;
    wdata->ts = hd_ts_read(master, buf, 0);
    wdata->id = ts_get_index(wdata->ts, fv_get_varname(buf, "mpt",
buf));
    if(wdata->id < 0)
      hd_quit("pt_params_init: The file '%s' does not contain the
mortality variable 'mpt' .\n", buf);
  }

  /* If the release rate is specified, then a start and end
*/
```

```
  /* coordinates for the continous line must be specified.
*/
  master->pt_nsource = 0;
  prm_set_errfn(hd_silent_warn);
  prm_read_int(fp, "PT_NSOURCE", &master->pt_nsource);
  prm_set_errfn(hd_quit);

  if (master->pt_nsource > 0) {
    master->pt_rate = d_alloc_1d(master->pt_nsource);
    master->pt_colour =
      (short *)malloc(sizeof(short) * master->pt_nsource);
    master->pt_x1 = d_alloc_1d(master->pt_nsource);
    master->pt_y1 = d_alloc_1d(master->pt_nsource);
    master->pt_z1 = d_alloc_1d(master->pt_nsource);
    master->pt_x2 = d_alloc_1d(master->pt_nsource);
    master->pt_y2 = d_alloc_1d(master->pt_nsource);
    master->pt_z2 = d_alloc_1d(master->pt_nsource);
    master->pt_accum = d_alloc_1d(master->pt_nsource);
    master->pt_size = d_alloc_1d(master->pt_nsource);
    master->pt_decay = d_alloc_1d(master->pt_nsource);
    master->pt_svel = d_alloc_1d(master->pt_nsource);
    master->pt_dens = d_alloc_1d(master->pt_nsource);
    master->svel_type = i_alloc_1d(master->pt_nsource);
    master->pt_sper = d_alloc_1d(master->pt_nsource);
    memset(master->pt_svel, 0, master->pt_nsource*sizeof(double));
```

Some code deleted

```
      /* Read the settling velocity type (ms-1)
*/
      /* Set the default value
*/
      master->svel_type[i] = NONE;
      /* Goes through the options
*/
      sprintf(key, "PT_Source%d.Stype",i);
      prm_read_char(fp, key, buf);
      if (strcmp(buf, "CONSTANT") == 0) {
      sprintf(key, "PT_Source%d.Svel", i);
      if (prm_read_double(fp, key, &master->pt_svel[i])) {
        master->svel_type[i]= CONSTANT;
      } else {
        hd_quit("pt_params_init: Constant settling velocity type
requires settling velocity attribute (PT_Source.Svel)#. \n");
      }
      } else if (strcmp(buf, "STOKES") == 0) {
      sprintf(key, "PT_Source%d.Dens", i);
      if (prm_read_double(fp, key, &master->pt_dens[i])) {
        if (master->pt_size[i] == 0.0)
          hd_quit("pt_params_init: Stokes settling velocity type
requires Size attribute(PT_Source#.Size).\n");
        master->svel_type[i] = STOKES;
      } else { hd_quit("pt_params_init: Stokes settling velocity type
requires Density attribute (PT_Source#.Dens).\n");
      }
      } else if (strcmp(buf, "DIURNAL") == 0) {
        sprintf(key, "PT_Source%d.Svel",i);
      if (prm_read_double(fp, key, &master->pt_svel[i])) {
        sprintf(key, "PT_Source%d.Sper",i);
        if (prm_read_char(fp, key, buf)){
          tm_scale_to_secs(buf, &master->pt_sper[i]);
          master->svel_type[i]= DIURNAL;
          } else {
          hd_quit("pt_params_init: Diurnal settling velocity type
requires Periodicity attribute (PT_Source#.Sper).\n ");
        }
      } else {
        hd_quit("pt_params_init: Diurnal settling velocity type
requires Settling Velocity attribute (PT_Source#.Svel).\n ");
      }
```

```
      } else if(strcmp(buf, "FILEIN") == 0) {
      char filename[MAXSTRLEN];
      sprintf(key, "PT_Source%d.File" ,i);
      if (prm_read_char(fp, key, filename)){
        if (i == 0)
          master->wvel_s = (pt_ts_t **)malloc(sizeof(pt_ts_t *) *
master->pt_nsource);
        master->wvel_s[i] = (pt_ts_t *)malloc(sizeof(pt_ts_t *));
        pt_ts_t *wdata = master->wvel_s[i];
        wdata->ts = hd_ts_read(master, filename, 0);
        wdata->id = ts_get_index(wdata->ts, fv_get_varname(filename,
"wpt", buf));
        if (wdata->id < 0)
          hd_quit("pt_params_init: The file '%s' does not contain the
settling variable 'wpt' .\n", filename);
        master->svel_type[i] = FILEIN;
      } else {
        hd_quit("pt_params_init: File input requires settling velocity
time series file.(PT_Source#.File)\n");
      }
      }
```

Some code deleted

```
/* END pt_params_init()
*/
/*----------------------------------------------------------------------
*/
```

Some code deleted

```
/*----------------------------------------------------------------------
*/
/* Routine to activate more particles randomly along a line source
*/
/* defined by the two points (pt_x1,pt_y1,pt_z1) and
*/
/* (pt_x2,pt_y2,pt_z2).
*/
/*----------------------------------------------------------------------
*/
```

Some code deleted

```
/*Evaluates the time series of settling velocities*/
      master->pt_svel[i] = ts_eval_xyz(w_s->ts, w_s->id,
                                master->t, master->pt_x2[i],
                                master->pt_y2[i],
                                master->pt_z2[i]);
```

Some code deleted

```
      /* Initialise the settling velocity */
      p[n].svel = 0.0;

/* END pt_new()
*/
/*----------------------------------------------------------------------
*/


/*----------------------------------------------------------------------
*/
/* Routine to activate more particles randomly along a line source
*/
/* defined by the two points (pt_x1,pt_y1,pt_z1) and
*/
/* (pt_x2,pt_y2,pt_z2).
*/
```

```
/*-------------------------------------------------------------------
*/

Some code deleted

/* Initialise the settling velocity */
      p[n].svel = 0.0;

Some code deleted

/* END pt_split()
*/
/*-------------------------------------------------------------------
*/

/*-------------------------------------------------------------------
*/
/* Routine to track all the particles for a single timestep
*/
/*-------------------------------------------------------------------
*/

Some code deleted

/*-------------------------------------------------------------------*/
/* Move particles if required                                        */
  if (master->t + master->dt / 2 >= master->ptnext_t) {
    int n;
    int cc, c, c2;
    double x, y, z;
    double maxdh;
    pt_ts_t *u_i = master->uvel_i;
    pt_ts_t *v_i = master->vvel_i;
    pt_ts_t *w_i = master->wvel_i;
    pt_ts_t *m_i = master->mort_i;

    if (DEBUG("particles"))
      dlog("particles", "Moving particles, t=%.0f\n", master->t);

Some code deleted

    /*-----------------------------------------------------------------
*/
    /* Set the settling velocity of each particle from an initial
*/
    /* release if required.
*/
    if(u_i && v_i) {
      double u, v;
      for (cc = 1; cc <= geom->b3_t; cc++) {
      c = geom->w3_t[cc];
      c2 = geom->m2d[c];
      u = ts_eval_xyz(u_i->ts, u_i->id, master->t,
                  geom->cellx[c2], geom->celly[c2],
                  geom->cellz[c]);
      v = ts_eval_xyz(v_i->ts, v_i->id, master->t,
                  geom->cellx[c2], geom->celly[c2],
                  geom->cellz[c]);
      u_i->val[c] = u * geom->costhcell[c2] + v * geom->sinthcell[c2];
      v_i->val[c] = -u * geom->sinthcell[c] + v * geom->costhcell[c2];
      }
    }
    if(w_i) {
      for (cc = 1; cc <= geom->b3_t; cc++) {
      c = geom->w3_t[cc];
      c2 = geom->m2d[c];
      w_i->val[c] = ts_eval_xyz(w_i->ts, w_i->id, master->t,
                          geom->cellx[c2], geom->celly[c2],
                          geom->cellz[c]);
      }
```

```
    }

    if (master->pt_nsource > 0)
      pt_new(master, master->ptn, master->ptp);

    /*---------------------------------------------------------------
*/
    /* Set the settling velocity of each particle from a source if
*/
    /* required.
*/
    if(master->pt_svel) {
      for (n = 0; n < master->ptn; n++) {
            pt_set_svel(master, &master->ptp[n], master->ptstep, n);
      }
    }

    /*---------------------------------------------------------------
*/
    /* Reads the mortality percentage from file if required
*/
    if (m_i) {
      int part_numb = 0;
      int part_numb_act = 0;
      int part_numb_lost = 0;
      m_i->data = ts_eval(m_i->ts, m_i->id, master->t);
      for (n = 0; n < master->ptn; n++) {
      part_numb++;
      if (((master->ptp[n].flag) & PT_ACTIVE) &&
          !((master->ptp[n].flag) & PT_LOST)) {
        part_numb_act++;
      } else if(((master->ptp[n].flag) & PT_LOST)) {
        part_numb_lost++;
      }
      }
      /* Make some of the particles lost due to mortality
*/
      double dp = round((m_i->data /100)* part_numb_act);
      if(dp > 0){
      int interval = round(part_numb_act/dp);
      for (n = 0; n < master->ptn; n += interval) {
        master->ptp[n].flag |= PT_LOST;
      }
      }
    }
```

Some code deleted

```
/* END pt_update()
*/
/*---------------------------------------------------------------
*/
```

Some code deleted

```
/*---------------------------------------------------------------
*/
/*This routine sets the settling velocity of all particles
*/
/*---------------------------------------------------------------
*/
void pt_set_svel(master_t *master, /* Master data
*/
                 particle_t *p,    /* Pointer to particle
*/
                 double dt,        /* Time interval for moving)
*/
                 int n             /* Particle number
*/
)
```

```
{
  int sm = master->pt_sm[n];         /* Particle source map
*/
  int stype = master->svel_type[sm]; /* Settling velocity type
*/
  double vel = master->pt_svel[sm];  /* Fixed settling velocity
*/
  double per = master->pt_sper[sm];  /* Fixed settling period
*/
  double dens = master->pt_dens[sm]; /* Water density in cell
*/
  double mu = 1.4e-3; /* Molecular viscocity of water at 20C
(kg/m/s)*/

  /* Set the settling type velocity
*/
  if ((p->flag & PT_ACTIVE) && !(p->flag & PT_LOST)) {
    if (stype == NONE) {
      /* No settling
*/
      p->svel = 0.0;
    } else if (stype == CONSTANT) {
      /* Constant settling
*/
      p->svel = vel;
    } else if (stype == STOKES) {
      /* Stokes settling
*/
      int c = ztoc_m(master, floor(p->e1), p->e3);
      p->svel = -master->g * (dens - master->dens[c]) *
      p->size * p->size / (18.0 * mu);
    } else if (stype == DIURNAL) {
      /* Diurnal settling
*/
      double frac = (master->t/(per))-(floor(master->t/(per)));
      p->svel = (-vel * cos(frac * 2*PI));
    } else if (stype == FILEIN) {
      /* Reading svel from a ts file
*/
      p->svel = vel;
    }
  }
}

/* END pt_set_vel()
*/
/*-----------------------------------------------------------------------
*/
```

Some code deleted

```
/*-----------------------------------------------------------------------
*/
/* This routine moves a single particle for a specified time
*/
/* The position of the particle is :
*/
/* Integer part of p->e1 = sparse location of the particle.
*/
/* Fractional part of p->e1 = x sub-grid distance of the particle in
*/
/*                            the cell.
*/
/* p->e2 = j location of particle (integer part) and y sub grid
*/
/*         distance (fractional part).
*/
/* p->e3 = depth of particle.
*/
```

```
/*--------------------------------------------------------------------
*/

Some code deleted

  /* Set the settling/swimming velocity for each particle from an
*/
  /* initial release if required.
*/
  if (u_i && v_i) {
    upt = u_i->val[c];
    vpt = v_i->val[c];
  } else {
    upt = 0.0;
    vpt = 0.0;
  }
  wpt = (w_i) ? w_i->val[c] : 0.0;

Some code deleted

/*--------------------------------------------------------------------*/
    /* Add diffusion velocities and scale the total by the cell
*/
    /* dimensions.
*/
    u1_l = (u1_l + diffu1 + upt) / geom->h1acell[c2];
    u1_r = (u1_r + diffu1 + upt) / geom->h1acell[c2];
    u2_b = (u2_b + diffu2 + vpt) / geom->h2acell[c2];
    u2_f = (u2_f + diffu2 + vpt) / geom->h2acell[c2];

Some code deleted

  /* Interpolate vertical advection velocities to the slice top    */
    /* and bottom. Note that the vertical diffusion velocity is
*/
    /* added later, at the third call to time_to_face() below, so
*/
    /* that vertical velocity values can be examined in detail if
*/
    /* the particle tries to leave the water surface (code further
*/
    /* below).
*/
    /* Also add the settling velocity if required.
*/
    w_b = (1 - frac_b) * wk + frac_b * wkp1 + wpt;
    w_t = (1 - frac_t) * wk + frac_t * wkp1 + wpt;

Some code deleted

/* END pt_move()
*/
/*--------------------------------------------------------------------*/
```

A2.2 Revision history:

April 7, 2010 - Revisions 1498-1523

Added temporal percentile computations (-ps mode) (Section 10, User's Manual).

Reworked particle settling and added swimming/mortality (Section 4.29, User's Manual).

A2.3 Shoc user manual:

4.27.5 Settling

Particles may be prescribed setting velocities as a function of the source, or as a function of position when an initial particle distribution is prescribed (i.e. no sources). For the former, different types of settling behaviour for particles released from each source may be prescribed using:

```
PT_Source0.Stype  NONE      # No settling imposed
                  CONSTANT  # Particles from this source settle with
                            # a constant settling velocity.
                  STOKES    # The stokes settling formula is used to
                            # compute the settling velocity. This is
                            # a function of particle size, density
                            # and water density.
```



```
                  DIURNAL   # A periodic settling velocity is used
                            # where the amplitude and period are
                            # prescribed.
                  FILEIN    # Velocity is read from file.
```

For all particles, a negative settling velocity means the particle will sink and a positive velocity will result in a buoyant particle. The `CONSTANT` settling velocity for particles released from each source may is prescribed using;

```
PT_Source0.Svel   1e-3        # velocity in ms-1
```

The `STOKES` settling velocity may be computes using Stokes settling formula:

$$v = \frac{g(\rho_w - \rho_p)d^2}{18\mu} \qquad 3.27.1$$

where g = 9.81 (m^2s^{-1}) is the acceleration due to gravity, ρ_w (kgm^{-3}) is the density of surrounding water, ρ_p (kgm^{-3}) is the density of the particle, d (m) is the particle diameter (size in this case) and m = 1.4e-3 ($kgm^{-1}s^{-1}$) is the viscosity of water at 20°C. This settling velocity is calculated and applied to each particle if the particle size is set (see Section 4.27.4) and the particle density is prescribed:

```
PT_Source0.Dens      1030  # Density in kgm-3
```

Hence if a growth rate is also prescribed, then as the particle grows its diameter increases and therefore settles faster.

The `DIURNAL` settling velocity is computed using the formula:

$$v = -svel.\cos(2\Pi(t/sper - floor(t/sper))) \qquad 3.27.2$$

where `svel` is the maximum vertical velocity (ms^{-1}) at which the particle will move, `t` is time and `sper` is the periodicity of the cosine function, e.g.

```
PT_Source0.Svel   1e-3    # Velocity in ms-1
PT_Source0.Sper   1 day   # Periodicity
```

The FILEIN settling velocity is prescribed using an ASCII or netCDF time series file.

```
PT_Source0.File svel.ts        # Time series file containing
                               # variable and 'wpt' (ms^-1).
```

The settling velocity variable in the file must be named 'wpt'. The settling velocity in the file may be a function of time or space (or both). The spatial coordinates of the source (i.e. StartLocation and EndLocation) are used to interpolate from the file onto the source location if spatial information is contained in the file.

Additionally, particles released from an initial distribution (i.e. without sources specified) may undergo settling as a function of their position in time and space as read from file. This is specified using:

```
PT_w_file    svel.nc      # File containing settling variable 'wpt'.
```

The settling velocity variable in the file must be named 'wpt', and the velocity may be a function of time, space or both. Spatially dependent velocities interpolate the settling velocity onto cell centres of the grid, and all particles within a particular cell will adopt that corresponding settling velocity.

NOTE: The differences between invoking PT_Source0.Svel settling velocity type and the PT_w_file are that the former is used for particles released from sources; in which case a continuous source of particles along a line is specified by a rate of release and the start/end positions of the line. Each source must have their own time series file. The second from is used for a release of particles determined with the particle input file, in which case the domain is seeded with an initial distribution of particles. In this case, the settling velocity can vary as a function of time t and space .

4.27.6 Swimming

Similar to the settling for particles released from an initial distribution, particles may be assigned horizontal swimming velocities applicable to an initial release. This swimming is read from netCDF file as a function of time and space and is specified via:

```
PT_uv_file  vel.nc       # File containing settling variable 'upt'
                         # for swimming in the x (east-west)
                         # direction and 'vpt' for swimming in the y
                         # (north-south) direction.
```

Note that upt and vpt are velocities are relative to the east-west / north-south axis rather than the numerical grid, and must generally undergo rotation (within the particle tracking code) to be transformed onto the grid.

4.27.7 Mortality

Mortality, or the loss of particles expressed as a percentage of active, unlost, particles at every time step, can be prescribed with a time series file (note: this input is not spatially dependent), e.g:

```
PT_mortality_file    mp.ts    # mortality percentage file
```